VOLUME 23 AUGUST, 1935 NUMBER 8

PROCEEDINGS
of
The Institute of Radio Engineers

Application Blank for Associate Membership on Page XIV

Institute of Radio Engineers Forthcoming Meetings

DETROIT SECTION
September 20, 1935

LOS ANGELES SECTION
September 17, 1935

NEW YORK MEETING
October 2, 1935

PHILADELPHIA SECTION
September 5, 1935

PITTSBURGH SECTION
October 15, 1935

WASHINGTON SECTION
September 9, 1935

INSTITUTE NEWS AND RADIO NOTES

Meeting of the Board of Directors

A special meeting of the Board of Directors was held in the Institute office on July 11 and those present were: Stuart Ballantine, president; Melville Eastham, treasurer; R. A. Heising, J. V. L. Hogan, Haradan Pratt, A. F. Van Dyck, William Wilson, and H. P. Westman, secretary.

H. S. Shaw was transferred to the grade of Fellow and J. A. Proctor admitted to that grade of membership. There were transferred to the grade of Member: E. C. Anderson, W. W. Garstang, and S. B. Smith and admitted to that grade A. R. Morton and H. H. Scott. Fifty-one applications for Associate and seventeen for Student membership were approved.

This special meeting was called to consider the possibility of the Institute sponsoring the preparation of a complete index of radio material to be prepared with the assistance of relief workers supplied by the New York City Emergency Relief Bureau. After careful examination of the situation, it was felt that although such an index might be obtained with a relatively small outlay of money, to be useful it would be necessary to maintain it continuously thereafter at what would probably be a substantial annual expense. The publication of such an index would be highly expensive. The maintenance of a service to supply bibliographical material although not requiring as large an initial outlay as publication, would, over a period of years, be just as expensive. In addition, a number of organizations at the present time are supplying index services and the potential use of an Institute service would, therefore, be substantially curtailed.

Survey of Engineering

The Bureau of Labor Statistics of the United States Department of Labor has distributed questionnaires to Institute members located in the United States in an effort to obtain statistical data on certain aspects of engineering employment. There has been some misunderstanding as to the purpose of this survey and it has been assumed by some that the Bureau is endeavoring to find positions for engineers. The Bureau has no facilities for placing unemployed engineers and the purpose of this survey is to obtain data on trends in engineering employment for such future value as this knowledge may provide. Those who have not filled in and returned the questionnaires are urged to do so.

Committee Work

STANDARDIZATION

Technical Committee on Electronics

A meeting of the Technical Committee on Electronics operating under the Institute's Standards Committee was held on June 22 in Schenectady, N. Y., and those present were: B. J. Thompson, acting chairman; Ben Kievit, Jr. (representing R. M. Wise), F. R. Lack (representing M. J. Kelly), E. A. Lederer, G. F. Metcalf, H. W. Parker, O. W. Pike, Dayton Ulrey, P. T. Weeks, and H. P. Westman, secretary.

Each of the subcommittees reported on the progress made by it and it is anticipated that reports from all of them will be available early in the Fall. Methods of handling these reports and their consolidation into a single document for action by the Technical Committee and later, the Institute's Standards Committee, were outlined.

Subcommittee on Electron Beam and Miscellaneous Tubes

A meeting of the Subcommittee on Electron Beam and Miscellaneous Tubes operating under the Technical Committee on Electronics was held in Schenectady on June 21. G. F. Metcalf, chairman; Ben Kievit, Jr., B. J. Thompson, Dayton Ulrey (representing Lee Sutherlin), and H. P. Westman, secretary, were present.

The committee revised certain recommendations made at previous meetings and prepared a list of terms which apply to electron beam tubes which it will define. A general discussion of a number of these terms was held to assist in crystallizing opinions as to suitable definitions. The committee expects to complete its work at its next meeting.

Subcommittee on Gas-Filled Tubes

This subcommittee met in Schenectady, N. Y. on June 21 and those present were O. W. Pike, chairman; H. E. Mendenhall, Dayton Ulrey, and H. P. Westman, secretary.

A preliminary report to the Electronics Committee was reviewed and slight revisions made in it. Modifications were made of several matters which were considered at two previous meetings of the committee.

Another meeting of this committee was held on June 22 in Schenectady and attended by O. W. Pike, chairman; Dayton Ulrey and

P. T. Weeks. It was devoted to modifying certain definitions to bring them into agreement with the types of definitions normally established by the Institute.

Subcommittee on Large High Vacuum Tubes

This subcommittee meeting, which was held in Schenectady, N. Y., on June 22, was attended by F. R. Lack (representing M. J. Kelly), C. M. Wheeler, E. E. Spitzer, and R. W. Larsen. A number of letter symbols were considered and several recommended for approval. The section on amplifier classifications in the 1933 Report was discussed and because it concerns the Subcommittee on Small High Vacuum Tubes, the committee visited that committee which was then in session and a satisfactory revision of that section was made jointly. Some work on definitions concluded the meeting.

Subcommittee on Small High Vacuum Tubes

This subcommittee met on June 22 in Schenectady, N. Y., and those present were P. T. Weeks, chairman; Ben Kievit, Jr., (representing R. M. Wise), E. A. Lederer, G. F. Metcalf, H. A. Pidgeon, E. W. Schafer and H. P. Westman, secretary. A number of definitions and methods of measurement were revised and during the visit of the Subcommittee on Large High Vacuum Tubes that portion of the 1933 report on amplifier classification was considered.

Institute Meetings

Buffalo-Niagara Section

A meeting of the Buffalo-Niagara Section was held on June 14 at the University of Buffalo. L. E. Hayslett, chairman, presided and thirty-five attended the meeting.

A paper on "Noise, Its Measurement and Analysis with Demonstrations of Actual Measuring and Analyzing Equipment" was presented by L. G. Hector, Professor of Physics at the University of Buffalo. Dr. Hector opened his paper with a discussion of the meaning of the decibel unit and its application in acoustics. He then pointed out that great interest is shown today in the acoustics of auditoriums and in the psychological effects of noises in offices, factories, on the street, and in vehicles. He then described the measurement and analysis of noise and demonstrated equipment designed for such purposes.

As this was the annual meeting, the election of officers was held and the previous officers were unanimously re-elected. These are L. E.

Hayslett, chief engineer for the Rudolph Wurlitzer Company as chairman; R. J. Kingsley, chief engineer of WBEN as vice chairman; and E. C. Waud as secretary-treasurer.

Chicago Section

The Chicago Section devoted its May 31 meeting to "The European Radio Situation" as described by Alfred Crossley, consulting engineer. The meeting was held in the Merchandise Mart and Mr. Crossley presided as chairman of the section. Ninety-five members and guests attended the meeting and twelve were at the informal dinner which preceded it.

The speaker spent two months abroad studying the European radio situation and compared European and American broadcast receiver technique. He discussed the trend in England, Holland, Belgium, Switzerland, Spain, Italy, France, and the Scandinavian countries. High fidelity receivers, latest type loud speaker designs, and the new type automatic volume control compensation system for the correction of output with respect to the percentage of modulation were described. The automobile radio situation in France was discussed in detail and the progress in this field of other European countries outlined. The short-wave feature of broadcast receivers as applied to all-wave receivers was presented from the European observer's standpoint and indicated that at the present time it is not as important as high fidelity reproduction. The meeting closed with a lively discussion on the merits of European and American tube technique.

Cleveland Section

The Cleveland Section met on May 24 at the Case School of Applied Science with K. J. Banfar, chairman, presiding. Twenty-two members were present.

Four papers were presented on the general subject of engineering investigations of sound. The first paper "A Study of Sound in Electrical Engineering" was presented by J. R. Martin. In it Professor Martin presented a short history of sound measurement and briefly described work being done at Case School of Applied Science. This work falls into three major divisions which cover traffic noise, noise in electrical machinery, and the psychological effects of noise. These subjects were then discussed in order by students of Case School.

The first of these was P. J. Kibler who spoke on "A survey of Traffic Noise." He described the audiometer method of sound measurement which is a comparison by ear of a calibrated noise level with the noise level to be determined. An 800-cycle note has been accepted as the

American standard for the calibrated source. Another method of measurement is an electrical one which involves a microphone, amplifier, and output meter calibrated in decibels from a standard sound pressure. The equipment used in the Cleveland traffic survey consisted of a General Radio sound meter supplied from a crystal microphone through an amplifier and weighting network. The network is used to compensate for the frequency characteristic of the ear and should have a different value for each loudness level because of the behavior of the ear. A map of the locations at which measurements were made was shown and a chart of the measurements made through a twenty-four-hour period at one particular point where readings were taken four times per minute was shown.

The subject of the second speaker, C. A. Bauman, was "Noise in Electrical Machinery." He pointed out that no machine has as yet been made noiseless and the problem resolves itself into reducing noise to an unobjectionable level without reducing the efficiency of the device. It often happens that a machine which is not inherently noisy may produce a slight noise which is amplified by resonance in adjacent parts. A study in this field has been concerned with determining the amount of noise generated at various frequencies including those of a supersonic nature.

The third speaker, G. L. Ross, discussed "The Psychological Effects of Noise." In this study, representative subjects were required to do certain tasks under the influence of noise at various levels. The subject was introduced to the noise for a short time before he was required to do the task and then was allowed five minutes to do a number of simple arithmetic problems. The result showed an increase of production up to a level of about 70 decibels and a dropping off above that. The efficiency decreased continuously with an increase in noise level.

Philadelphia Section

The June 6 meeting of the Philadelphia Section was held at the WCAU Auditorium in Philadelphia. Two hundred and fifty-five members and guests attended and sixteen were present at the informal dinner which preceded the meeting. E. D. Cook, chairman, presided.

The first paper presented was by Raymond Sooy of the RCA Manufacturing Company who described his "Personal Experiences with Old and New Types of Recording." The author had charge of recording for the Victor Company for over thirty years and described the methods used in recording the music of famous artists and orchestras in the early days of the art when they had to sing and play into

large horns. Frequently a number of horns were connected to a single recording mica diaphragm which operated a cutter to engrave the vibrations into the recording wax. The equipment covered a frequency range from about 300 to 2000 cycles and some sounds which would not record properly had to be faked to make an acceptable record. Many artists were temperamental and were rarely satisfied with their recordings. Only small orchestras could be accommodated.

The introduction of electrical recording made possible many improvements and the ability to record all instruments including a symphony orchestra. The present technique permits sound picked up in different studios to be transmitted by wire to a central recording room where two records are usually made. One is played back to permit the artist to criticize it and to avoid the need of processing if it is not satisfactory.

Among other uses, has been the recording of noises from different types of airplanes to permit student flying officers to recognize the type of plane from the motor noise. Many private records are made for various purposes, some being used in place of letters. The paper was discussed by Mr. Bowers and Professor Rittenhouse.

"The WCAU Photona, A New Electronic Musical Instrument" was the subject of a paper by J. G. Leitch, technical supervisor of WCAU. He outlined the early experimental work done in the mechanical and electrical generation of tone and illustrated the methods used at the present time for this purpose. The early work done by I. I. Eremeeff who was largely responsible for the construction of the WCAU Photona, was described. Experimental work on moving film was covered and pieces of film exhibited. The instrument uses rotating disks acting as shutters between a source of light and a photoelectric cell. A demonstration was given of a simple tone and its change in character when tremolo and a harmonic were added to it.

Mr. Eremeeff was introduced and after a short statement the Photona was played by Hayes Watson. After the meeting all were invited to inspect the studios of WCAU and KYW.

Pittsburgh Section

The annual meeting of the Pittsburgh Section was held on June 11 at the Stratford Club with C. K. Krause, chairman, presiding. It was in the form of a dinner meeting and eighteen members were present. The nominating committee presented its recommendations which were approved by those present and the following officers elected for next year: R. D. Wyckoff, Gulf Research and Development Corporation, as chairman; H. V. Noble, Gulf Research and Development Corpora-

tion, as vice-chairman; and Branko Lazich of the Union Switch and Signal Company as secretary-treasurer. The meeting was closed with the projection of several motion picture films.

San Francisco Section

A meeting of the San Francisco Section was held on May 18 and was in the form of an inspection trip to Oakland airport. One hundred and twenty attended and sixty-five were present at the dinner which was part of the trip. Ralph Shermund, vice chairman, presided and a paper on "Aeronautical Radio Aids" was presented by E. J. Krenz.

Many applications of radio to air navigation were described and included the teletype communication network, meteorological station operations and methods used for condensing and transmitting data to planes, radio beacon transmitters, weather information transmitters, and ultra-high-frequency landing beam equipment. The radio laboratory, shops, and planes of the Boeing School of Aeronautics were then visited. After the dinner, motion pictures were shown and a talk was given by Mr. Krenz.

"Automobile Radio Receiver Development" was the subject of a paper by A. E. Towne, an engineer for the Remler Company, presented at the June 19 meeting of the San Francisco Section. Twenty-one members and guests attended the meeting which was held at the Hotel Bellevue and presided over by Ralph Shermund, vice-chairman. Six attended the informal dinner which preceded the meeting.

In his paper, Mr. Towne covered in detail many problems involved in the design of modern automobile radio receivers. He gave particular attention to the antenna and sensitivity problems and methods of avoiding disturbances due to ignition systems of cars.

Seattle Section

The Seattle Section met on May 31 at the University of Washington. Thirty-two members and guests were present and R. C. Fisher presided.

H. K. Scramstead, Teaching Fellow, Department of Physics of the University of Washington, presented a paper on "The Application of the Wilson Expansion Chamber to Investigations in Atomic Physics."

Dr. Scramstead introduced the subject with an outline of atomic structure and the quantum theory of radiation. The operation and use of the Wilson expansion chamber were described in detail and illustrated with lantern slides showing various ionization paths. This was followed by a demonstration of the duplex camera and the projector

arrangement whereby the radius of curvature of the ionization track could be accurately determined. The slides which were projected showed the existence of both positrons and electrons which Dr. Scramstead has confirmed in the course of his experimental research.

Washington Section

On June 10 a meeting of the Washington Section was held at the Potomac Electric Power Company Auditorium. E. K. Jett, chairman, presided and fifty-one members and guests were present. Of these, twenty attended the informal dinner which preceded the meeting.

A paper on "Some Continued Observations of Ultra-High Frequency Signals Over Long Indirect Paths" was presented by Ross A. Hull, Associate Editor, *QST*. In it Mr. Hull discussed the propagation of sixty-megacycle signals over paths involving the bending of waves to give strong signals at points well below the optical path. Assumptions well established by facts have been made that stratification of the low atmosphere is responsible for the bending and that changes in air mass conditions particularly with respect to humidity may be studied more effectively with the aid of radio transmitters and recorders.

Personal Mention

E. J. T. Moore, formerly of Stromberg-Carlson in Sydney, has established a consulting practice at Sydney, Australia.

G. B. Myers, Lieutenant, U.S.N., has been transferred from the U.S.S. *Chicago* to the U.S.S. *California* with base at San Pedro, Calif.

Formerly in the Electrotechnical Laboratory in the Ministry of Communication, Tomozo Nakai has become Assistant Professor of Electrical Engineering at Tohoku Imperial University, Sendai, Japan.

P. J. Neimo, Lieutenant, U. S. N., has been transferred from Washington, D. C., to the U.S.S. *Augusta* basing at Seattle, Wash.

Formerly with the Prabhat Film Company, R. K. Phatak has become sound engineer for Serog Movie Tone at Bombay, India.

R. J. Renton of the Federal Communications Commission has been transferred from Boston, Mass., to the central monitoring station at Grand Island, Neb.

Henry Shore, formerly with RCA Communications, is now with the patent department of the Radio Corporation of America in New York City.

Previously with Hygrade Sylvania Corporation, E. M. Stuckert has become a senior radio electrician of the Department of commerce Lighthouse Service at Portland, Maine.

Previously with Electrical Research Products, R. T. Van Niman is now with Muyak Corporation of Ohio, Lakewood, Ohio.

William Waterman has joined the engineering staff of RCA Manufacturing Company, Victor Division at Camden having previously been with Lang Radio Corporation.

Harry Wilkie, a radio engineer for the Signal Corp has been transferred from Honolulu to Fort Sam Houston, San Antonio, Texas.

Jack Yolles has left the Radio Corporation of America to join the staff of Sonora, Paris, France.

An honorary degree of Doctor of Science was conferred upon Alfred N. Goldsmith by Lawrence College, Appleton, Wisconsin. The citation made by President Henry Wriston of the College states that it was conferred in part "in recognition of the unique place which Dr. Goldsmith had made in his chosen field."

Siro Akuzawa formerly with the Hirosima Broadcasting Station has joined the Design Department of the Radio Broadcasting Corporation of Japan at Tokio.

J. L. Barnes formerly on the staff of Massachusetts Institute of Technology has been named Assistant Professor of Mathematics at Tufts College, Mass.

H. H. Gleason has left Pilot Radio and Tube Corporation to join the engineering staff of the RCA Manufacturing Company at Camden, N. J.

L. K. Gould is now a geophysical engineer for the Western Geophysical Company in Los Angeles, California, having severed his connections with RKO Studios of that city.

Previously with Pilot Radio and Tube Corporation, A. G. Manke has joined the staff of General Household Utilities Corporation of Chicago.

F. J. Marco, consulting radio engineer has moved from Northbrook, Illinois, to Chicago.

P. C. Michel recently received a Ph.D. from Yale University and has entered the general engineering department of the General Electric Company at Schnectady, N. Y.

E. H. Pierce, Lieutenant, U.S.N., has been transferred from the Naval Research Laboratory to the U.S.S. *Zane*, basing at San Diego, Calif.

J. S. Reese, Lieutenant, U.S.N., has been transferred from New London, Connecticut, to the U.S.S.-S33 with headquarters at the submarine base Pearl Harbor, Hawaii.

Previously with the General Electric Company, Ltd., John Stewart has become a scientific officer of the Royal Aircraft Establishment at South Farnborough, Hants, England.

E. N. Wendell previously with Compania Telefonica Nacional de Espana is now with Les Laboratories L.M.T., Paris, France.

Proceedings of the Institute of Radio Engineers
Volume 23, Number 8 *August, 1935*

TECHNICAL PAPERS

ON SUPERREGENERATION OF AN ULTRA-SHORT-WAVE RECEIVER*

By

Hikosaburo Ataka

(Meidi College of Technology, Tobata, Japan)

Summary—*The superregeneration of an ultra-short-wave receiver is investigated theoretically and experimentally under the following four headings:*

Part I. Theory of Quenching Action.
Part II. Experiments on Quenching Action.
Part III. Effects of Signal Wave.
Part IV. Amplification by Superregeneration.

In Part I is developed an analysis of a quenching action, when the quenching electromotive force is assumed to operate by varying sinusoidally the amount of effective resistance of the oscillatory circuit. A simple criterion is given on the stability of the oscillation in the receiver. It states that the higher the quenching frequency and the greater the amplitude of the periodic resistance, the more unstable the oscillation becomes. The oscillatory current is of a nature of a modulated carrier wave, where the modulation varies the frequency as well as the amplitude of the carrier and a number of component frequencies are comprised in it.

In Part II are described the experiments on the quenching action. The stable and the unstable regions of the oscillation under the influence of quenching action are determined. The results are of a somewhat complicated aspect, but the above criterion is generally satisfied. The transient phenomena at the start or at the end of the oscillation are investigated by means of a Braun tube oscillograph. The characteristic noise of the superregenerative receiver is concluded to be generated with the irregularities of the electromotive forces which initiate the oscillation. In the absence of any signal whatever, these irregular electromotive forces are produced by the shot effect, thermal agitation, etc.

In Part III are studied the effects of an incoming signal on the receiver. The striking phenomenon due to the signal wave of the resonant frequency is the suppression of the characteristic noise (Uda phenomenon). After the detailed investigation on synchronization, the suppression of the characteristic noise is concluded to be ascribed to a synchronization of the oscillation in the receiver with that of the incoming signal wave. By means of the Braun tube, it is shown that (1) the higher the intensity of the signal, the more early the oscillation starts, and (2) the maximum amplitude of the oscillatory current remains almost constant, irrespective of the intensity of the signal.

Owing to the high sensitivity of the superregenerative receiver, up to the sixty-fourth synchronizations are observed.

* Decimal classification: R 163. Original manuscript received by the Institute, March 30, 1934.

In Part IV is considered the amplification by superregeneration. In the first place, the effects of the various factors which affect sensitivity are studied experimentally. Contrary to the usual expectation that the sensitivity of the superregenerative receiver increases rapidly with the decrease of the quenching frequency, it results in (1) for too low quenching frequencies, the sensitivity is as low as for too high quenching frequencies. There is an optimum quenching frequency which gives the best sensitivity, (2) except for the case of very low quenching frequencies, the sensitivity increases generally as the quenching voltage increases, and (3) the optimum frequency displaces to the low-frequency side when the quenching voltage decreases.

Next the mechanism of amplification is studied in detail, and it is shown that there are three important factors which determine the amplification. These are the quenching frequency, the quenching voltage, and the time of advance by which the oscillation is initiated early in the presence of the signal. Basing on the experimental results obtained, a theory of amplification by superregeneration is developed and the effects of the various factors are considered theoretically.

Part I. Theory of Quenching Action

1. Introduction

In 1922, E. H. Armstrong[1] proposed a new method of amplification which was the extension of regeneration into a field beyond its theoretical limit, and he termed, therefore, the process of amplification "superregeneration." The method has often been applied to the reception of medium and short waves since his discovery, but the principle has not come into common use, on account of other superior means which replaced it.

Of late years, however, with the rapid development of ultra-short-wave communication, superregeneration has been gaining in favor for the reception of these waves.

The action of the receiver on this principle is in general, quite complicated, especially in the reception of ultra-short waves. Several valuable papers have recently appeared on this subject. Of its action, however, some important phenomena remain, as yet very imperfectly explored. The object of this paper is to present some systematic studies on its action.

2. Deduction of the Differential Equation

The fundamental principle of superregeneration is based on the impression of a low-frequency variation, usually called "quenching action," which changes the effective resistance of the oscillatory circuit periodically. The quenching action may be performed by varying either the plate voltage or the grid-bias voltage of the detector tube. An analysis of the quenching action is extremely simplified by sub-

[1] E. H. Armstrong, Proc. I.R.E., vol. 10, p. 244: August, (1922).

stituting for the quenching voltage the equivalent variation of the effective resistance.

Then the effective resistance of the oscillatory circuit of the superregenerative receiver may be taken to be composed of the following three terms:

(1) The ohmic resistance γ of the circuit,

(2) The negative resistance $\rho(i)$ by regeneration which is a function of the oscillatory current i,

(3) The periodic resistance $R_m \sin pt$ due to the quenching action, of which the angular frequency is p.

Thus we have

$$R = \gamma + \rho(i) + R_m \sin pt.$$

The differential equation for the oscillatory circuit, consisting of a constant inductance L, a constant capacity C, and the variable resistance R can be written in the form

$$L\frac{di}{dt} + Ri + \frac{1}{C}\int i\,dt = 0, \qquad (1)$$

where no electromotive forces are assumed to be present. Now the problem resolves itself into the study of an electric oscillation in a circuit, as indicated in Fig. 1.

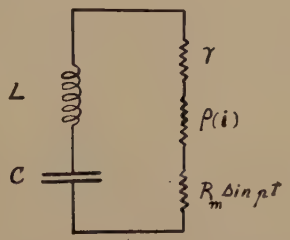

Fig. 1—Equivalent circuit of superregenerative receiver.

The negative resistance due to regeneration $\rho(i)$ is usually expressed by a certain polynomial of i, of which the higher powers play an important rôle in taking the effect of the signal wave into account. But in the absence of any signal whatever, it may be assumed that

$$\gamma + \rho(i) \ll R_m \sin pt.$$

Then the differential equation under consideration is simplified into the form

$$L\frac{di}{dt} + R_m \sin pt \cdot i + \frac{1}{C}\int i\,dt = 0,$$

or differentiating once more, we have

$$\frac{d^2i}{dt^2} + \frac{R_m}{L}\sin pt\frac{di}{dt} + \left(\frac{1}{CL} + \frac{pR_m}{L}\cos\ pt\right)\cdot i = 0.$$

The second term of this equation vanishes by the well-known substitution

$$i = I\cdot y\cdot \epsilon^{-\int(R_m/2L)\sin pt\cdot dt} = I\cdot y\cdot \epsilon^{(\alpha/p)\cos pt}, \tag{2}$$

where,

$$\alpha = \frac{R_m}{2L}\cdot$$

Equation (1) is then transformed into

$$\frac{d^2y}{dt^2} + \left(\omega^2 - \frac{\alpha^2}{2} + p\alpha\cos pt + \frac{\alpha^2}{2}\cos\ 2pt\right)\cdot y = 0, \tag{3}$$

where,

$$\omega = \frac{1}{\sqrt{CL}},$$

and ω is the angular frequency of the natural oscillation of the circuit.

This equation is a special form of Hill's equation. We shall consider the following two extreme cases.

Case (1): $\alpha \ll p$.

Equation (3) reduces to

$$\frac{d^2y}{dx^2} + (\omega^2 + p\alpha\cos pt)\cdot y = 0.$$

Case (2): $\alpha \gg p$.

Equation (3) reduces to

$$\frac{d^2y}{dx^2} + \left(\omega^2 - \frac{\alpha^2}{2} + \frac{\alpha^2}{2}\cos\ 2pt\right)\cdot y = 0.$$

By a slight change of independent variable, both of these equations can be transformed into the form

$$\frac{d^2y}{d\tau^2} + (W + A\cos\tau)y = 0 \tag{4}$$

which is a standard type of Mathieu's equation. The substitutions necessary for this transformation are shown in Table I.

TABLE I

	τ	W	A
Case (1): $\alpha \ll p$	pt	$\frac{\omega^2}{p^2}$	$\frac{\alpha}{p}$
Case (2): $\alpha \gg p$	$2pt$	$\frac{2\omega^2-\alpha^2}{8p^2}$	$\frac{\alpha^2}{8p^2}$

It should be noted that the actual case which is expressed by (3) will lie between these two extreme cases.

One of the particular solutions of (4) may be assumed to be given by the real part of

$$y = \epsilon^{i\mu\tau} \sum_{n=-\infty}^{+\infty} b_n \cdot \epsilon^{in\tau} \tag{5}$$

where μ is a coefficient independent of τ, generally called a "characteristic exponent."

Substituting (5) into the differential equation (4) and equating coefficients of equal powers of ϵ to zero, we have a set of equations

$$[W - (\mu + n)^2]b_n + \tfrac{1}{2}A[b_{n-1} + b_{n+1}] = 0 \tag{6}$$

where,

$$n = \cdots, -2, -1, 0, 1, 2, \cdots .$$

Eliminating the coefficients b determinantally, we have a determinantal expression which constitutes an equation for μ:

$$\Delta(\mu) = \begin{vmatrix} \cdots, & \cdots, & \cdots, & \cdots, & \cdots, \\ \frac{A}{2[W-(\mu+1)^2]}, & 1, & \frac{A}{2[W-(\mu+1)^2]}, & 0, & 0 \\ 0, & \frac{A}{2[W-\mu^2]}, & 1, & \frac{A}{2[W-\mu^2]}, & 0 \\ 0, & 0, & \frac{A}{2[W-(\mu-1)^2]}, & 1, & \frac{A}{2[W-(\mu-1)^2]} \\ \cdots, & \cdots, & \cdots, & \cdots, & \cdots, \end{vmatrix} = 0.$$

Following Hill's analysis, the determinantal equation may be written in the form

$$\sin^2 \pi\mu = \sin^2 \pi\sqrt{W} \cdot \Delta(0) \tag{7}$$

where,

$$\Delta(0) = [\Delta(\mu)]_{\mu=0}.$$

When μ is determined in terms of W and A by (7), the coefficient b_n can be found in terms of b_0 and μ from (6), and the solution of Mathieu's equation (4) is complete. We shall now proceed to discuss some properties of the solution.

3. Stability of the Solution

From (5), the solution is found to remain always finite, if the value of μ is real, including zero. In this case the solution is of an oscillatory character and is called stable. On the other hand, if μ has an imaginary part, the solution increases or decreases indefinitely as the time in-

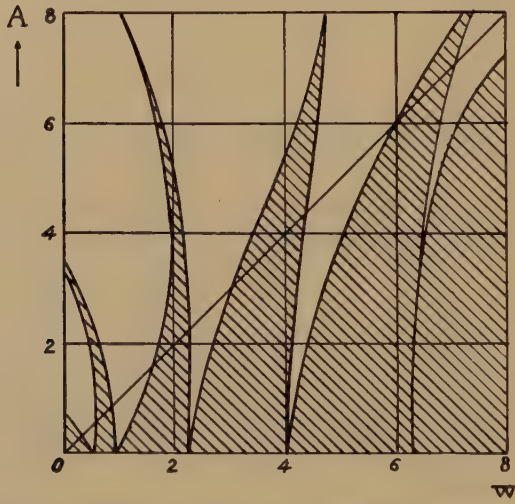

Fig. 2—Stable (shaded) and unstable (unshaded) regions of solution of Mathieu's equation.

creases. The solution is of a logarithmic character and is called unstable.

μ is determined by the values of W and A. Thus a point in the WA plane corresponds to a certain value of μ which makes the solution stable or unstable. The WA plane is divided into areas where the solution is stable and those where it is unstable. Such a diagram is shown[2] in Fig. 2.

In general, from this diagram we may make the following deductions:

(1) Below a 45-degree radial line from the origin, that is, in the region $W > A > 0$, the solution is generally stable, the stable areas being separated by relatively small unstable areas.

[2] G. Gorelik and G. Hintz, *Zeit. für Hochfrequenz.*, Bd. 38, s.222, (1931).

(2) Above the 45-degree radial line from the origin, that is, in the region $A > W > 0$, the solution is generally unstable, the unstable areas being cut by relatively small stable areas.

Thus, to the first approximation, we may take the 45-degree radial line, $W = A$ as a partition of the stable and the unstable regions. Hence for the stability of the solution, that is, for oscillations under the influence of the quenching action, the following simplified criterion can be deduced:

$$W > A : \text{stable}$$
$$W = A : \text{neutral}$$
$$W < A : \text{unstable.}$$

Referring to Table I, the above criterion is expressed by, in case (1), that is, $\alpha \ll p$,

$$\omega^2 > \alpha \cdot p : \text{stable}$$
$$\omega^2 = \alpha \cdot p : \text{neutral}$$
$$\omega^2 < \alpha \cdot p : \text{unstable,}$$

and in case (2), that is, $\alpha \gg p$,

$$\omega^2 > \alpha^2 : \text{stable}$$
$$\omega^2 = \alpha^2 : \text{neutral}$$
$$\omega^2 < \alpha^2 : \text{unstable.}$$

Now consider the stability of the solution in the αp plane. For $\alpha \gg p$, that is, in the left upper part of the plane, the partition is given by a straight line $\alpha^2 = \omega^2$, and for $\alpha \ll p$, that is, in the right lower part of the plane, the partition is given by a hyperbola $\alpha \cdot p = \omega^2$. Interpolating these two extreme curves, we can obtain a curve as shown in Fig. 3, as the partition of the stable and unstable regions.

As α is a quantity which is proportional to the amplitude of the variation of the effective resistance and p stands for its angular frequency, this diagram illustrates the effects of the quenching frequency and the quenching voltage on the stability of the oscillation. It is clear that the stability of the oscillation would actually be more complicated than that which is indicated by this simplified criterion. But in general it may be stated that the higher the quenching frequency and the greater the amplitude of the variation of the effective resistance, the more unstable the oscillation becomes.

The stability of the oscillation is, as will be shown later, of considerable importance in the operation of the superregenerative receiver.

4. Oscillatory Currents

In the practical condition, the quenching frequency $p/2\pi$ is far less than the natural frequency of the circuit $\omega/2\pi$. For example, in the reception of a wave, of which the wavelength is 5 meters, a quenching frequency of 100 kilocycles is commonly employed. Then we have $\omega/p = 500$. Hence it may be put with a close approximation that

$$\omega \gg p .$$

In what follows we shall consider only case (1), as case (2) would produce similar results with only some quantitative differences.

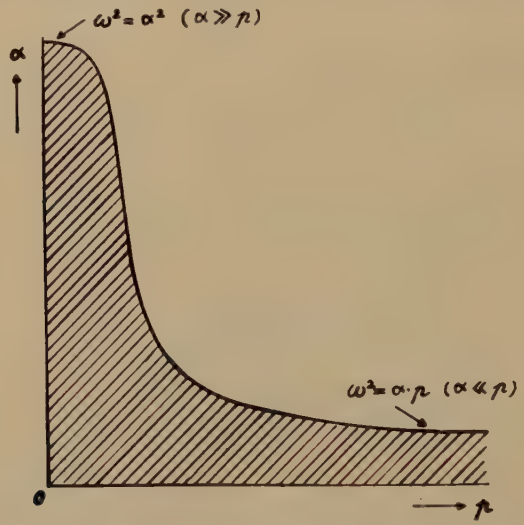

Fig. 3—Stable (shaded) and unstable (unshaded) regions given by a criterion.

Referring to Table I, W becomes exceedingly great as compared with A, so that it may be taken

$$\Delta(0) = 1 .$$

Then from (7), we have

$$\mu = \sqrt{W} = \frac{\omega}{p} ,$$

and the recurrence equation (6) is transformed into

$$-n(2\omega + np)b_n + \frac{\alpha}{2}(b_{n-1} + b_{n+1}) = 0 .$$

Neglecting np with respect to ω, we get

$$b_{n-1} + b_{n+1} = \frac{2n}{\frac{\alpha}{2\omega}} b_n. \tag{8}$$

This relation is, fortunately, satisfied by the Bessel function

$$b_n = J_n(m), \tag{9}$$

where,

$$m = \frac{\alpha}{2\omega}.$$

Substituting the above values of b_n and μ into (5), we have

$$y = \sum_{n=-\infty}^{n=+\infty} J_n(m) \cdot \cos (a + np)t.$$

Or employing the formula

$$J_{-n}(m) = (-1)^n \cdot J_n(m),$$

and,

$$\cos (m \sin \theta) = J_0(m) + 2J_2(m) \cos 2\theta + 2J_4(m) \cos 4\theta + \cdots$$

$$\sin (m \sin \theta) = 2J_1(m) \sin \theta + 2J_3(m) \sin 3\theta + 2J_5(m) \sin 5\theta + \cdots,$$

we have finally,

$$\begin{aligned} y &= J_0(m) \cos \omega t \\ &\quad - J_1(m)\{\cos (\omega - p)t - \cos (\omega + p)t\} \\ &\quad + J_2(m)\{\cos (\omega - 2p)t + \cos (\omega + 2p)t\} \\ &\quad - J_3(m)\{\cos (\omega - 3p)t - \cos (\omega + 3p)t\} \\ &\quad + \cdots \\ &= \cos (\omega t + m \sin pt). \end{aligned} \tag{10}$$

Thus the maximum amplitude of y is always unity, but its frequency varies with the time. In Fig. 4(a), y is shown in rectangular coördinates.

The oscillatory current is expressed by the product of y and $\epsilon^{(\alpha/p)\cos pt}$.

$$\begin{aligned} i &= I \cdot \epsilon^{(\alpha/p)\cos pt} \cdot y \\ &= \epsilon^{(\alpha/p)\cos pt} \cdot \cos (\omega t + m \sin pt), \end{aligned} \tag{11}$$

where the arbitrary current I is assumed to be unity for simplicity. In this expression the factor $\epsilon^{(\alpha/p)\cos pt}$ gives the amplitude modulation of the oscillatory current and is shown in Fig. 4(*b*). The oscillatory current varies along this curve as its envelope. i is shown in Fig. 4(*c*), in which $R_m \sin pt$ is also represented by a broken line. Comparing these two curves, it is easily seen that there is a phase difference $\pi/2$ between the variation of the oscillatory current and that of the effective resistance.

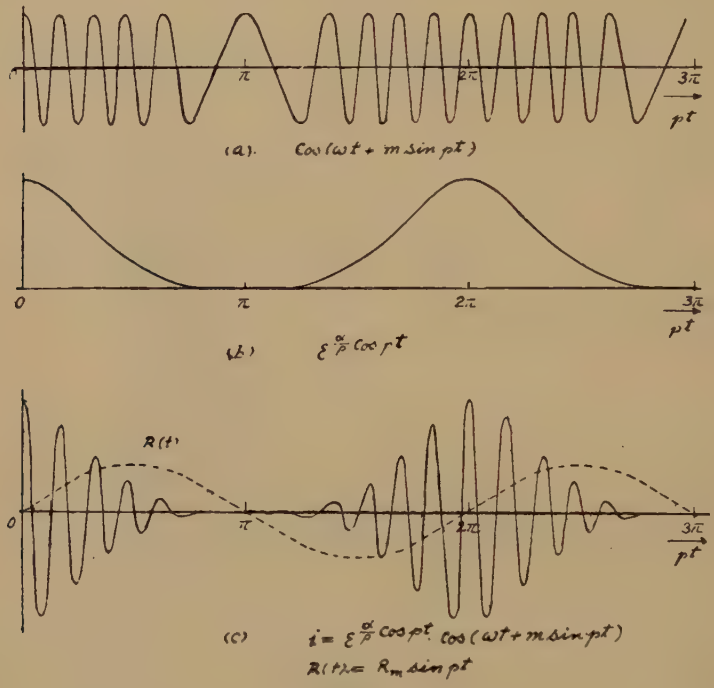

Fig. 4

The component frequencies which are comprised in the oscillatory current can be found from the expansion of (11), that is,

$$i = \epsilon^{(\alpha/p)\cos pt} \cdot \cos(\omega t + m \sin pt)$$

$$= \left(1 + \frac{\alpha}{p} \cos pt\right) \cdot \cos(\omega t + m \sin pt). \qquad (12)$$

The amplitude and the frequency of the component oscillation are shown in Table II.

Accordingly if we analyze the oscillatory current by means of a sensitive wavemeter, then we shall have a resonance curve as indicated

TABLE II

Amplitude	Angular Frequency		Amplitude
$J_0(m)$	ω		
$J_1(m)\left(1-\frac{\alpha}{p}\right)$	$\omega-p$	$\omega+p$	$J_1(m)\left(1+\frac{\alpha}{p}\right)$
$J_2(m)\left(1-2\frac{\alpha}{p}\right)$	$\omega-2p$	$\omega+2p$	$J_2(m)\left(1+2\frac{\alpha}{p}\right)$
$J_3(m)\left(1-3\frac{\alpha}{p}\right)$	$\omega-3p$	$\omega+3p$	$J_3(m)\left(1+3\frac{\alpha}{p}\right)$
. . .	. . .	. . .	. . .

Fig. 5—Multiple resonance curve.

in Fig. 5. It is composed of a number of component resonance curves. The phenomenon is usually called "multiple resonance," and it is thoroughly studied by G. Gorelik and G. Hintz.[2]

Before going into the experiments on the quenching action, it will be helpful, in discussing the experimental results, to consider the theoretical form of a Lissajous figure which is described by the periodic resistance and the oscillatory current. It can easily be found from the curves shown in Fig. 4(*c*). Suppose that along the *X*-axis (horizontal) the periodic resistance is taken and along the *Y*-axis (vertical) the oscillatory current is taken. Then the Lissajous figure will be of a form shown in Fig. 6. It appears like a lozenge having a narrow band on its center. The lozenge is made from a deformation of an ellipse, since the envelope of the oscillatory current is not a sinusoidal curve, but an exponential one. The central band is caused from the suppression of

the oscillation during a certain interval of the periodic resistance, and it may be taken to be one of the characteristic features of the quenching action.

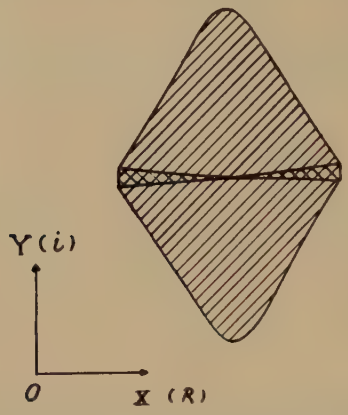

Fig. 6—The theoretical form of the Lissajous figure.

Part II. Experiments on Quenching Action

1. Preliminary Experiments

For the experiments in the following paragraphs, we have employed chiefly the arrangements which are shown in Fig. 7, except when otherwise stated. In the plate circuit of the ultra-short-wave oscillator of

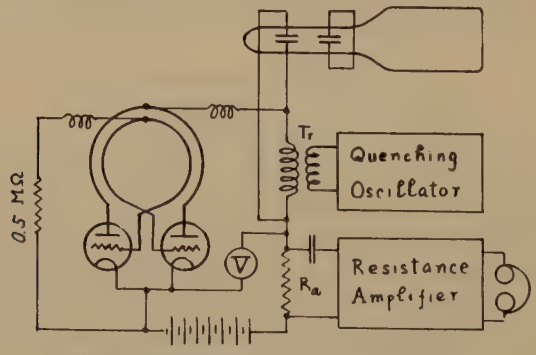

Fig. 7—Experimental arrangements.

Mesny's push-pull type (wavelength $\fallingdotseq$ 4 meters), a high-frequency transformer T_r and a resistance R_a are inserted in series. A quenching voltage is impressed upon the plate circuit through T_r. A resistance amplifier is connected to the terminals of R_a and a characteristic noise accompanying the quenching action is observed. The quenching os-

cillator and the resistance amplifier are both carefully shielded. The quenching oscillator has a wide range of frequency (30–1600 kilocycles) and of output voltage (0–250 volts), both of which can be adjusted smoothly. The crest value of the quenching voltage, which is impressed on the oscillator, is accurately measured by means of a Braun tube. But in some cases a thermovoltmeter was also employed, for the sake of convenience, assuming the voltage under measurement to be sinusoidal.

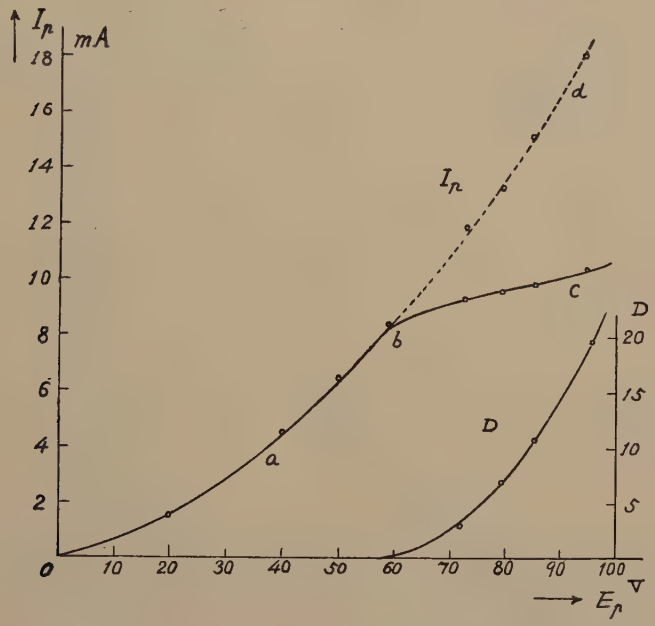

Fig. 8—Static characteristic of the ultra-short-wave oscillator.

With this arrangement some preliminary experiments were carried out.

(*a*). Static Characteristic of the Ultra-Short-Wave Oscillator

When the quenching voltage is removed and $R_a=0$, the relation between the direct plate voltage E_p and the plate current I_p is observed. The result is shown in Fig. 8. On increasing the plate voltage gradually, the plate current increases along a curve *oab;* at the point *b* ($E_p=58$ volts) the oscillation starts smoothly. With the further increase of the plate voltage, the increase of the plate current becomes somewhat slow along a curve *bc*. But when the oscillation is suppressed, the relation is given by a curve *bd* which is an extension of the original

curve *oab*. Curve *D* shows the deflection of the galvanometer in the dipole receiving set and it is nearly proportional to the square of the oscillatory current.

(*b*). Calibration of a Braun Tube as a Crest Voltmeter

The crest value of the high-frequency voltage can very conveniently be measured by means of the Braun tube. The cathode ray is excited under a constant plate voltage (300 volts) and the voltage under measurement is impressed upon a set of the deflecting plates, while the other set of the deflecting plates is short-circuited. This yields on the

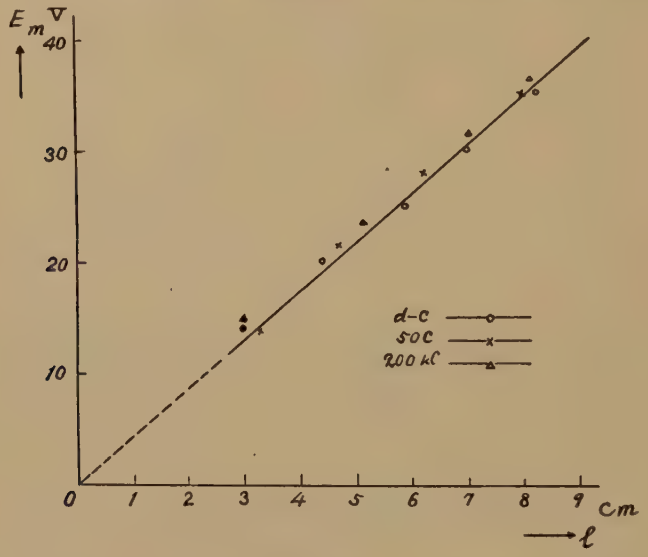

Fig. 9—Calibration curve of a Braun tube as a crest voltmeter.

screen a straight line, of which the length is directly proportional to the crest value of the impressed voltage. The calibration was carried out at frequencies of 50 cycles and 200 kilocycles, and also at the direct voltage. The results are shown in Fig. 9, in which the deflection at the direct voltage is doubled.

2. Stability of the Oscillation

When a quenching action is impressed upon an ultra-short-wave oscillator, in general there are produced three different states of oscillation, according to its frequency and its voltage.

If the quenching voltage is less than a certain critical value, the ultra-short-wave oscillation would merely be modulated by the quenching oscillation. This will be called a state of "modulation." The state

is of great importance in the transmitter but almost of no interest in the superregenerative receiver. In the receiver which is usually operated in a weak oscillatory state, the state of modulation occurs only for a *very* low quenching voltage.

When the quenching voltage passes over the critical value, some striking changes are produced in the oscillator. For the lower quenching frequencies, the oscillation is interrupted intermittently, being accompanied with a characteristic noise. This will be called a state of

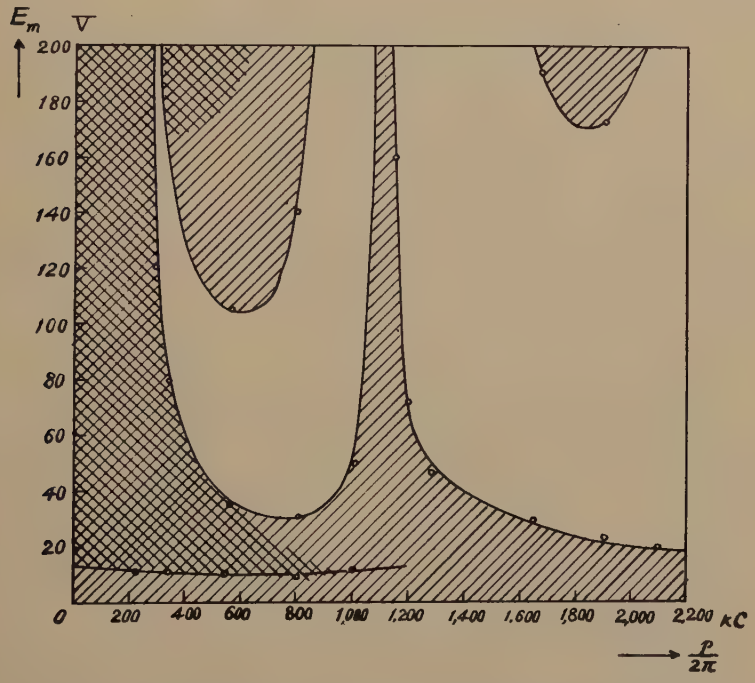

Fig. 10—State of mush (doubly shaded), state of quenching (shaded), and state without self-excitation (unshaded).

"quenching." Since the superregenerative receiver is operated in this state, our interest lies chiefly on it. For the higher quenching frequencies, however, the oscillation becomes generally very unstable and is usually suppressed perfectly. This will be called a state "without self-excitation."

Experimentally the state without self-excitation can conveniently be differentiated from the other states by the following method. An open coil of a single turn is coupled closely with the oscillator. If any variations are observed in the plate current, on closing the coil, then

the oscillator is in the state of quenching or in the state of modulation, while on the other hand if no variations are observed, then the oscillator is in the state without self-excitation. The method is very sensitive and a feeble oscillation in the receiver can easily be detected.

By this method, we have mapped the plane of the quenching voltage and the quenching frequency into states of stable oscillation and states of unstable oscillation. The results are shown in Fig. 10. In this diagram the shaded areas correspond to the stable oscillation, that is, the states of quenching or modulation, and the unshaded areas correspond to the unstable oscillation, that is, the state without self-excitation. The doubly shaded areas correspond to the state in which the characteristic noise is produced. This will be called a state of "mush." The state of mush is usually considered to coincide with the state of quenching,[3] but it is clear that the former is but a part of the latter.

In general, from this diagram, we can see that the higher the quenching frequency and the greater the quenching voltage, the more unstable the oscillation becomes, as indicated by theory in Part I, Section 3.

3. Transient Phenomena

In the theory which has been developed in the Part I, Section 4, the increase or the decrease of the oscillatory current occurs symmetrically according to the same exponential law. Also the oscillation exists continuously, however small its amplitude may become. Actually the oscillation has its end, when its amplitude becomes less than a certain value, and has its start when the conditions of the circuit become favorable for its generation. Thus there would exist no oscillation in the circuit during a certain interval of the quenching action.

Hence the two following problems arise:

(1). To determine at what point of the quenching voltage cycle, the oscillation starts or stops.

(2). To determine in what way the amplitude of the oscillation increases or decreases.

The Braun tube oscillograph has proved to be very helpful for attacking these problems. Fig. 11 shows the experimental arrangements which are those of Fig. 7 with some modifications. On one set (horizontal) of deflecting plates, the quenching voltage is impressed through a suitable coupling coil L_1 from the quenching oscillator, and on the other set (vertical) of deflecting plates, the voltage of the ultra-short-wave oscillation is impressed through a coupling coil L_2. By means of these two voltages, a Lissajous figure is formed on the fluo-

[3] W. L. Barrow, Proc. I.R.E., vol. 21, p. 1182; August, (1933).

rescent screen of the Braun tube. Sketches of the figures obtained under various conditions are given in Figs. 12 to 15. Owing to the linear

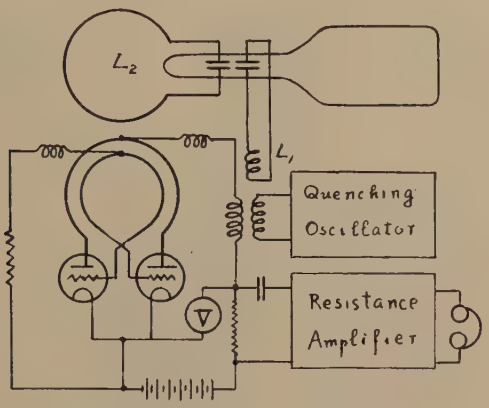

Fig. 11—Experimental arrangements.

relation between the voltage and the deflection, the length of the figure in the vertical direction or in the horizontal direction is nearly proportional to the amplitude of the voltage of the ultra-short-wave

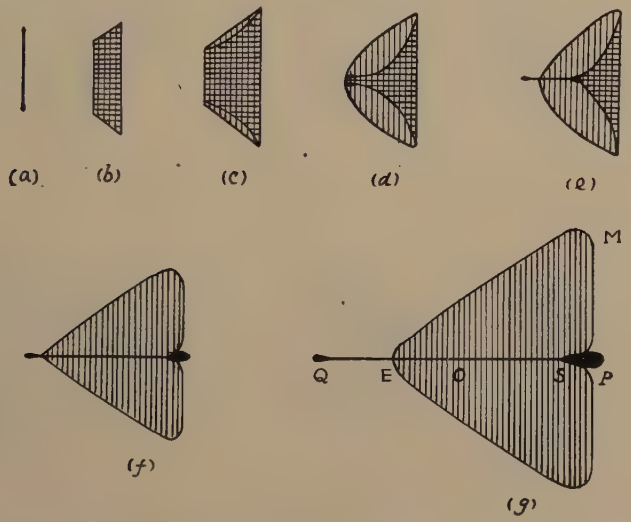

Fig. 12—Lissajous figures at $E_p = 102V$, $p/2\pi = 90$ kilocycles.

oscillation or that of the quenching voltage, respectively. The figures (a), (b), (c), . . . are obtained by the gradual increase in the quenching voltage. In general the deflection due to the ultra-short-wave oscilla-

tion is very dim, so that it is necessary to observe the figure with sufficient care.

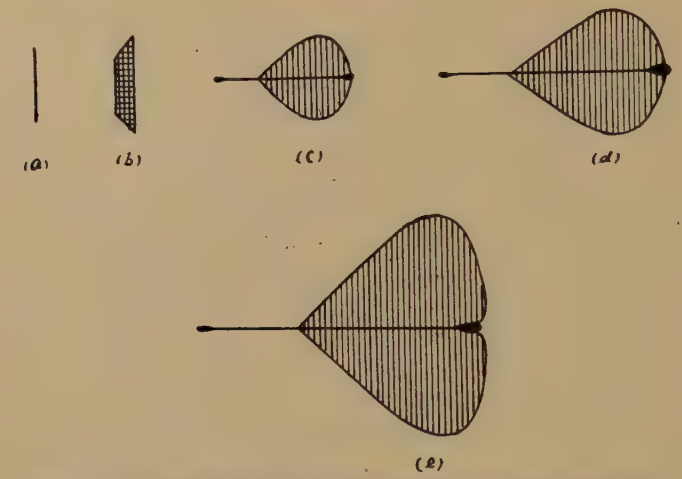

Fig. 13—Lissajous figures at $E_p = 88V$, $p/2\pi = 90$ kilocycles.

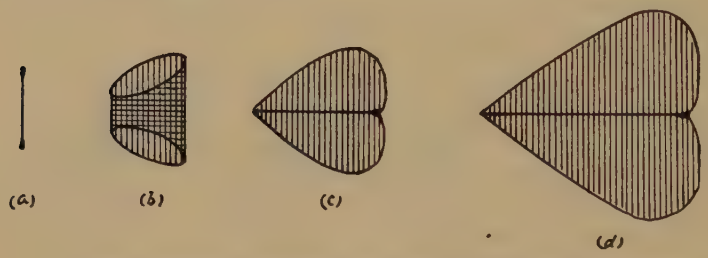

Fig. 14—Lissajous figures at $E_p = 103V$, $p/2\pi = 550$ kilocycles.

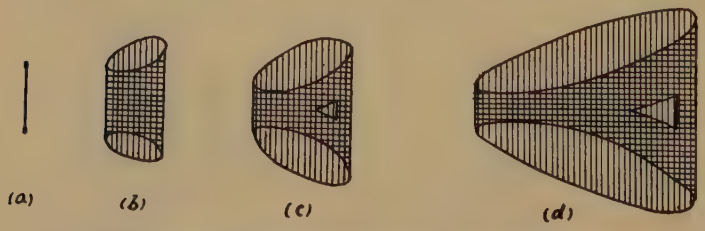

Fig. 15—Lissajous figures at $E_p = 109V$, $p/2\pi = 910$ kilocycles.

The conditions under which the various Lissajous figures were taken are as follows:

(1) $E_p = 102V$, $p/2\pi = 90$kc (Fig. 12.)

(2) $E_p = 88V$, $p/2\pi = 90$kc (Fig. 13.)

(3) $E_p = 103V$, $p/2\pi = 550\text{kc}$ (Fig. 14.)

(4) $E_p = 109V$, $p/2\pi = 910\text{kc}$ (Fig. 15.)

where E_p denotes the direct plate voltage of the ultra-short-wave oscillator, and $p/2\pi$ the quenching frequency.

4. Discussion of the Lissajous Figures

In Part I, Section 4, we found the theoretical form of the Lissajous figure which has for components the effective resistance and the oscillatory current. Comparing the experimental results with this theoretical form, we shall discuss the actual phenomena at the start or at the end of the oscillation in the superregenerative receiver.

In the experiments the Lissajous figures have as components the quenching voltage and the oscillatory voltage. To the first approximation we may take the variation of the effective resistance to be in the opposite phase to the variation of the quenching voltage, and the form of a Lissajous figure may be assumed not to be altered appreciably by this cause.

In Fig. 12(a) the quenching voltage is zero and the figure has but one component, namely the ultra-short-wave oscillation. In (b) the quenching voltage is relatively small, so that the oscillator is found to be in the state of modulation. From the lengths of two parallel sides of the trapezoidal figure, the modulation factor can, as is well known, be determined. In (c) the oscillator is found to be still in the state of modulation. The hypotenuses are found to be twofold. (d) shows a transition from the state of modulation to the state of quenching. One of the twofold hypotenuses grows to an exponential curve. The figures (f) and (g) are of a type which is most commonly observed in the state of mush.

We shall proceed to consider the composition of the Lissajous figure more in detail, referring to this typical form (g). Let the horizontal axis of the Lissajous figure be PQ and the center of PQ be O. During the interval OP the quenching voltage acts in the same direction as the direct plate voltage of the oscillator, and during the interval QO the quenching voltage acts in the opposite direction to the direct plate voltage. The oscillation starts at a point S on OP, and its amplitude increases rapidly to the point M (where it becomes maximum), almost according to an exponential law. Then the amplitude of the oscillation begins to decrease gradually with the decrease of the quenching voltage, until at the point E the oscillation has its end. During the interval from E to Q, and the reverse one from Q to S, passing through E and O, there exists no ultra-short-wave oscillation in the receiver. It

starts again only when the quenching voltage increases to the point S. The same process is repeated for each cycle of the quenching action. If the Lissajous figure (g) is transformed into a rectangular diagram as shown in Fig. 16 the above relations will be made more clear.

It should also be mentioned that the heavy spot in the neighborhood of the point S has a close relation to the production of the characteristic noise. This spot disappears, as will be shown later, at the same time with the suppression of the characteristic noise, when the signal wave of resonant frequency is impressed on the receiver.

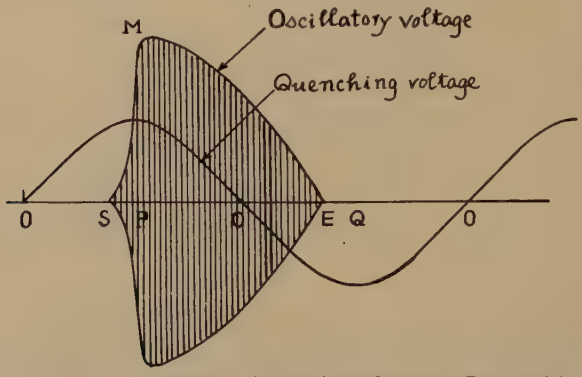

Fig. 16—Transformation of Lissajous figure in Fig. 12(g) into a rectangular diagram.

The Lissajous figures shown in Fig. 13 are obtained with a relatively low value of the direct plate voltage. The increase of the amplitude at the start of the oscillation becomes somewhat slow.

The Lissajous figures shown in Fig. 14 are obtained with a relatively high quenching frequency. Although the oscillator is found to be in the state of quenching, the characteristic noise is very small.

The Lissajous figures shown in Fig. 15 are of a somewhat peculiar shape. As each of these figures has no horizontal line which is a characteristic feature in the state of quenching the oscillator is found to be in the state of modulation.

From a survey of these figures we may make the following deductions:

(1). In the neighborhood of the maximum value of the quenching voltage, the ultra-short-wave oscillation generally has its start, and its amplitude increases rapidly almost according to an exponential law.

(2). The decrease of the amplitude of the oscillation occurs very slowly, almost according to a sinusoidal law, and the oscillation ceases

at a value of the quenching voltage, which is far less than that of its start.

(3). At the start of the oscillation, some irregularities are found.

5. Generation of the Characteristic Noise

An important phenomenon which accompanies the quenching action but which has not been taken into any consideration in the theory is the generation of the characteristic noise. Usually the superregenerative receiver has its best operating condition in the state of mush.

From the preceding investigations, it is obvious that the generation of the characteristic noise occurs at the start of the oscillation when the ultra-short-wave oscillator is in the state of quenching. It should also be noted that although the effective resistance of the circuit is reduced to be sufficiently negative to start the oscillation by means of the quenching action, the oscillation will not occur until some electromotive force, no matter how small it may be, is impressed upon the circuit.

Even in the absence of any signal whatever, a number of electromotive forces may be supposed to act upon the oscillatory circuit from various internal causes such as the shot effect, the flicker effect, thermal agitation, etc. When the effective resistance of the circuit is reduced to be sufficiently negative, the oscillation will be initiated by an impulse from that electromotive force which is the greatest among them. As will be shown later, the greater the impulse of the electromotive force, the earlier the oscillation starts. Owing to irregularities in the inducing electromotive force the initial condition at the start of the oscillation must be considered to be very irregular, as indicated by the heavy spot in the neighborhood of the starting point S in the Lissajous figures which are shown in Fig. 12. The characteristic noise is thus considered to be caused by the irregular electromotive forces which initiate the oscillation.

Part III. Effects of Signal Wave

1. Uda Phenomenon

In order to study the effects of signal wave on the superregenerative receiver generally, we have employed the experimental arrangements as indicated in Fig. 17. A transmitter of a small output is placed at a corner of a passage at a distance of 30 meters from the receiver. The filament circuit of the transmitter can be operated by means of a key K at the receiving position. A superregenerative receiver is of a ultra-audion type with the separate quenching. The range of the wavelength

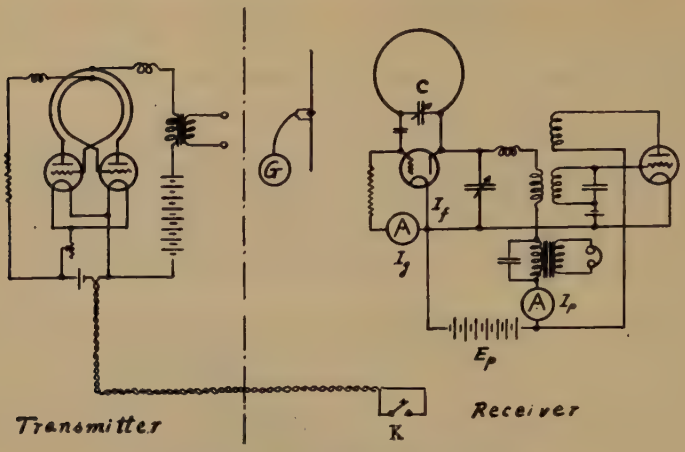

Fig. 17—Experimental arrangements.

to be received is 4.72 to 5.30 meters (Fig. 18). The wavelength of the transmitter is 5.03 meters and it is seen that the tuning occurs at $C=63$.

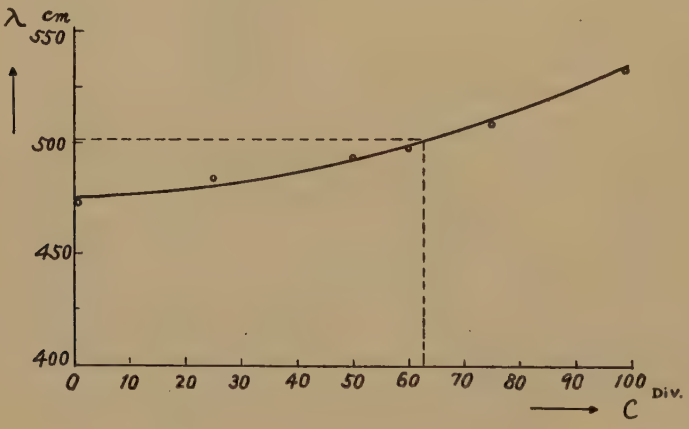

Fig. 18—Range of wave length of the receiver.

On closing the key and adjusting the variable condenser C to tune with the unmodulated signal wave, the following changes are observed in the superregenerative receiver:

(1) Suppression of the characteristic noise (Fig. 19).

(2) Increase of the grid current and decrease of the plate current (Fig. 20).

(3) Increase of the oscillatory current (Fig. 21).

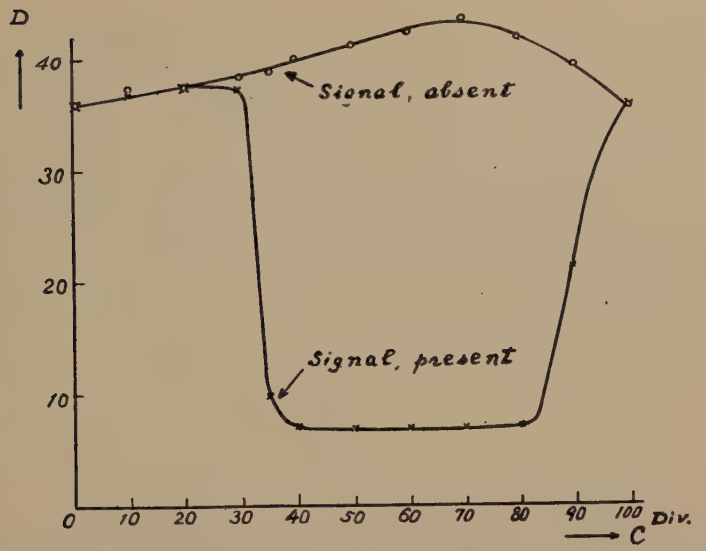

Fig. 19—Suppression of the characteristic noise by the signal wave.

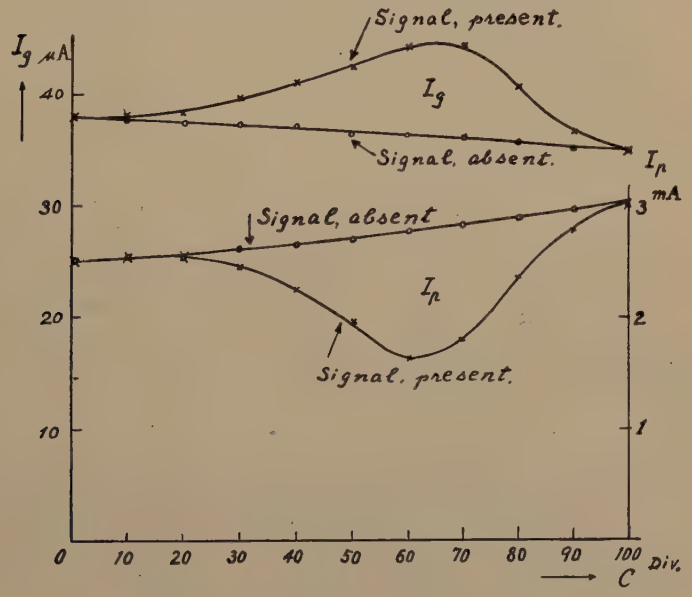

Fig. 20—Increase of the grid current and decrease of the plate current by the signal wave.

In order to measure the characteristic noise, a crystal detector and a galvanometer were inserted in parallel with the headphones. The deflections of the galvanometer are shown in Fig. 19. The oscillatory

current in the receiver is measured by a dipole receiving set. The deflection due to the incoming wave is, of course, negligible.

The above changes are not mutually independent, but certain close relations exist between them. Suppose that an electromotive force of resonant frequency is impressed on the grid circuit by the signal wave. Then the oscillation in the receiver is accordingly enforced, resulting in an increase of the grid current and also an increase of the grid bias voltage. The increase of the bias causes, in turn, the decrease of the plate current.

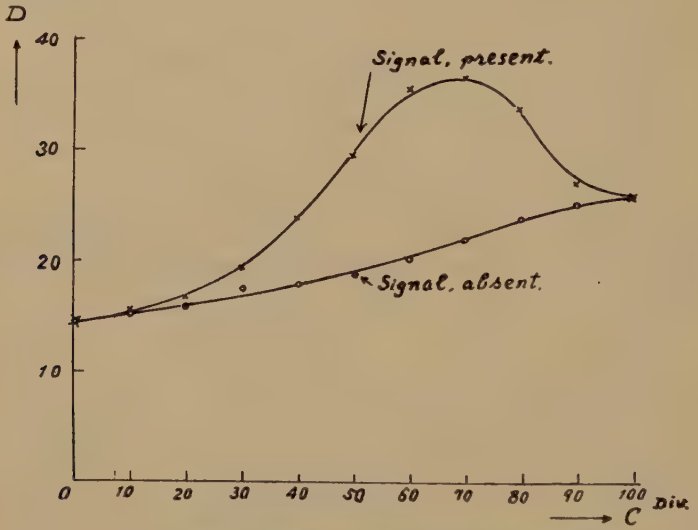

Fig. 21—Increase of oscillatory current by the signal wave.

Among the changes due to signal wave, the suppression of the characteristic noise is the most remarkable. S. Uda early noticed the phenomenon and applied it to a relay system which acts on the signal wave with a high sensitivity. The phenomenon will, therefore, be called after his name.

This is of great importance in the superregenerative receiver. Because if the characteristic noise were not in the least suppressed, the reception of the signal would be greatly disturbed by it. The following paragraphs are chiefly devoted to the study of this phenomenon.

2. Synchronization of Ultra-Short-Wave Oscillators

In the absence of any signal whatever, the superregenerative receiver is in some complicated oscillatory state as theoretically investigated in Part I, Section 4. In general, a triode oscillator shows a peculiar behavior in the presence of the incoming wave, of which the frequency

is in a simple relation to that of its natural oscillation. The phenomenon is usually called a "synchronization" or a "pull-in" effect. On the synchronization of triode oscillators, there have appeared several interesting papers. But almost all of them deal with the case of relatively low frequency. Hence, we shall consider first the synchronization of the ultra-short-wave oscillators without the quenching action.

Consider two ultra-short-wave oscillators which will be called oscillator I and oscillator II, and a third resonant circuit III which is coupled with each of them (Fig. 22). By means of the condenser C, the frequency of oscillator II is varied gradually to tune with that of

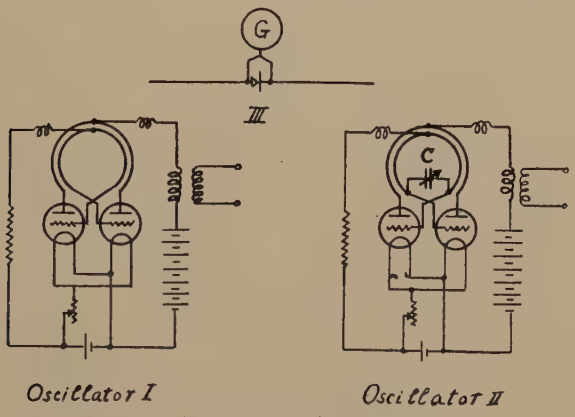

Fig. 22—Experimental arrangements.

oscillator I ($\lambda \doteqdot 4$ meters). The deflection of the galvanometer in III and the plate current of I are measured simultaneously. The results are shown in Fig. 23.

The induced electromotive force in the resonant circuit may be written

$$e = E_1 \sin(\omega_1 t + \phi_1) + E_2 \sin(\omega_2 t + \phi_2), \qquad (13)$$

where the first term represents the electromotive force due to I and the second term that due to II. When the frequency of oscillator II is varied gradually to tune with that of oscillator I, two oscillators will step into synchronization at a point L and will step out at a point M. In the interval LM the frequencies of two oscillators may be taken exactly equal, but the phase difference between the oscillatory voltages will vary with the variation of the capacity C.

The deflection of the galvanometer is approximately proportional to

$$\frac{1}{T}\int_0^T e^2 dt.$$

In the synchronous state, however, $\omega_1 = \omega_2$, so that we have

$$D = \frac{k}{2}[E_1^2 + E_2^2 + 2E_1E_2 \cos(\phi_1 - \phi_2)], \qquad (14)$$

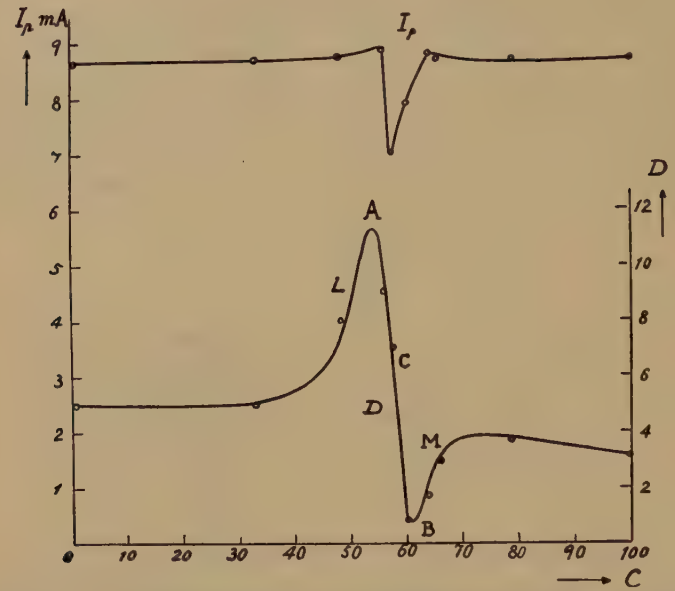

Fig. 23—The plate current I_p and the deflection of galvanometer D at the synchronization.

where k is a constant of proportionality. Thus, referring to Fig. 23, we have

(1). $D = \frac{k}{2}(E_1 + E_2)^2$, for $\phi_1 - \phi_2 = 0$ which occurs at A

(2). $D = \frac{k}{2}(E_1^2 + E_2)^2$, for $\phi_1 - \phi_2 = \frac{\pi}{2}$ which occurs at C

(3). $D = \frac{k}{2}(E_1 - E_2)^2$, for $\phi_1 - \phi_2 = \pi$ which occurs at B.

If the oscillatory voltages are impressed upon two sets of deflecting plates of the Braun tube, then we shall have the Lissajous figures which are shown in Fig. 24. The figures (A), (B), and (C) are obtained in the states which are indicated by the points AB and C in Fig. 23, respectively.

In the above representation of the action the amplitudes of the oscillatory voltages are supposed to remain constant irrespective of

the variation of the capacity C, but strictly this will not be the case. Hence the results are only qualitative.

The decrease of plate current is important in the reception of the signal when the oscillator is used as a receiver. In general, the great variation of the plate current occurs when the oscillator is in the weak oscillatory state.

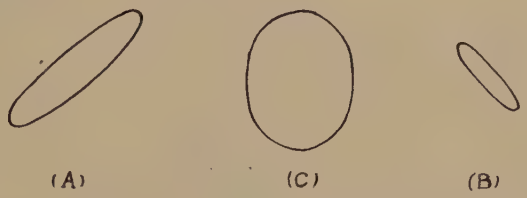

Fig. 24—Lissajous figures at the synchronization.

3. Synchronization in the Superregenerative Receiver

With the experimental arrangements as indicated in Fig. 22, oscillators I and II may be taken as the receiver and the transmitter, respectively.

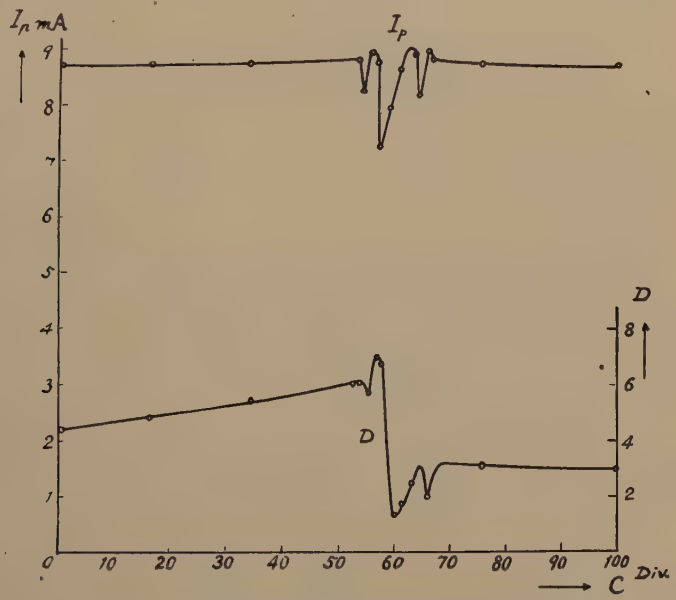

Fig. 25—Synchronization for a modulated wave.

If the incoming wave on the receiver is modulated with a frequency of 850 kilocycles, then the synchronization is observed at three different points, which correspond to the carrier and the side bands, as indicated in Fig. 25.

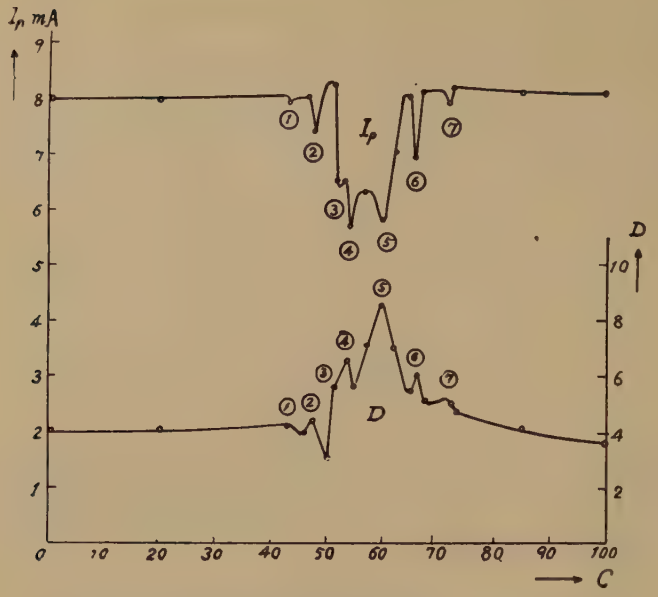

Fig. 26—Synchronization when the receiver is in a state of modulation.

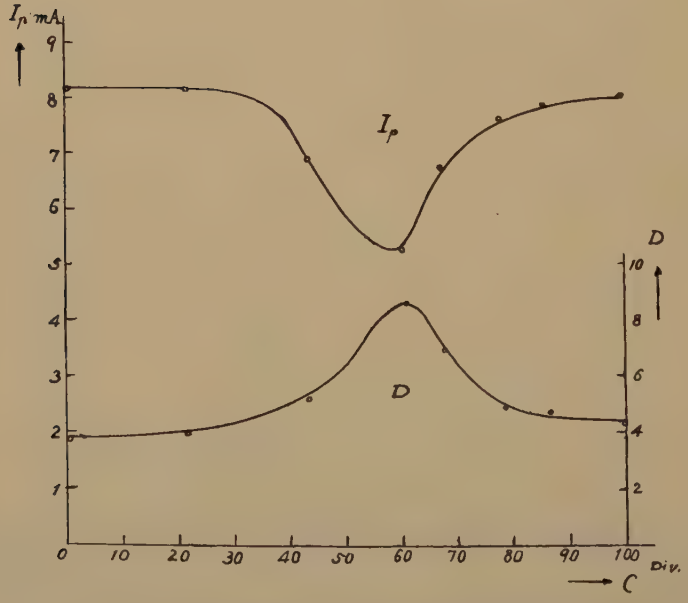

Fig. 27—Synchronization in the superregenerative receiver.

On the other hand, if the receiver is in a state of modulation with a frequency of 850 kilocycles, while the incoming wave is unmodulated, then the phenomenon appears in a more complicated aspect, as shown in Fig. 26. The synchronization occurs at seven points which are numbered from the left. The numbers on the curves I_p and D are corresponding synchronization points.

If the receiver is in a state of quenching ($p/2\pi = 52.6$ kilocycles), then it would be expected to observe very jaggy curves at the synchronization, owing to the presence of a number of component frequencies. But actually we have nothing but very flat curves as shown in Fig. 27. Thus for a low quenching frequency each synchronization cannot be observed separately, since they occur so closely together that they merge into one.

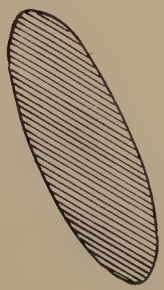

Fig. 28—Lissajous figure in the synchronization of the superregenerative receiver.

If the oscillatory voltages of the transmitter and of the superregenerative receiver are impressed upon the two sets of deflecting plates of a Braun tube, then we have the Lissajous figure which is shown in Fig. 28. From this it is obvious that in the state of synchronization the frequency of the superregenerative receiver is equal to that of the incoming wave, although its amplitude varies periodically.

It should also be noted that in the state of synchronization of the superregenerative receiver there occurs a suppression of the characteristic noise, with the mechanism of which we shall deal in the next paragraph.

4. Suppression of the Characteristic Noise

In Part II, Section 3, we obtained the Lissajous figure which were composed of the oscillatory voltage and the quenching voltage, in the absence of the signal wave. Now we shall study the effects of the signal wave on this figure. In the experimental arrangements as shown in Fig. 11, the superregenerative receiver is kept in the state of mush and

the typical Lissajous figure is reproduced on the screen of the Braun tube. When an unmodulated signal wave of resonant frequency is impressed upon the receiver, some changes are produced on the figure. The figures which are shown in Fig. 29 are obtained under conditions $E_p = 102V$, and $p/2\pi = 90$ kilocycles, and the intensity of the signal wave increases in the direction (*a*), (*b*), (*c*), $\cdots$ gradually.

The figure in (*a*) shows the state without the signal wave, and corresponds to that in Fig. 12 (*g*). The figure in (*b*) shows the state with a very weak signal wave and the characteristic noise is suppressed partially. For relatively strong signals we have figures in (*c*), (*d*), and (*e*), and the characteristic noise is suppressed perfectly.

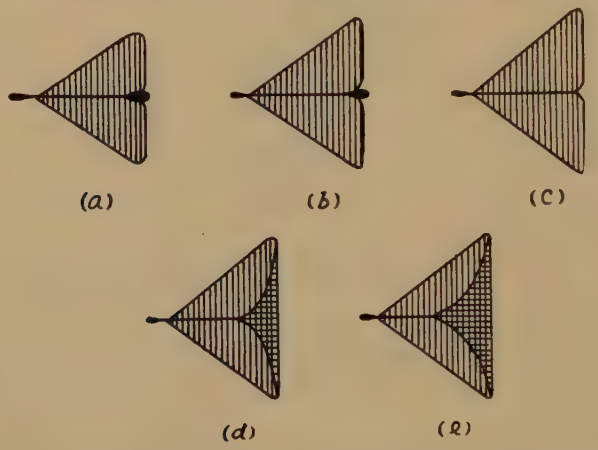

Fig. 29—Effects of the signal wave on the Lissajous figures.

From a survey of these figures, we may make the following deductions:

(1). The heavy spot at the start of the oscillation, disappears with a relatively strong signal and at the same time the characteristic noise is suppressed.

(2). The greater the intensity of the signal, the earlier the oscillation starts.

(3). The maximum amplitude of the oscillatory current remains almost constant, irrespective of the intensity of the signal wave.

If the induced electromotive force due to the signal wave becomes greater than those due to the shot effect, thermal agitation, flicker effect, etc., the oscillation can no longer be initiated with the impulse of the latter, but with that of the former. The initial condition at the start of the oscillation would nevertheless be very irregular. This con-

dition becomes, however, very regular in the state of synchronization, since there is a simple relation between the oscillation in the receiver and that of the signal wave. Thus the heavy spot at the start of the oscillation disappears and at the same time, the characteristic noise is suppressed.

Incidentally the above deductions, as will be shown later, give us a clue as to the mechanism of amplification by superregeneration.

5. General Form of Synchronization

In general, a synchronization of two triode oscillators takes place in the case when between their wavelengths λ_0 and λ there holds a relation

$$\lambda = \frac{m}{n}\lambda_0, \tag{15}$$

where m and n are both positive integers.

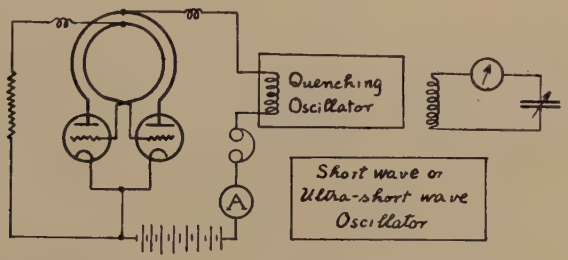

Fig. 30—Experimental arrangements.

Now we shall consider the case where one oscillator is a superregenerative receiver. On account of the enhanced sensitivity of superregeneration, we can observe a synchronization of an extremely high order. The experimental arrangements are shown in Fig. 30. An electromotive force of a variable frequency is generated by a short-wave or a ultra-short-wave oscillator and it is impressed upon a superregenerative receiver of which the wavelength of the principal oscillation is 4.12 meters. Then the synchronization is found to occur in the receiver whenever the relation

$$\lambda = 4.12m \text{ meters} \quad (n = 1),$$

is satisfied, where λ is the wave length of the impressed electromotive force.

The detection of the synchronization can easily be performed by either a sudden suppression of the characteristic noise or a sudden decrease of the plate current. The latter is usually very sharp as compared with the former, and can easily be measured.

A relation between the wavelength of the impressed electromotive force and the plate current is shown in Fig. 31. The minimum of the plate current occurs exactly at intervals of 4.12 meters. In the figure up to the sixty-fourth synchronization is shown. The number shown in the figure denotes the order. The higher the number of the order becomes, the smaller the variation of the plate current.

This phenomenon can very conveniently be applied to the calibration of a wave meter. In the same experimental arrangements as

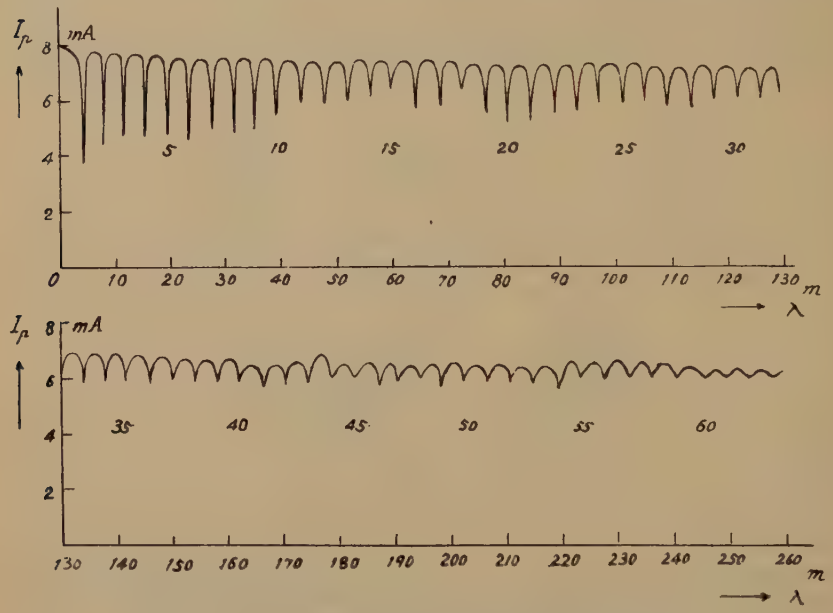

Fig. 31—The variation of the plate current with the wavelength of the signal wave.

in Fig. 30, suppose that a wave meter on the right is under calibration. Varying the frequency of the oscillator, we take in order the points at which the synchronization occurs in the superregenerative receiver. Then we can obtain the results as shown in Fig. 32. Thus if the wavelength of the superregenerative receiver is determined once for all accurately, say, by means of a Lecher wire system, then the later process is very simple.

The above phenomenon can also be applied to the superregenerative wave meter.[4] The range of the wave meter can greatly be increased.

Next we shall consider the case where the wavelength of the signal wave is shorter than that of the oscillation in the receiver. In this case

[4] H. Ataka, Proc. I.R.E., vol. 21, p. 1590; November, (1933).

the synchronization occurs in the similar way as in the preceding case when a relation

$$\lambda = \frac{1}{n}\lambda_0 = \frac{4.12}{n} \text{ meters} \quad (m = 1)$$

is satisfied.

But the experiment has been carried out only in two cases $n=1$ and $n=2$.

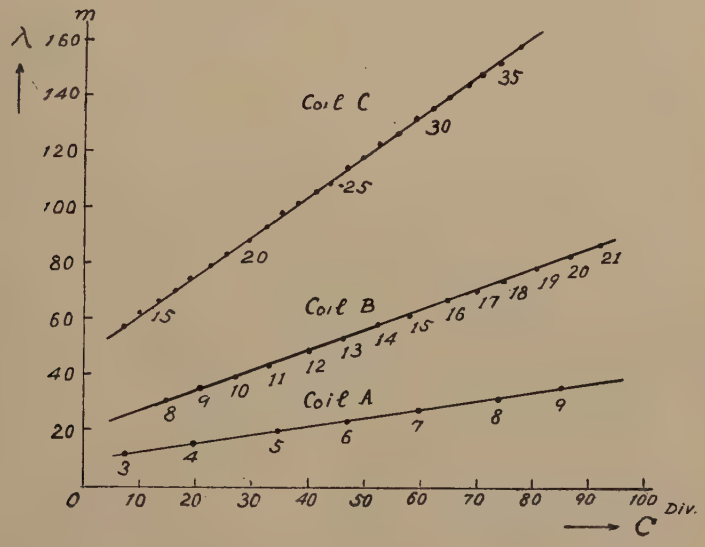

Fig. 32—Calibration curves of a wave meter by means of a superregenerative receiver.

Part IV. Amplification by Superregeneration

1. Effects of Quenching Action on Sensitivity

The effect of the superregenerative receiver lies in its high sensitivity which is caused by the extraordinary amplification of superregeneration. The last part of this paper is chiefly devoted to this important subject. In the first place, we shall study the effects of the various factors which affect the sensitivity, especially that of the quenching action.

The same superregenerative receiver as shown in Fig. 7 is employed for this purpose. As a measure of the sensitivity we have taken the variation in the plate current due to the signal for the sake of convenience.

(*a*). Effects of the Intensity of the Signal Wave

When the receiver is operated in the usual condition, the plate current is observed with the variation of the intensity of signal. The in-

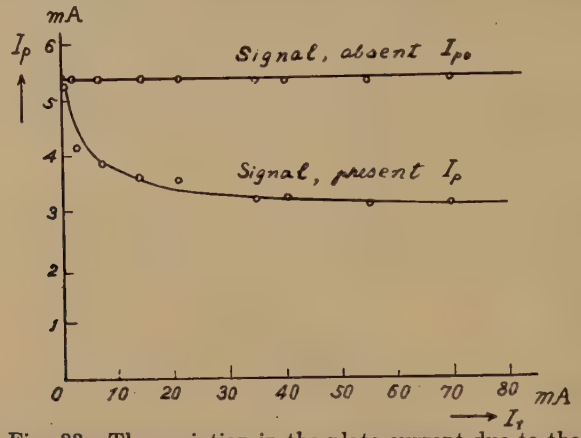

Fig. 33—The variation in the plate current due to the intensity of signal.

tensity of the signal is measured by the antenna current I_t of the transmitter. The result is shown in Fig. 33. In the absence of the signal the plate current is constant ($I_p = 5.4$ milliamperes), as given by the

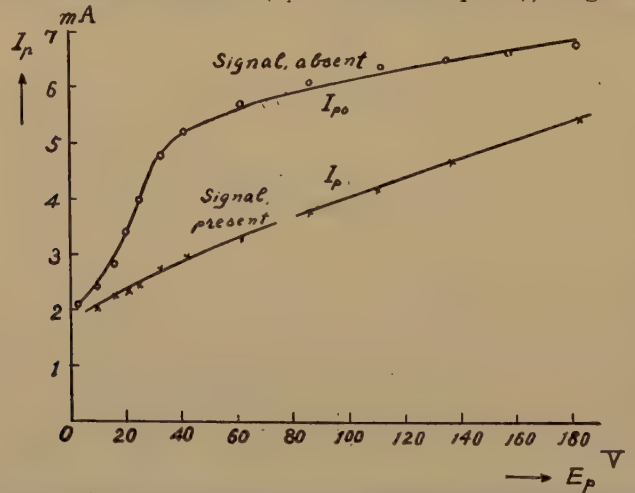

Fig. 34—Effect of the direct plate voltage on the plate current.

upper curve, while in the presence of the signal it decreases to the value given by the lower curve. The variation due to the signal is given by the area between two curves. For the relatively strong signals, the variation in the plate current remains almost constant.

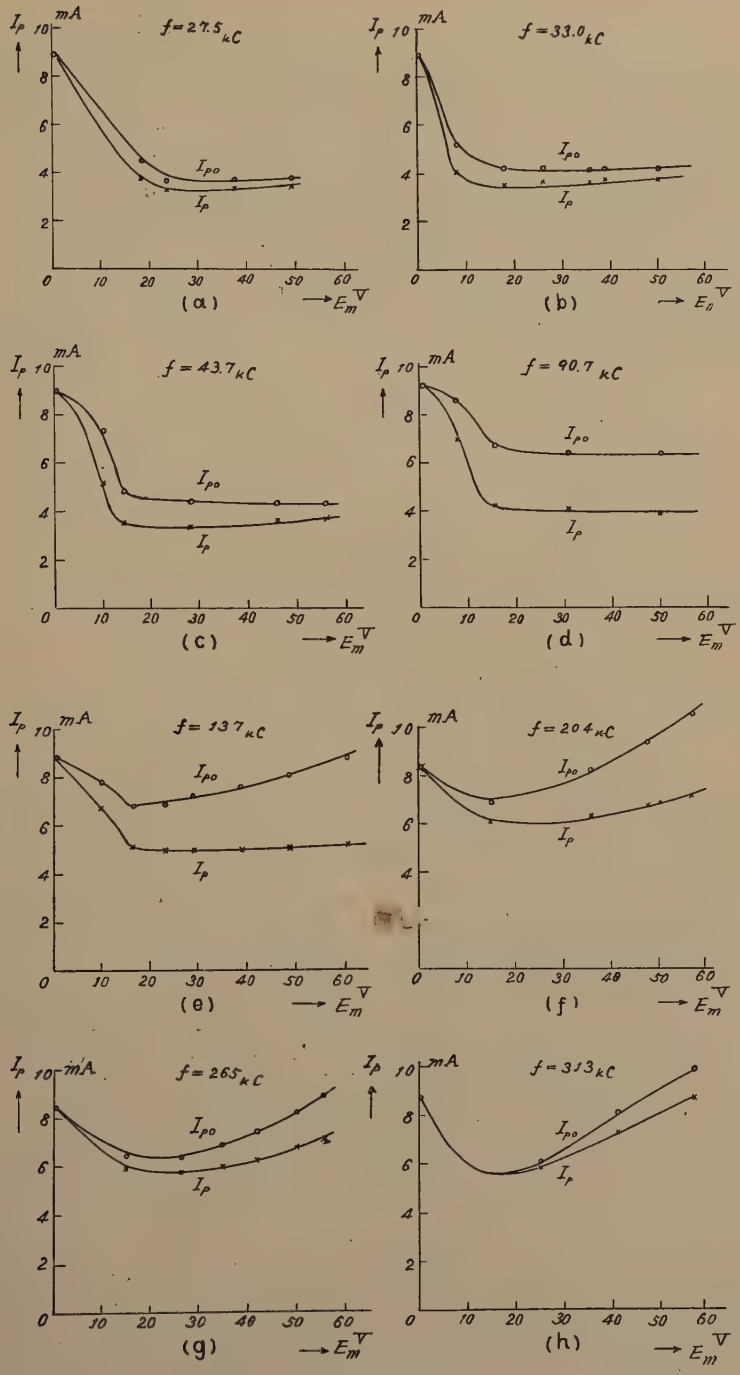

Fig. 35 (a)-(h)—Effects of the quenching voltage on the sensitivity at the various quenching frequencies.

(*b*). Effect of the Direct Plate Voltage

The effect of the direct plate voltage of the receiver on the sensitivity is shown in Fig. 34. Thus the variation of the plate current is greatest when the receiver is operated at the voltage $E_p = 50$ volts. For the higher plate voltages the receiver enters a strong oscillatory state and the sensitivity decreases gradually, while for the lower plate voltages the receiver enters a state without self-excitation and the sensitivity again decreases rapidly. Referring to Fig. 8, the optimum direct plate voltage is such that the receiver is just brought to an oscillatory state.

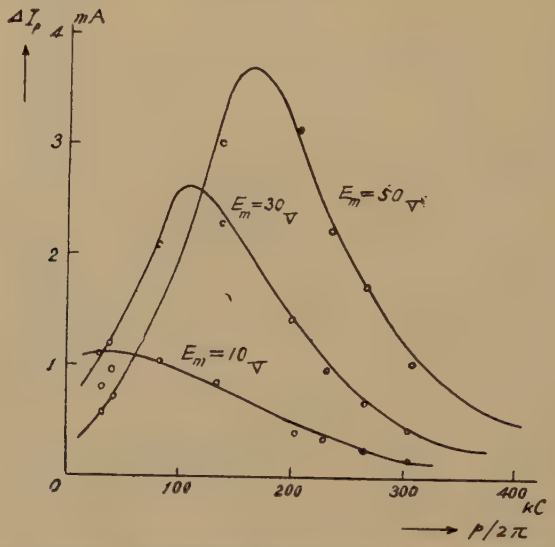

Fig. 36—Variation of the sensitivity due to the quenching action.

(*c*). The Effects of the Quenching Action

In order to see the effects of the quenching action on the sensitivity the plate current is observed with the variation of the quenching voltage at the various quenching frequencies. Throughout the experiments the plate voltage of the receiver and the antenna current of the transmitter are both kept constant. The results are shown in Fig. 35.

In each of these figures, the upper curve shows the plate current in the absence of the signal, and the lower curve shows it in the presence of the signal. Hence the greater the area between these two curves, the higher the sensitivity of the receiver.

From these curves, the variation of the plate current ΔI_p is plotted against the quenching frequency at constant quenching voltage, in Fig. 36.

From this diagram we can make the following deductions:

(1). For too low quenching frequencies, the sensitivity is as low as for too high quenching frequencies. There is an optimum quenching frequency which gives the best sensitivity.

(2). Except for the case of very low quenching frequencies, the sensitivity increases generally as the quenching voltage increases.

(3). The optimum frequency displaces to the lower frequency side when the quenching voltage decreases.

Usually it is considered that the sensitivity of the superregenerative receiver increases very rapidly as the quenching frequency is decreased. From the above results it is obvious that this will occur only for the very low quenching voltages.

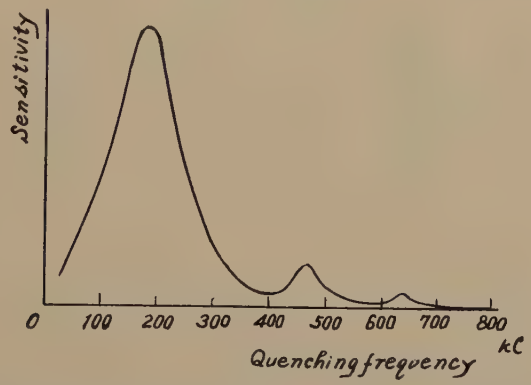

Fig. 37—Variation of the sensitivity due to the quenching frequency at the constant quenching voltage.

The above results have been obtained from the relation between the unmodulated signal and the detected continuous current. Similar results can also be obtained when the signal wave is modulated by an audio frequency and the detected current is received by the headphone. In this case however, a curious phenomenon is observed. If the sensitivity of the superregenerative receiver is measured with the variation of the quenching frequency at constant quenching voltage, then we shall have a curve shown in Fig. 37. Thus beside a single large maximum as already shown in Fig. 36, there occur several small maxima for the higher quenching frequencies.

2. Mechanism of Amplification

A theory of amplification by superregeneration was proposed by E. O. Hulburt[5] in 1923, the next year after Amstrong's discovery. The fundamental assumption of this theory is that the time of build-

[5] E. O. Hulburt, Proc. I.R.E., vol. 11, p. 391; August, (1923).

ing-up of a free oscillation is constant, irrespective of the intensity of the signal.

On the other hand a new theory recently has been developed on this line by H. O. Roosenstein,[6] who assumed that the time of building-up of the free oscillation varies with the intensity of the signal. The greater the intensity of the signal, the longer the time of building-up becomes. This assumption is in general in accord with our experimental results.

In each of these theories, the quenching electromotive force is assumed to operate by varying the amount of the effective resistance of the oscillatory circuit according to a rectangular wave form which

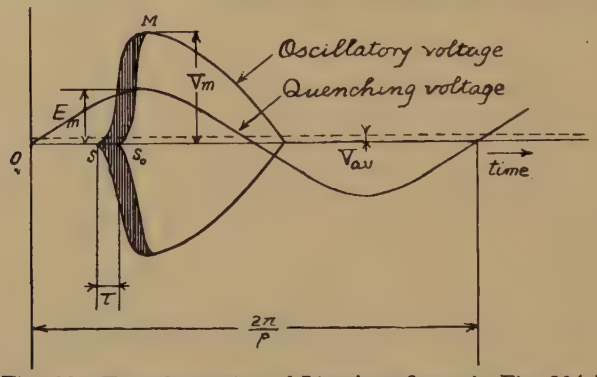

Fig. 38—Transformation of Lissajous figure in Fig. 29(*a*) and (*e*) into the rectangular coördinates.

is far different from the actual condition. Hence before going into a development of the theory, it will be necessary to consider the mechanism of amplification by superregeneration precisely, basing it on the experimental results obtained.

For this purpose, the Lissajous figures in Fig. 29 (*a*) and (*e*) are transformed into rectangular coördinates as shown in Fig. 38. In the absence of any signal whatever, the oscillation starts at the point S_0 and its amplitude increases rapidly to the point M almost according to the exponential law, while in the presence of the signal the oscillation starts at the point S and its amplitude increases in a similar manner to the point M. Thus the incoming signal affects chiefly the start and the building-up of the oscillation, but the decay of the oscillation which occupies a greater part of the oscillatory voltage remains almost independent of the incoming signal.

The amount of the increase in the oscillatory voltage due to the signal is of great importance for the receiver; it is shown by the shaded

[6] H. O. Roosenstein, *Hochfrequenz. und Elektroakustik*, Bd. 42, s.85, (1933).

area. Assuming the characteristic of the detector to be linear for simplicity, the detected current is proportional to the mean value of the upper half of the shaded area, which is shown by a broken line in the same figure.

The amplification by superregeneration depends on three important factors, that is, the number of shaded areas per second $p/2\pi$, the maximum amplitude of the oscillatory voltage, and the time τ by which the oscillation starts early in the presence of the signal. This will be called a time of "advance." The number of shaded areas per second is nothing but the quenching frequency. The maximum amplitude of the oscillatory voltage is chiefly determined by the amplitude of the quenching voltage. The time of advance will be a function of the quenching frequency, the quenching voltage, the characteristic constants of the triode, and also the intensity of the signal. If the quenching frequency is low, that is, the period of the quenching action is long, the time of advance will accordingly become long. On the other hand, if the quenching voltage becomes high, then this time is considered to increase again.

For lower quenching frequencies, the number of shaded areas per second is small, while the time of advance will become great. But the latter is seen not to be so great as to cover the loss due to the former. Hence the sensitivity will become poor.

For higher quenching frequencies which bring the receiver into a state without self-excitation, the time of advance will be null as no oscillation starts in the receiver. The sensitivity of the receiver again becomes poor.

An optimum quenching frequency which gives the best sensitivity lies between these two extreme frequencies. For this frequency the number of shaded areas per second and the time of advance are both relatively great.

In Fig. 39 the influence of various factors on the amplification are shown schematically. (*a*) shows the case where the quenching frequency is very low. The sensitivity is very poor as indicated by a broken line which shows the mean shaded area. (*b*) shows the case where the quenching frequency is relatively high, but the quenching voltage is still low. The sensitivity improves slightly as indicated by a broken line. (*c*) shows the case where both the quenching frequency and the quenching voltage are high and the sensitivity becomes high, as indicated by a broken line.

Let us now formulate the above relations in a mathematical expression. Assuming that the building-up of the free oscillation follows according to the same exponential law either in the absence or in the

presence of the signal, the mean value of the upper half shaded area in Fig. 39 is given by

$$V_{av} = \frac{1}{2\pi} \tau \cdot p \cdot V_m.$$

The increase of the oscillatory current causes, as described in Part III, Section 1, an increase of the grid current and a decrease of the plate current.

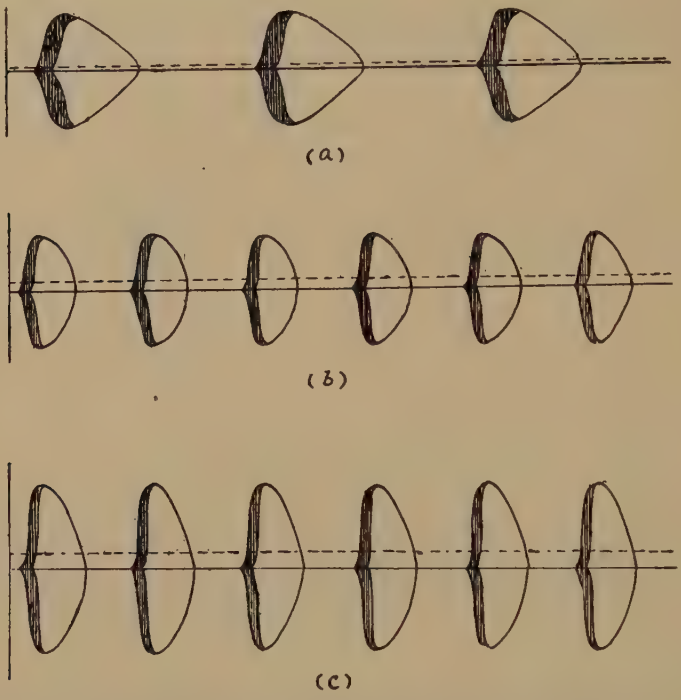

Fig. 39—Various modes of amplification by superregeneration.

Accordingly the variation of the plate current due to the signal is

$$\Delta Ip = Ip_0 - Ip = \frac{G}{2\pi} \cdot \tau \cdot p \cdot V_m, \tag{16}$$

where G is a constant depending on the characteristic of the detector and I_{p0} and I_p are the plate currents in the absence and in the presence of the signal, relatively.

The time of advance τ depends on the intensity of the incoming signal and can be written in the form[7]

$$\tau = \tau_0 \log \frac{v}{v_0}, \tag{17}$$

where τ_0 is a constant depending on the quenching frequency and the quenching voltage, v is the induced electromotive force due to the signal, and v_0 the induced electromotive force due to the shot effect, thermal agitation, etc., which initiate the oscillation in the absence of the signal.

In considering the effects of the quenching action on the amplification, it will be necessary to express τ_0 in terms of p and E_m. For this purpose we shall develop τ_0 in the series of p and E_m by the aid of Taylor's theorem:

$$\tau_0 = (\tau_0)_0 + \left(\frac{\partial \tau_0}{\partial p}\right)_0 \cdot p + \left(\frac{\partial \tau_0}{\partial E_m}\right)_0 E_m + \cdots . \tag{18}$$

From the fact that the time of advance τ decreases as the quenching frequency p increases and increases as the quenching voltage E_m increases, it may be taken that

$$\alpha = (\tau_0)_0 > 0$$

$$\beta = -\left(\frac{\partial \tau_0}{\partial p}\right)_0 > 0$$

$$\gamma = \left(\frac{\partial \tau_0}{\partial E_m}\right)_0 > 0.$$

Hence, we have,

$$\tau_0 = \alpha - \beta p + \gamma E_m. \tag{19}$$

To the first approximation we may take also

$$V_m = K E_m, \tag{20}$$

where K is a constant of proportionality.

Substituting (17), (19), and (20) into (16), we have finally

$$\Delta I_p = I_{p0} - I_p = \frac{GK}{2\pi} (\alpha - \beta p + \gamma E_m) \cdot p \cdot E_m \cdot \log \frac{v}{v_0} \cdot \tag{21}$$

From this expression we can find the effects of the signal intensity v, the quenching frequency p, and the quenching voltage E_m on the variation of the plate current ΔI_p.

[7] H. Barkhausen and G. Hässler, *Hochfrequenz. und Elektroakustik*, Bd. 42, s.41, (1933).

In Fig. 40, the relation between ΔI_p and v with constant p and E_m is shown. ΔI_p varies with v according to the logarithmic function and

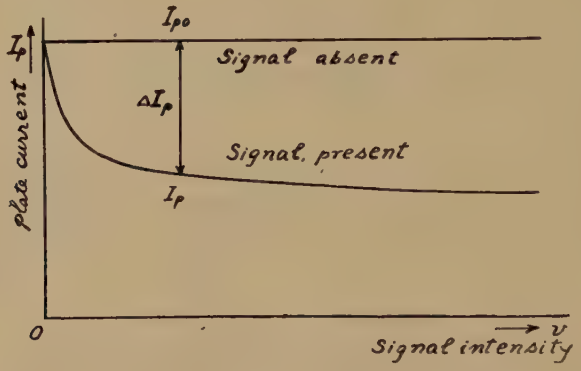

Fig. 40—Variation of the plate current due to the intensity of signal.

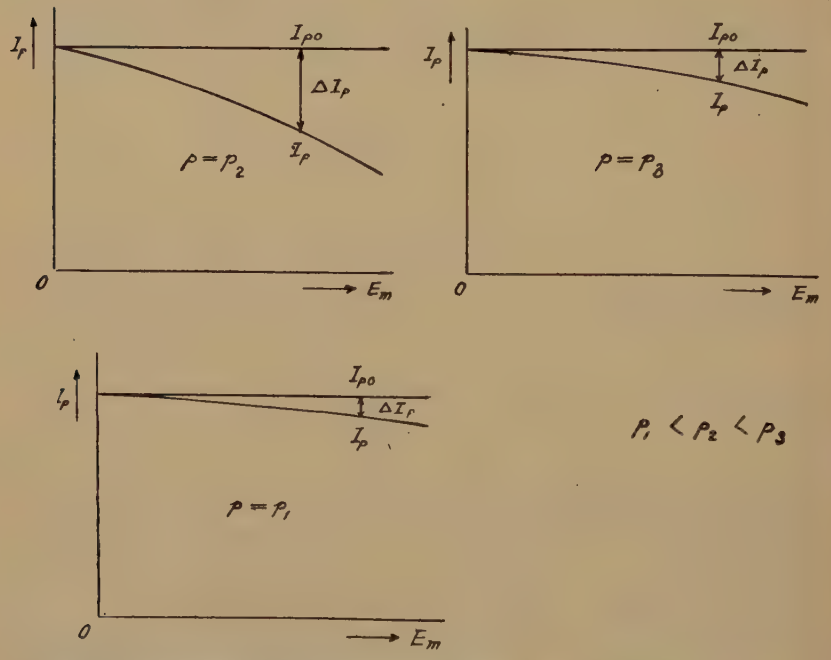

Fig. 41—Variation of the plate current due to the quenching voltage at the various quenching frequencies.

it agrees with the experimental results given in Fig. 33. The relation between I_p and E_m for various values of p shown in Fig. 41, which

may be compared with the experimental results in Fig. 35. The relation between ΔI_p and p at the various values of E_m is shown in Fig. 42.

The results given in this figure are in general in accord with the experimental results given in Fig. 36. The optimum frequency which gives the maximum value of ΔI_p is easily found from (21), that is,

$$p = \frac{\alpha + \gamma E_m}{2\beta} \tag{22}$$

which displaces to the lower frequency side as E_m decreases.

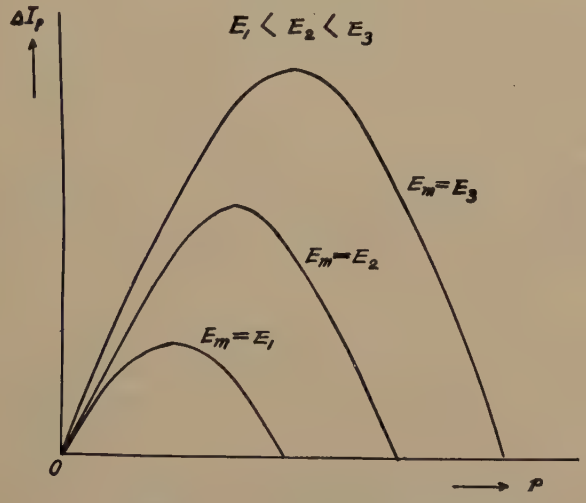

Fig. 42—Effect of the quenching frequency on the variation of the plate current.

Conclusion

The amplification by superregeneration is performed by the building-up of the free oscillation which is initiated by the impulse of the signal. When the effective resistance of the oscillatory circuit in the receiver is brought to be sufficiently negative to start the oscillation, the receiver becomes very sensitive for the impulses of the impressed electromotive forces. The slightest impulse is sufficient to start the oscillation.

Thus it is of essential importance in the amplification by superregeneration that the receiver be in a state of quenching. Any type of oscillatory circuit and any method of quenching action may be employed to produce the state. For example, if a usual regenerative receiver is brought to an oscillatory state by applying a relatively high

plate voltage, it is often observed that the receiver operates with an abnormally high sensitivity. This can be explained by the fact that a parasitic oscillation is generated under certain conditions in the receiver and it performs the quenching action on the principal oscillation.[8] Thus the regenerative receiver acts implicitly as a superregenerative one.

The high sensitivity and the relatively simple construction are two great merits of the superregenerative receiver. But this receiver is not free from certain defects. In the first place, the reception of a very weak signal is disturbed by the characteristic noise. This noise will, however, be decreased by the proper design of the vacuum tube. The ultimate intensity of the signal to be received by the superregenerative receiver is limited by this noise. Next stands the poor selectivity of the receiver. It is caused by the presence of a number of component frequencies which are produced by the quenching action.

It is emphasized that the receiver should be operated with the optimum quenching frequency and the optimum quenching voltage both of which are relatively high. By means of them the above two inherent defects can be remedied to a great extent.

Acknowledgment

In conclusion, the writer wishes to express his deep appreciation to the Hashimoto Research Fund of the Institute of Electrical Engineers of Japan, which gave the financial support for this work.

[8] H. Ataka, *Hochfrequenz. und Elektrokustic*, Bd. 42, s.155, (1933).

Proceedings of the Institute of Radio Engineers
Volume 23, Number 8 *August, 1935*

ELECTRICAL MEASUREMENTS AT ULTRA-HIGH FREQUENCIES*

By

Ronold King

(Formerly, University of Wisconsin, Madision, Wisconsin; now, Physics Department, Lafayette College, Easton, Pennsylvania)

Summary—*Part I. A modified form of the long-line equations for use at ultra-high frequencies is given. A complete solution is obtained for a pair of parallel wires bridged at each end by a general impedance. The solution is in the form of expressions giving the voltage across, and the current through one of these impedances. Conditions are given under which the current or voltage becomes a maximum, as well as formulas for these maximum amplitudes. Special cases are discussed and expressions are derived for use in the measurement of reactance and resistance.*

Part II. A convenient form of parallel wire system for ultra-high-frequency measurements is briefly described, and its constants are listed. The use of a tandem bridge is explained. The general problem of measuring current and voltage at ultra-high frequencies is considered. A method is mathematically derived for obtaining the calibration characteristics of current and voltage indicators; the method is applied experimentally to determine such characteristics for a thermal milliammeter and for the symmetrical screen-grid voltmeter. The scale factor is discussed.

Part III. The mathematical theory of Part I is applied to obtain two methods for measuring respectively high and low reactances. These are used to measure the reactances of various wires, coils, condensers, thermal milliammeters, vacuum thermocouples, etc., and to study series and parallel resonance circuits at ultra-high frequencies.

Part IV. The general problem of resistance at ultra-high frequencies is discussed. The mathematical theory of Part I is applied to the measurement of resistance. Methods are described for measuring the resistances of wires and coils, and of high resistance leaks. A method is suggested for measuring the permeability of wires. Experimental results are given.

Part V. A method is described for determining the component frequencies present in an ultra-high frequency source, and for measuring their relative amplitudes.

Part I—Outline of the Mathematical Theory

THE purpose of this part is to lay the mathematical foundations for methods of measuring current, voltage, reactance, and resistance at ultra frequencies.

A. The Long-Line Equations at Ultra-High Frequencies

The differential equations expressing the relations between increments of current and voltage in a pair of parallel conductors are usually written in the symbolic form

* Decimal classification: R200. Original manuscript received by the Institute May 24, 1934; revised manuscript received by the Institute, August 7, 1934.

$$(j\omega l + r)I = -dv/dx$$
$$(j\omega c + g)v = -dI/dx. \qquad (1)$$

Here r, l, c, and g are, respectively, resistance, inductance, capacitance, and leakance per loop unit length of the parallel wires. These equations are usually derived in a way presupposing a knowledge of the fact that r, l, c, and g are the only circuit parameters which enter into the long-line problem.[1] Formulas for these parameters are then derived separately.[2] This method of analysis is entirely adequate for low and intermediate frequencies. At ultra-high frequencies, on the other hand, neither (1), nor all of the low-frequency parameters are accurate.

In discussing circuit analysis at high frequencies, Brainard[3] has pointed out that a better approximation is obtained in handling lumped circuits by writing the impedance operator in the form, $(R+j\omega L + \omega^2 N)$, instead of in the usual form, $(R+j\omega L)$. The added term, in which N is a constant, represents the radiation resistance.

In order to take this radiation term into account in circuits with distributed constants, it is necessary to rederive the long-line equations directly from the Maxwell field equations. By including the leading term in $\dot{I}$ as well as that in I, and considering retardation, the following equations are obtained:

$$(r + j\omega l + \omega^4 ns)I = -dv/dx$$
$$(g + j\omega c)v = -dI/dx. \qquad (2)$$

Here the usual four parameters are defined at ultra-high frequencies, and $n = 10a^2/C^4$. C is the velocity of light; a the spacing of the parallel wires; s the length of the conductor.*

By differentiating (2) with respect to x, two second order equations are obtained. Since the coefficients are functions of x, the simple exponential solution characteristic of equations with constant coefficients does not apply. An exact solution of the long-line equations at ultra-high frequencies is, therefore, complicated. Fortunately the requirements of the problem encountered in the measurements to be discussed below are such that a simplifying approximation is possible. It can be shown that if $nC\omega^2/l \ll 1$, an approximate solution of (2) is obtained by setting $r' = r + \omega^4 ns$ and treating this as a constant. If this is done, the high-frequency equations (2) reduce to the same form as

[1] A. Hund, Scientific Paper of the Bureau of Standards, No. 491, p. 520.
[2] E. Bennett, "Electrodynamics for Engineers," McGraw-Hill Book Co., pp. 193, 534.
[3] Brainerd, Proc. I.R.E., vol. 22, p. 395; March, (1934).
* These equations have been derived and discussed in detail by the author under the title, "The telegraphists equations at ultra-high frequencies," *Physics*, vol. 6, p. 121; April, (1935).

the low-frequency ones (1). In the following analysis a general solution of (1) will be obtained and interpreted for ultra-high frequencies at the proper point.

B. The General Mathematical Problem

The mathematical problem is to derive formulas for current or voltage maxima, and for the maximizing conditions related to a terminal impedance at one end of a pair of parallel wires, in terms of the constants and length of these wires, the general terminal impedances, and the position of the driving electromotive force relative to the wires.

Consider a pair of parallel wires extending from $x=0$ to $x=s$. At $x=0$ they are bridged by an impedance Z_0; at $x=s$ by an impedance Z_s. A sinusoidal electromotive force is impressed in the circuit in series with the impedance Z_0. From a formula given by Cohen[4] written in admittance notation, the steady-state current i_x at a point x along the wires is given by

$$i_x = E_0 Y_0 \left\{ \frac{NY_s \cosh Ky + \sinh Ky}{(N^2 Y_0 Y_s + 1) \sinh Ks + N(Y_0 + Y_s) \cosh Ks} \right\}. \quad (3)$$

Here, $K^2=(lp+r)(cp+g)$, and $p=j\omega$ for the sinusoidal electromotive force here assumed. The following abbreviations have been used:

$$N = \sqrt{\frac{lp + r}{cp + g}} = (lp + r)/K = \text{surge impedance}$$

$$y = s - x.$$

By a general reciprocity theorem[5] it follows that the current i_0 through the impedance Z_0 due to a driving electromotive force E_x at a point x along the line is given by

$$i_0 = E_x Y_0 \left\{ \frac{NY_s \cosh Ky + \sinh Ky}{(N^2 Y_0 Y_s + 1) \sinh Ks + N(Y_0 + Y_s) \cosh Ks} \right\}. \quad (4)$$

The voltage across Z_0 is, then, simply

$$v_0 = i_0/Y_0 \quad (5)$$

where i_0 is given by (4).

In expanding the general and symbolic solution (5), the same restrictions on the line constants as were previously imposed[6] will be found convenient. Briefly, these are

[4] Cohen, "Heaviside's Electrical Circuit Theory," p. 119, formula 99.
[5] Pierce, "Electric Oscillations and Electric Waves," p. 204.
[6] R. King, Proc. I.R.E., vol. 21, pp. 1146–7, 1157–8; August, (1933).

$$\begin{cases} K = \alpha + j\beta \doteq r/2N + j\omega/v \\ N \doteq lv \\ \alpha \ll \beta < 1 \end{cases} \quad \text{(a)}$$

$$\alpha^2 s^2 \ll 1. \quad \text{(c)}$$

Let the following notation be introduced:

$$NY_0 = N(G_0 - jB_0) = g_0 - jb_0$$
$$NY_s = N(G_s - jB_s) = g_s - jb_s$$
$$N(Y_0 + Y_s) = (g_0 + g_s) - j(b_0 + b_s) = g_2 - jb_2$$
$$N^2 Y_0 Y_s + 1 = 1 - b_0 b_s + g_0 g_s - j(b_0 g_s + (+b_s g_0) = (b_1 - jg_1).$$

Equation (5) may be written in the following form:

$$v_0 = E_x P/Q. \quad (6)$$

Here P, the numerator, is a function of y; Q, the denominator, is a function of s. It is clear that P can be obtained at once from Q by writing y for s and setting Y_0 equal to zero. It is, therefore, sufficient to operate with Q. From (5) using restriction (c) one obtains for the absolute value of Q,

$$Q = \{A^2 \cos^2 \beta s + D^2 \sin^2 \beta s - 2F \sin \beta s \cos \beta s\}^{1/2}. \quad (7)$$

The coefficients are

$$A^2 = (\alpha s b_1 + g_2)^2 + (b_2 + \alpha s g_1)^2$$
$$D^2 = (b_1 + \alpha s g_2)^2 + (\alpha s b_2 + g_1)^2 \quad (8)$$
$$F = (b_1 b_2 - g_1 g_2)(1 - \alpha^2 s^2).$$

In order to obtain the positions and amplitudes of the maximum values of v_0 it is necessary to derive expressions for the maxima and minima of Q with respect to s. It can be shown that after neglecting small quantities and imposing restriction (e) the values of s for which Q has extreme values are given by

$$\tan \beta s = \quad (9)$$
$$\frac{(b_2^2 + g_2^2) - (b_1^2 + g_1^2) \pm \sqrt{(b_2^2 + g_2^2)^2 + 2(b_1 b_2 - g_1 g_2)^2 - 2(b_1 g_2 + b_2 g_1)^2 + (b_1^2 + g_1^2)^2}}{2\{(b_1 b_2 - g_1 g_2) + \alpha/\beta)(b_1 g_2 + b_2 g_1)\}}$$

$$\alpha^2 s(b_2^2 + g_2^2) \ll \alpha(b_1 g_2 + b_2 g_1) + \beta(b_1 b_2 - g_1 g_2). \quad \text{(e)}$$

From (6) and the statements following it, the voltage amplitude across the impedance Z_0 is given by

$$v_0 = E_x \left\{ \frac{A_y^2 \cos^2 \beta y + D_y^2 \sin^2 \beta y - 2F_y \sin \beta y \cos \beta y}{A_s^2 \cos^2 \beta s + D_s^2 \sin^2 \beta s - 2F_s \sin \beta s \cos \beta s} \right\}^{1/2}. \quad (10)$$

The maximum value of this amplitude is obtained when the numerator is maximized and the denominator minimized. This is accomplished by substituting the proper values of s and y from (9), y being obtained by setting $Y_0=0$ and writing y for s. The coefficients are obtained from (8) in the same way.

The complete general solution for the positions and the amplitudes of resonance voltages across the terminal impedance Z_0 has thus been obtained. By positions is meant the values of y and s which produce the resonance condition. From (5) it is evident that the expression for maximum current through Z_0 differs from the above only by a constant factor in the amplitude. This factor is the absolute value of the admittance Y_0. The maximizing values of s and y will again be obtained from (9), but the choice of signs will be the opposite of that for maximum voltage. Furthermore, since it is merely a convention of notation which distinguishes the end $x=0$ from the end $x=s$, it is clear that the above expressions may be used equally well for obtaining the resonance current or voltage associated with the impedance Z_s. By reapplying the reciprocity theorem, current and voltage at any point x along the wires may be obtained in terms of a driving voltage in series with Z_0.

C. Correlation with Previous Theory; the Shape of Resonance Curves; Terminal Impedances with Distributed Constants

In the general solution of the preceding section nothing was said regarding the shapes of resonance curves, nor about a terminal impedance which includes a secondary length of parallel wires. These questions have been solved completely for an important special case of the general theory,[6] so that nothing further need be said. To show that this is true, it is merely necessary to allow Z_0 to approach zero in the fundamental relation (4) of the preceding section. The resulting expression is identical with the fundamental equation (3) of the earlier analysis.[6] It is, therefore, not necessary to reconsider the question of the shape of resonance curves, nor of a secondary length of parallel wires.

D. Special Cases of the General Theory

The formulas derived in Section *B* for the positions and amplitudes of resonance maxima in the general case are complicated, and not convenient for purposes of computation from experimentally determined values of s and y, or of relative amplitudes. Fortunately it is possible to simplify the formulas very materially for the two special cases which are of primary importance. In the following analysis the neces-

sary approximations will be introduced as mathematical hypotheses; a discussion of their physical significance and of the degree in which actual conditions are approached is reserved for later sections dealing with actual measurements.

1. Special Case A

Let it be assumed that the terminal impedances are of such a nature that the following inequalities are good approximations:

$$B_0^2 \gg G_0^2 \text{ so that } B_0 \doteq 1/X_0;\ G_0 \doteq R_0/X_0^2 \tag{1}$$

$$B_s^2 \gg G_s^2 \text{ so that } B_s \doteq 1/X_s;\ G_s \doteq R_s/X_s^2 \tag{2}$$

$$B_0 B_s \gg G_0 G_s. \tag{3}$$

It can be shown that these conditions are included in the following more general ones

$$\begin{aligned} b_1^2 &\gg g_1^2 \\ b_2^2 &\gg g_2^2. \end{aligned} \tag{4}$$

With these conditions, Q is minimized with the positive sign in Section B, equation (9), and P is maximized with the negative sign. Neglecting small terms in accordance with (4), the following results are obtained:

$$\tan \beta s = b_2/b_1 = N(B_0 + B_s)/(1 - N^2 B_0 B_s) \tag{5}$$

$$\tan \beta y = -1/b_s = -1/NB_s. \tag{6}$$

With these, (10) gives for the maximum amplitude:

$$|v_0|_{\max} = \frac{E_x}{\sqrt{1+b_0^2}} \left\{ \frac{1}{\alpha s + \dfrac{g_0}{b_0^2+1} + \dfrac{g_s}{b_s^2+1}} \right\}. \tag{7}$$

For some purposes it is convenient to introduce equivalent damping lengths of parallel conductors for the terminal impedances. Thus, by defining,

$$\alpha s_0 = g_0/(1 + b_0^2); \qquad \alpha s_s = g_s/(1 + b_s^2)$$

where s_0 and s_s are the equivalent damping lengths, respectively, of Z_0 and Z_s, (7) may be written in the compact form

$$|v_0|_{\max} = \frac{E_x}{\sqrt{1+b_0^2}} \frac{1}{\alpha s_e} \tag{8}$$

with,

$$s_e = (s + s_0 + s_e). \tag{9}$$

It is clear from (5) that the maximizing value of s depends as well upon B_0 as upon B_s. In order to determine experimentally unknown values of B_0 and B_s it is much more convenient to transform (5) into two equations which involve, the one only B_0, the other only B_s. This can be done readily mathematically by defining a length S between the impedances such that,

$$\tan \beta S = 1/(-b_0) = 1/(-NB_0). \tag{10}$$

This is obtained from (5) by setting $B_s = \infty$; i.e., $X_s = 0$. In other words, the value $s = S$ represents a length of parallel wires, such that the voltage amplitude across Z_0 will be a maximum for $X_s = 0$. The experimental significance of this length S will be discussed at a later point. By combining (10) with (5) and using formula 648 of Pierce's tables, one obtains,

$$\tan \beta(s - S) = -1/NB_s = -X_s/N. \tag{11}$$

This formula resembles corresponding relations given by other writers.

If the reactance X_s is sufficiently small and inductive, (11) may be written in the following form:

$$\beta(s - S) = \omega L/N = -\beta k; \quad \text{or } s - S = k \tag{12}$$

with $k = L/l$. This agrees with (32a) of reference 6.

Equation (6) indicates that the position, x, at which the driving electromotive force E_x must be applied for the voltage across Z_0 to be a maximum, depends upon both B_0 and B_s. This dependence upon B_s is only apparent, however. It can easily be shown that

$$\tan \beta x = 1/(-NB_0) = -X_0/N. \tag{13}$$

From this it is clear that the maximum voltage is obtained across Z_0 when the driving electromotive force is applied at a current loop along the wires.

The complete solution of Special Case A is obtained, then, from (7) using either (5) and (6) or (11) and (13). It is subject to restrictions (a) and (c) of the general case. Restriction (e) becomes

$$\alpha^2 s/\beta \ll \left|(1 - N^2 B_0 B_s)/(B_0 + B_s)N\right| \tag{e'}$$
$$\alpha^2 y/\beta \ll \left| X_s/N \right|.$$

This simply means that instead of $\tan \beta y$ vanishing, and $\tan \beta s$ becoming infinite according to (5) and (6) as B_s and the quantity $(1 - N^2 B_0 B_s)$ vanish, they approach, respectively, very small and very large values.

2. Special Case B

The desired conditions for this case are the following:

$$B_s^2 \ll G_s^2 \ll 1 \text{ so that } B_s \doteq X_s/R_s^2;\ G_s \doteq 1/R_s$$
$$B_0^2 \gg G_0^2. \tag{14}$$

It can easily be shown that these restrictions are included in (4) provided that,

$$1/g_s^2 \gg b_0^2 \gg g_s^2. \tag{15}$$

It follows, then, that (5) applies to this case in the form:

$$\tan \beta s = (b_0 + b_s)/(1 - b_0 b_s) \doteq b_0. \tag{16}$$

The maximizing value of y is obtained from Section B equation (9) using (14). It is,

$$\tan \beta y = -1/\left(b_s + \frac{\alpha}{\beta} g_s\right) = \text{very large.}$$

As a first approximation this is the same as (6), so that (7) is the expression for maximum amplitude in this case too. As a result of (14),

$$|v_0|_{\max} = \frac{E_x}{\sqrt{1 + b_0^2}} \frac{1}{\{\alpha s + g_s + g_0/(1 + b_0^2)\}}. \tag{18}$$

From (16) above and (10), it follows that,

$$\tan \beta(s - S) \doteq \infty. \tag{19}$$

Equation (13) is also true in this case. The first inequality of restriction (e) cannot be simplified; the second inequality is obviously satisfied.

In concluding the discussion of the two special cases, it is interesting to note that the solutions are practically the same in form. But it must not be forgotten that the relative orders of magnitude of the quantities involved in each case are different; i.e., the resemblance is a purely symbolic one.

E. Interpretation of the Solution at Ultra-High Frequencies

Throughout the analysis of Sections B, C, and D, no mention was made of the conditions implied as a result of the conclusions drawn in Section A. That, is, the solution was carried out for the conventional long-line equations. Subject to the condition stated in Section A, a good approximation is obtained at ultra-high frequencies by writing

$r' = r + \omega^4 ns$ for r. This is the same as replacing the damping constant α by a new damping factor given by

$$\alpha' = r'/2N = (r + \omega^4 ns)/2N \tag{1}$$

or,

$$\alpha' s = rs/2N + \omega^4 ns^2/2N. \tag{2}$$

In this expression rs is the total effective ohmic resistance, and the quantity $\omega^4 ns^2$ is the radiation resistance of the parallel wires at resonance. Let this latter be denoted by R_r. Then,

$$R_r = 10\alpha^2 s^2 \beta^4 = 40\pi^2 (s/\lambda)^2 (2\pi a/\lambda)^2 \qquad (\beta = \omega/v \doteq \omega/C). \tag{3}$$

The radiation resistance determined in this way is the same as that obtained using Poynting's theorem assuming uniform current distribution.

It hardly seems necessary to point out, that at ultra-high frequencies it is not sufficient to consider merely the radiation from the parallel wires. Clearly, there will also be energy radiated from the terminal impedances, and the resistance terms in these impedances must include a radiation as well as an ohmic part.

In concluding the mathematical study it seems well to point out that the conditions imposed throughout the analysis are such that the solutions are very general. If the frequency is not too high and the spacing of the wires is not too large, the solution indicated for ultra-high frequencies is quite accurate. It is evident, however, that the solution obtained above is entirely inadequate in discussing radiation from two parallel antennas, unless these are very close together.

Part II—Experimental Technique; the Measurement of Current and Voltage

The purpose of this part is to describe a convenient parallel wire system, and to make use of it in the measurement of current and voltage.

A. Notes on Experimental Technique

The general form of the apparatus used in the ultra-high-frequency measurements to be described in this and subsequent parts is the same as that used in earlier work[6,7], but with numerous refinements. In particular, the movable oscillator has been retained, and its significance will become apparent below. The complete arrangement is pictured and explained in Figs. 1 and 2. The constants of the wire system are

[7] R. King, *Ann. der Phys.*, Folge five, vol. 7, p. 806, (1930).

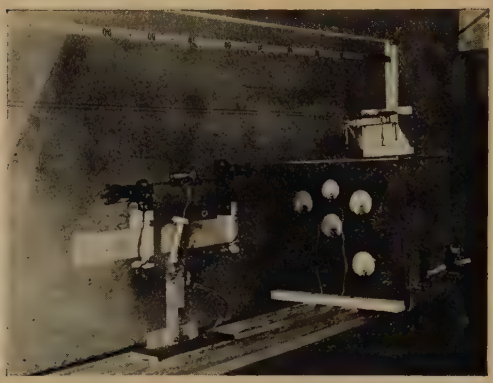

Fig. 1—The voltmeter end of the parallel wire system. At the extreme right is the screen-grid voltmeter; the variable series capacitances C are visible directly above the voltmeter case. The small lower plates of these capacitances are flush with the cover and tied directly to the control grids of the 224 tubes. At the left is the oscillator, freely movable over the entire length of the wooden track. The small coil hanging at an angle is a variable length coil tuned to resonance at the generated frequency. The parallel wires and the tape scale are shown.

Fig. 2—The far end of the parallel wire system. At the left are two meters in series with the total plate current and ΔI_p meters of the voltmeter. The third meter reads the oscillator plate current. The two control knobs vary the field current of the double motor generator set used to supply the oscillator and voltmeter voltages. The resistance box is a variable shunt for the $\Delta I_p'$ meter; the calibration card for different shunts is visible. The tandem bridge is shown tied to the mounting for unknown Z_s circuit elements at the extreme right. A single turn coil is shown mounted in place. The thermal milliammeter shown is not actually connected. However, the coil may be removed and the short meter leads connected in its place in the grooves of the support.

listed in Table I for the frequency used throughout the measurements; viz., $\omega = 10^9$. Restrictions (a) and (c) of the general theory are also shown to be satisfied.

TABLE I

CONSTANTS OF THE PARALLEL WIRE SYSTEM

Symbol	Name of Quantity	Formula	Numerical Value
a	Separation of wires		5 cm
d	Diameter of wires		0.080 cm
r_0	Direct-current resistance per loop cm		7.0×10^{-4} ohms
r	Resistance per loop cm at $\omega=10^9$	$r=\sqrt{\frac{r_0\omega}{1-(d/a)^2}}$ (e. m. u.)	2.65×10^{-2} ohms
	Inductance per loop cm at $\omega=10^9$	$l=4\log\left\{\frac{1+\sqrt{1-(d/a)^2}}{d/a}\right\}+\sqrt{\frac{r_0}{\omega[1-(d/a)^2]}}$	1.93×10^{-8} henrys
v	Velocity of propagation	$v=v_0\left(1-\frac{r}{2\omega l}\right)\doteq v_0$	3.0×10^{10} cm/sec
N	Surge impedance	$N=vl$	579 ohms
α	Damping constant	$\alpha=r/2N$	2.29×10^{-5} cm^{-1}
Λ	Wavelength		188.8 cm
β	Propagation constant	$\beta=2\pi/\Lambda$	0.0332 cm^{-1}
$\omega^4\eta$	Radiation factor per loop cm	$\omega^4\eta=10\alpha^2\beta^4$	2.08×10^{-4} cm^{-2}
r'	Effective resistance per loop cm	$r'=r+\eta s\omega^4$	5.07×10^{-2} ohms*
α'	Effective damping constant	$\alpha'=r'/2N$	4.38×10^{-5} cm^{-1}*
	Restriction (a)	$\alpha'<<\beta<1$	$4.38\times10^{-5}<<0.0332<1$
	Restriction (c)	$\alpha'^2s^2<<1$	$s<3000$ cm

* The value of s is chosen to be that of $S=116.4$ cm in most of the following measurements.

Before proceeding to describe methods of measurement using the parallel wire system, it is necessary to discuss a point of primary importance. It will be recalled that the general theory for parallel wires with terminal impedances was derived on the assumption that the wire length s between the impedances is continuously variable. Experimentally this might be realized, by using telescoping tubes. But such an arrangement is cumbersome, and has the disadvantage, that the line constants are not the same over the entire length. A simple method of eliminating this difficulty is the following. Let the terminal impedance Z_s be composed of two parallel branches such that,

$$Y_s = Y_1 + Y_i.$$

Here Y_1 is the admittance of the bridge connected across the parallel wires. The quantity Y_i is the input admittance of a secondary length of parallel wires extending beyond Y_1. If the inequality $Y_1 \gg Y_i$ is satisfied at all times, then Y_i may be neglected, and Y_1 written for Y_s. It can be shown that the minimum value of Y_i for a length s_2-s_1 of parallel wires bridged by a low impedance bridge of equivalent length k_2 is 2.6×10^{-6} mhos. This value is reached when $s_2-s_1=\Lambda/4-k_2$. Hence, if the secondary is kept adjusted to this value, Y_i may be

neglected so long as $Y_1 > 10^{-4}$. This is readily accomplished by means of a tandem bridge. Suppose a bridge of admittance Y_1 is placed in a suitable movable support. Let a second similar support be tied rigidly to the first one so that the distance from the point s_1 at which Y_1 makes contact with the parallel wires to a heavy copper bridge of equivalent

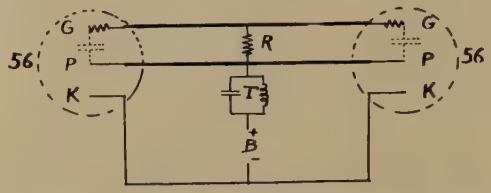

Fig. 3—Schematic circuit diagram of the regenerative oscillator. T = tuned circuit formed by single turn coil pictured in Fig. 1. R = 3000-ohm resistance. The operating voltage is from 70 to 100 volts; plate current varies from about 40 to 100 milliamperes. The inductance rods were of telescoping brass, spaced 3 centimeters, and about 20 centimeters long for the 188.8-centimeter wavelength.

length k_2 is always $\Lambda/4 - k_2$. The input admittance of the secondary in parallel with Y_1 is, then, always a minimum.[8] It will be presupposed in all measurements in which an impedance Z_s is moved along the wires as a bridge, that a suitably placed tandem bridge moves with it, so that $Z_1 \doteq Z_s$. $(Z_1 < 10^4)$.

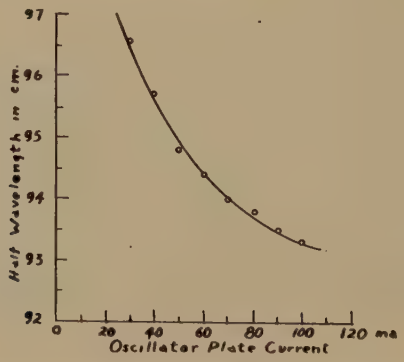

Fig. 4—Variation of wavelength generated by the oscillator with plate current.

The source of ultra-high-frequency voltage was a two-tube regenerative oscillator. The circuit diagram is shown in Fig. 3. The wave-

[8] The possible reaction of the tertiary length of parallel wires beyond the tandem bridge is assumed negligible. If a heavy copper bridge is used in the tandem, this will certainly be true except possibly at lengths of the tertiary which bring it exactly into resonance. Such lengths, when they occur, are easily avoided by placing a third bridge across the wires. Or, if it is desired, a third bridge of heavy copper may be attached ten or more centimeters beyond the tandem bridge and moved with this.

length characteristics of this type of oscillator have been derived;[9] the lower wavelength limit using 56 or 37 type tubes is about 125 centimeters. The dependence of wavelength upon plate current is shown in Fig. 4. With the two-tube circuit it is possible to eliminate the grid lead, according to the suggestion of Shoemon Ohtaka,[10] by placing a high resistance leak across the current loop of the oscillatory circuit. This is shown in Fig. 3.

B. Current and Voltage at Ultra-High Frequencies

A fundamental difference exists between the measurement of current and voltage at low frequencies and at ultra-high frequencies. In the former, one is justified in almost every case in speaking of the current in a given circuit branch. One assumes that the same current flows in every part of a series circuit. An exception to these statements is found in the case of long transmission lines, where current and voltage are functions of the space dimensions. In the case of ultra-high frequencies this is always true, due to the enormous change in the relative orders of magnitude of wavelength and circuit dimensions. As a result of distributed capacitance and radiation, no coil, no pair of wires, not even a single wire is equivalent to a series circuit in the low-frequency sense. At ultra-high frequencies it is always a question of distributed circuit constants, (including radiation), nearly always of resonance circuits, and consequently, of current and voltage which are functions of position.

The definition of current and voltage in relation to a particular circuit configuration depends upon a knowledge of the fundamental field vectors **B** and **E**. Such a definition has already been obtained for the parallel wire system with terminal impedances by integrating the field equations. Thus, the voltage amplitude between two points on the parallel wires connected by an impedance Z_0 is defined, except for a scale factor, by (10) of Part I, Section B. The current amplitude through Z_0 is defined by the same equation with both sides divided by the absolute value of Z_0. But this second definition is ambiguous unless it is specified that Z_0 is a "lumped" impedance, since otherwise the phrase, "current through Z_0," is meaningless. Strictly speaking, there is no such thing as a "lumped" impedance at ultra-high frequencies. But electrically an impedance may be considered "lumped," if the same current flows in every part. Now, the current distribution along a pair of parallel wires is very nearly sinusoidal. Hence, the current through a short (relative to the wavelength) piece of one of the wires

[9] R. King, Proc., I.R.E., vol. 20, p. 1370; August, (1932).

[10] Shoemon Ohtaka, "On a new type of ultra-short wave oscillator," *Jour. I. E. E.* (Japan), vol. 54, p. 1; January, (1934).

at a current loop will be very nearly uniform. This means that if the impedance Z_0 consists of a short straight conductor placed across the parallel wires at a current loop, the current through the conductor will be practically uniform over its length. If by Z_0 is meant such a conductor, then (10) of Part I, Section B with both sides divided by $|Z_0|$ may be used as a definition of current. It will be on the basis of these definitions that methods will be described for measuring current and voltage.

C. The Measurement of Current and Voltage

1. General Discussion

It follows from the above statements that the only difference between the measurement of current and voltage lies in the determination of the scale factor. Moreover any device which is sensitive at the desired frequency, may be used to read current or voltage if connected to a suitable length of parallel wires. If k is the equivalent length of a low resistance thermal milliammeter or of a vacuum tube voltmeter, then the input impedance of either device may be made extremely small if parallel wires of length $\Lambda/2-k$ are attached, and extremely high if the wires are of length $\Lambda/4-k$. If the characteristics are known, it is merely necessary to determine the scale factor for the complete device including the attached parallel wires.

2. The Relative Calibration of Indicating Devices

From (10), Part I, Section B, the voltage across an impedance Z_0 may be written in the form

$$|v_0| = \frac{E_x}{Q(s)}\{[b_s \cos \beta y - \sin \beta y]^2 + f(\alpha, y, g_s)\}^{1/2}. \qquad (1)$$

Here $Q(s)$ represents the denominator of (10), and $f(\alpha,y,g_s)$ is a small quantity which is significant only when the other term in (1) becomes vanishingly small. Except when,

$$\tan \beta y = b_s \qquad (2)$$

(1) becomes, (using (6), Part I, Section D, and remembering that $y=(s-x)$,

$$|v_0| = (E_x/Q) \cos \beta(x_m - x). \qquad (3)$$

If Q is minimized, the maximum amplitude in (3) is simply (7), Part I, Section D.

Equation (3) shows that if an indicating device of impedance Z_0 is placed across one end of a pair of parallel wires, and if an impedance Z_s is moved to a point sufficiently distant from Z_0 for which the voltage

across Z_0 is a maximum or near maximum, then the voltage across Z_0 is essentially a cosine function of the displacement of the oscillator relative to the wires between the two impedances.

3. Relative Calibration of a Thermal Milliammeter

The heater unit of the Weston thermal milliammeters, model 425, satisfies the conditions of Special Case A of Part I, Section D. By placing such a meter (125-milliampere range) across one end of the parallel wires, and adjusting a copper bridge about three half wavelengths from the meter until this showed a maximum deflection, it was merely necessary to move the oscillator parallel to the wires between meter and bridge to obtain the curve of Fig. 5. To show that the curve drawn

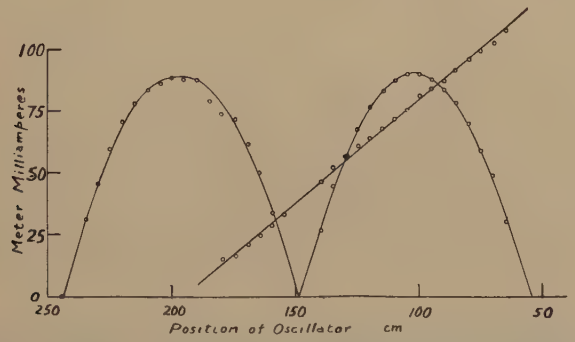

Fig. 5—Deflection of 125-milliampere Weston thermal milliammeter, model 425, as the oscillator was moved parallel to the wires. The meter bridged the wires at a current loop.

through the experimentally determined points of Fig. 5 is indeed a cosine curve, the arc-cosine of the amplitudes was taken and plotted. This gave the straight line of slope $2\pi/\Lambda$ shown in Fig. 5. The theory is thus seen to be verified, and the relative correctness of the milliammeter scale is assured. A similar calibration was made for a Western Electric vacuum thermocouple. A cosine curve was obtained.

4. Relative Calibration of the Symmetrical Screen-Grid Voltmeter

Transrectification characteristics of the two-tube screen-grid voltmeter without external leak were given in a recent paper[11] for audio and radio frequencies. It was suggested that the ultra-high-frequency characteristics might be expected to be similar. This will now be verified. The complete circuit for the voltmeter in the form in which it was used is shown in Fig. 6. It is pictured in Fig. 1. Before carrying out the calibration, the sensitivity of the device as a function of the

[11] R. King, Proc., I.R.E., vol. 22, p. 771; June, (1934).

series capacitances C (Figs. 1 and 6) had to be examined. At low or radio frequencies such series capacitances would act simply as a capacitive voltage divider, so that a definite fraction of the voltage impressed across W_1W_2 would be applied across the input admittances of the two tetrodes in series. At ultra-high frequencies this lumped circuit behavior is no longer true: a variation in the series capacitances C not only changes the input admittance of the voltmeter (if the condensers are assumed a part of this), but also shifts the position of the current loops and nodes relative to the input capacitances of the screen grid tubes. This effect is shown in Fig. 7. It is clear that for a condenser separation of about 0.6 centimeter the sensitivity is greatest and that

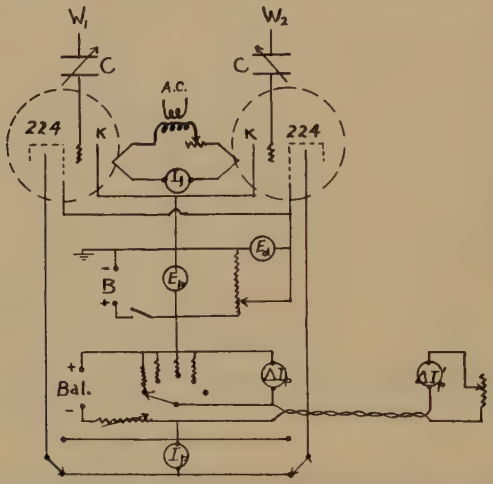

Fig. 6—Complete circuit diagram of the screen-grid voltmeter. W_1 and W_2 are the parallel wires. The series capacitances C consist, respectively, of two semicircular brass plates about 2 centimeters in diameter arranged on screws to permit moving the upper plate from contact with the lower one to a 4-centimeter separation. Operating voltages are: $E_p = 150$ volts; $E_d = 125$ volts (to give maximum plate current).

a maximum voltage is established across the input capacitances of the tubes. By adjusting the condensers C, the sensitivity of the voltmeter can be varied over a wide range.

In order to obtain the relative transrectification characteristic of the symmetrical voltmeter at ultra-high frequencies, a preliminary examination of the radio-frequency characteristic is valuable. This indicates that there are two regions of curvature, the first for very low, the second for high input voltages; the intermediate range is very nearly linear. Since the ultra-high-frequency characteristic may be assumed to resemble this in shape, it will be convenient to carry

out the calibration in two parts. First, the maximum input voltage across the tube capacitances will be kept sufficiently low to make sure

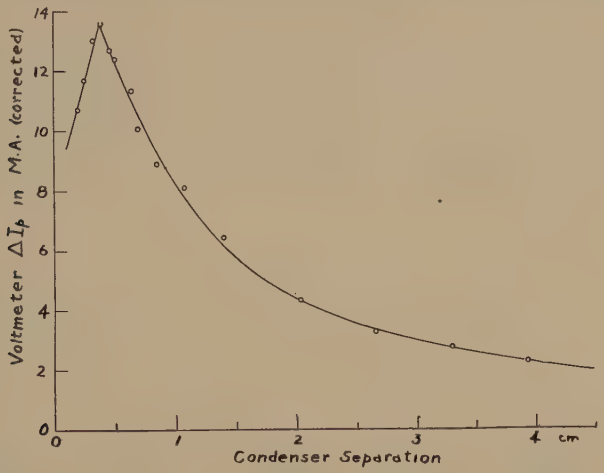

Fig. 7—Effect of separation of the condenser plates of the series capacitances C upon the voltmeter deflection with constant impressed voltage.

that the high voltage curvature is not reached. The calibration will then be repeated with a much higher voltage amplitude.

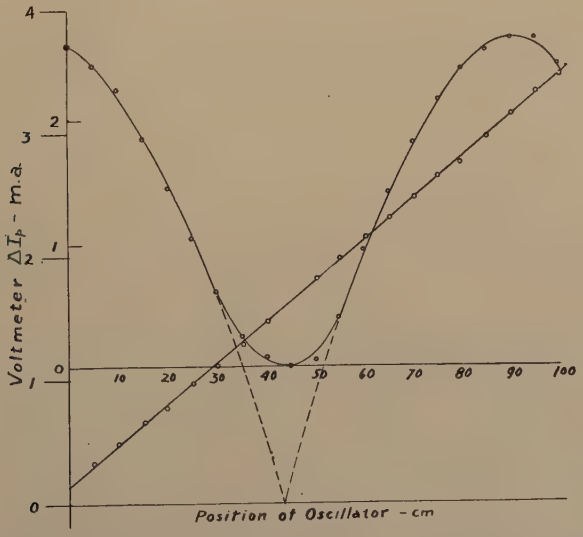

Fig. 8—Low range voltmeter deflection as the oscillator was moved.

With the voltmeter fixed at one end of the parallel wires as shown in Fig. 1, a copper bridge was adjusted to produce a maximum de-

flection when placed about three half wavelengths from the voltmeter. The oscillator was then moved parallel to the wires; the voltmeter ΔI_p was recorded every five centimeters. A zero reading was taken each time by bridging the wire system at a voltage loop. The experimental curve is shown in Fig. 8. The departure from the ideal or rectified cosine curve is evident at the lower amplitudes. The true cosine curve is shown dotted; it was obtained by the construction indicated, and verified by plotting the arc-cosine. From the observed curve and

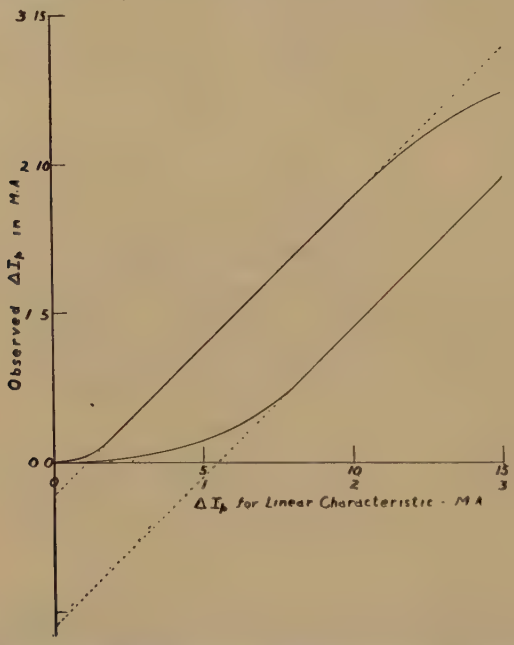

Fig. 9—Low and high range calibration curve of voltmeter.

the ideal curve for a straight line characteristic, the lower range of the calibration curve of Fig. 9 was easily obtained.

The upper range was determined in much the same way. By increasing the oscillator output and adjusting the series condensers for greater sensitivity the voltmeter deflection was very much increased. The oscillator was moved parallel to the wires, and deflections and zero readings were again taken as before. The observed curve is shown in Fig. 10. The low range correction was now made as shown using the results of the previous determination. From the known ratio of the width of a cosine curve at the base to the width at half amplitude, the amplitude of a true cosine curve to fit the lower deflection range of the observed curve was determined. Using this value, a true cosine

curve was constructed; it is shown dotted in Fig. 10. From the observed amplitudes and the ideal amplitudes for a straight line characteristic, the upper range of the calibration curve of Fig. 9 was constructed. The relative transrectification characteristics of the symmetrical voltmeter at $\omega = 10^9$ were thus determined. Their shape is very much like the low- and radio-frequency curve as predicted.[11] The scale factor depends upon the adjustment of the series capacitances; a method for determining it will be described below.

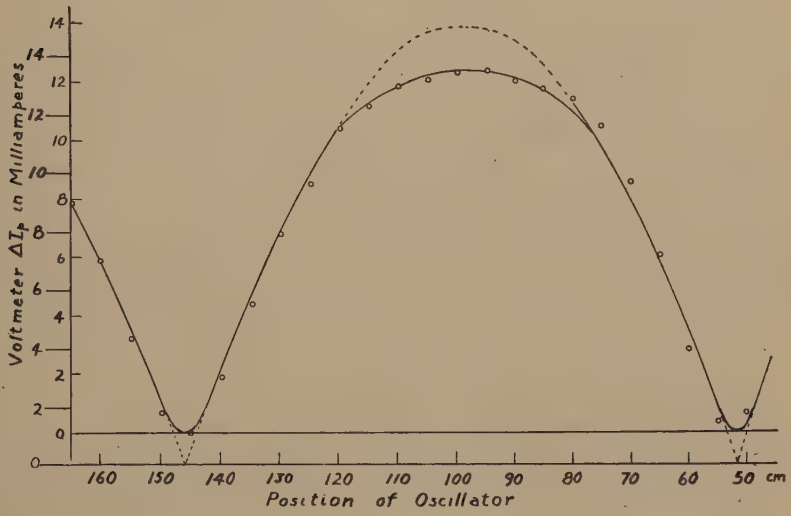

Fig. 10—High range voltmeter deflection as the oscillator was moved.

D. The Scale Factors for Current and Voltage Calibration Curves

For many ultra-high-frequency measurements it is sufficient to know the relative values of current and voltage. This is true, for example, in the measurement of reactance and resistance to be described in the following parts of this paper. It is possible to determine the scale factors for some milliammeters and voltmeters with reasonable accuracy. However, such a scale factor even if accurate to a high degree, has no great significance. Thus it seems clear that merely to insert a current reading or voltage reading device in an ultra-high-frequency circuit, must almost inevitably completely change the characteristics of that circuit. Furthermore, even if the current through the meter is known, a knowledge of the current in an adjacent part of the circuit is not thereby obtained. And if the voltage across a coil, say, is meas-

[11] *Loc. cit.*, Figs. 5 and 11.

ured, nothing about the voltage distribution is known except that one value. In general, therefore, precision measurements in the low-frequency sense have little significance at ultra-high frequencies.

The scale factor of a thermal milliammeter of the Weston model 425 type may be determined if the ultra-high-frequency resistance of the meter is available. Clearly, such a factor will in any case be true only for that frequency for which the resistance is known. The ultra-high-frequency resistances of thermal milliammeters were measured by a method to be described in Part IV. Since the heater wire in the resistance bridges of these meters is very fine, skin effect is not important. In fact, the effective ultra-high-frequency resistance of the heater unit alone, when this is removed from the meter case, differs from the low-frequency value chiefly in its radiation resistance. When the unit is mounted in the case, the effective resistance is somewhat increased due to capacitance in parallel. An examination of the construction of meters of this type reveals this immediately. The formula for the resistance R' at an angular frequency ω of a simple circuit consisting of a resistance R in series with an inductance L, and both in parallel with a capacitance C, is given by the following expression if $R<\omega L$:

$$\frac{R'}{R} \doteq \frac{1}{(1-\omega^2 LC)^2}. \tag{4}$$

Here R includes the radiation resistance. Similarly the current I_r through the inductive branch of the circuit is given by

$$\frac{I_r}{I} \doteq \frac{1}{(1-\omega^2 LC)}. \tag{5}$$

In this equation I is the algebraic sum of the currents through the two branches. Combining (4) with (5) gives

$$I_r/I = \sqrt{R'/R}. \tag{6}$$

Now, at low frequencies $I_r = I$, so that (6) gives the ratio of the current through the inductive branch at an angular frequency ω to the current at low frequency. This is the desired scale factor. From resistance measurements to be described later, this factor was found to be about 0.9 for the model 425 meter of range 250 milliamperes, and practically unity for the 125-milliampere meter, and for the heater unit alone of the 250-milliampere meter. Capacitance in parallel causes the meters to read somewhat high, whereas the radiated energy has a compensating effect, tending to make the reading too low. The net effect was to make these meters read slightly high. It is not to be expected that

such scale factors are extremely accurate; they do, however, represent the true order of magnitude.

To determine the scale factor of the symmetrical screen-grid voltmeter, or of any other device, the following theoretical considerations are pertinent. The voltage amplitude across an impedance Z_0 was given by (7), Part I, Section D. This formula is equally valid if the subscripts o and s are interchanged. Hence the current through an approximately lumped impedance Z_s is given by

$$|I_s| = \frac{E_x}{N} \frac{b_s}{\sqrt{b_0^2 + 1}} \left\{ \frac{1}{\alpha s + \frac{g_0}{1 + b_0^2} + \frac{g_s}{1 + b_s^2}} \right\}. \tag{7}$$

Taking the ratio of (7), Part I, Section D, and (7) above, one easily obtains

$$|v_0/I_s| = X_0 \sqrt{(N^2 + X_s^2)/(N^2 + X_0^2)}. \tag{8}$$

Thus, if a current meter with a known scale factor is available, the scale factor of the voltmeter may be obtained if the reactances of the two instruments at the ultra-high frequency concerned are known. The method consists simply in connecting the voltmeter across one end of the wires, and moving the current meter as a bridge (always with correctly adjusted tandem bridge) until a satisfactory deflection is obtained in both current meter and voltmeter. If the current is accurately known, the corresponding voltage is determined from (8). This, in conjunction with the relative calibration characteristics, completely determines the voltage scale of the device.

In conclusion it may be said that methods have been theoretically derived and experimentally carried out for determining the calibration characteristics of current and voltage indicators at ultra-high frequencies. The relative calibration curves are quite accurately obtained; the scale factor rather less precisely.

Part III—The Measurement of Reactance

The purpose of this part is to describe two methods for measuring reactances at ultra-high frequencies using the mathematical theory of Part I and the experimental technique of Part II as bases.

A. Reactance, Inductance, and Capacitance at Ultra-High Frequencies

The measurement of the reactances of coils and condensers at ultra-high frequencies is not unlike the problem of determining the reactance

of a complicated network of capacitances and inductances in various series and parallel combinations at low frequencies. If capacitive reactance is defined by $1/\omega C$, and inductive reactance by ωL, two problems present themselves. The first of these deals with the relative orders of magnitude of these two types of reactance. Thus, with $\omega = 10^9$, the reactance of capacitances as small as $C = 10^{-11}$ or $C = 10^{-12}$ farads or even smaller, is of the order of a few hundreds or thousands of ohms, whereas even at a radio-frequency such as $\omega = 10^6$, the reactance of the same capacitances would be measured in hundreds of thousands or millions of ohms. The inverse situation is true of inductive reactance. Small inductances of the order of 10^{-8} henrys have reactances at $\omega = 10^9$ of ten or more ohms, where at $\omega = 10^6$ these would be vanishingly small.

The second problem is a consequence of the fact that inductance and capacitance, in the usual low-frequency sense, are themselves functions of the frequency as this becomes sufficiently high. Inductance and capacitance both increase with frequency as a result of skin effect.[12] In general, however, reactances which are purely inductive or purely capacitive are extremely rare. Thus a coil, a variable condenser with its mountings and connecting leads, wires connected to binding posts, or placed near each other, all correspond to complicated low-frequency networks of inductances and capacitances in series and parallel combinations.

As a logical consequence of these considerations, it seems preferable to speak of inductive and capacitive reactance (or susceptance), rather than of inductance or capacitance at ultra-high frequencies. Reactance, like susceptance, is a quantity which definitely depends upon frequency, and which has a meaning only at a specified frequency. To be sure, it is customary in the case of some commercial bridges to speak of negative and positive inductance or capacitance. Some writers also seem to invite this terminology. Thus, Hund[13] defines the inductance of a coil with distributed capacitance by

$$L_e \doteq L/(1 - \omega^2 LC)$$

and Southworth[14] writes for the capacitance of a condenser with leads, the formula

$$C_a \doteq C/(1 - \omega^2 LC).$$

[12] *Cf.* Ollendorf, "Grundlagen der Hochfrequenztechnik," p. 45, Julius Springer, (1926).

[13] A. Hund, "High Frequency Measurements," p. 6, McGraw-Hill Book Co., (1933).

[14] G. C. Southworth, "Electric measurements at ultra-radio frequencies," *Rad. Rev.*, vol. 2, p. 30, (1921).

Both of these equations imply that when $|\omega^2 LC| > 1$, a condition which may very readily arise, the inductance L_e in the one case, or the capacitance C_a in the other become negative. In the present paper this terminology will be discarded as confusing and ambiguous. The above formulas will be written in the form:

$$X_e = X/(1 - \omega^2 LC)$$
$$B_e = B/(1 - \omega^2 LC)$$

where, now, the reactance or susceptance is inductive or capacitive depending upon whether the positive or the negative sign prevails.

The measurement of reactance using parallel wires is no new idea. It is referred to in most books on radio- and high-frequency measurements, usually under the separate headings of the measurement of capacitance and the measurement of inductance. It will become definitely clear from the reactance measurements to be discussed below, that a "capacitance" or an "inductance" measured at ultra-high frequencies using a parallel wire method (and this method is really useful only at such frequencies), has in almost every case little in common with the same inductance or capacitance measured at low frequencies. It is possible to measure reactance to a high degree of accuracy with the parallel wire system, but, as is characteristic of reactance, the value obtained is true only for the frequency at which it was determined, regardless of whether it be divided by ω and called inductance, or whether its reciprocal (with low resistance) be divided by ω and called capacitance—positive or negative. Furthermore, the reactance measured is the effective reactance across the parallel wires, including the capacitances to the wires, to binding posts, etc. The reactance is also assumed measured with a current loop at its electrical center.

The measurement of capacitance and inductance by a parallel wire method is briefly referred to by Southworth[14] and by Englund.[15] However, a detailed theoretical study of the method, a careful consideration of the approximations and conditions which it implies in its simpler form, and an extensive application to an examination of reactive circuits at ultra-high frequencies is not available. The present study, in conjunction with the preceding mathematical investigation, is intended to provide a brief but complete analysis of the theoretical and experimental problem.

B. The Measurement of Reactance

1. The Measurement of Wavelength

By moving a No. 20 copper wire bridge ($k = 2.2$ centimeters) in tandem with a second bridge at $\Lambda/4 - k$ along the parallel wires, maxi-

[15] Englund, "Wave limit of oscillations," Proc. I.R.E., vol. 15, p. 920; November, (1927).

mum voltage across Z_0 was indicated with the bridge at $x=210.7$ centimeters and at $x=116.3$ centimeters. Neglecting a very small correction for the velocity of propagation, $\Lambda/2=94.4$ centimeters, or $\beta=0.0333$. This wavelength, which corresponds to $\omega=10^9$, was retained throughout the following measurements. It was frequently checked, but found very constant.

2. The Determination of the Lengths $(S+n\Lambda/2)$ at which a Non-reactive Bridge Produces a Maximum Voltage Across Z_0.[16]

(a) Experimental method.

According to results previously obtained,[6] the distance between a first bridge placed at a point x_1 to produce maximum V_0, and a second identical bridge placed at a point x_2 beyond x_1 to reduce this maximum to a minimum, is given by

$$x_2 - x_1 = \Lambda/2 - 2k$$

where $k=L/l$, is the inductive shift or equivalent length of each of the two identical bridges. The length S is, then, given by

$$S = x_1 - x_0 + k.$$

Although the minimum obtained by moving the second bridge is reasonably sharp, using a No. 20 copper wire, it is nevertheless not easy to locate it accurately by merely shifting the bridge. A convenient way of determining this point is to plot the amplitudes in the neighborhood of the minimum using a sensitive scale on the ΔI_p milliammeter of the screen-grid voltmeter. This range is shown in Fig. 11. From the curve the minimum point is found to be at $x=206.4$ centimeters. Hence,

$$\begin{aligned} x_2 - x_1 &= 206.4 - 116.3 = 90.1 \text{ cm} \\ 2k &= 94.4 - 90.1 = 4.3 \text{ cm} \\ k &\doteq 2.2 \text{ cm}. \end{aligned}$$

To the nearest millimeter, therefore, the equivalent length of a No. 20 copper wire bridge five centimeters long is 2.2 centimeters. This is practically independent of frequency.

(b). Theoretical Method.

By definition $k=L/l$. Hence, by computing the self-inductance L of a straight round wire, and the inductance l per loop unit length of

[16] *Cf.* formula (10) and what follows in Part I, Section D.
[6] *Loc. cit.*, page 1174.

the wire system, k can be evaluated. From formula (131), Bureau of Standards Circular No. 74, one obtains

$$L = 0.0025[2.303 \log_{10}(4s/d) - 1]. \quad (1)$$

For the case at hand, s = length of bridge = 5 centimeters; d = diameter of wire = 0.081 centimeter. Then,

$$L = 0.045 \ \mu\text{h}.$$

From Table I, $l = 0.0193 \ \mu\text{h}$

hence, $k = L/l = 2.3$ cm.

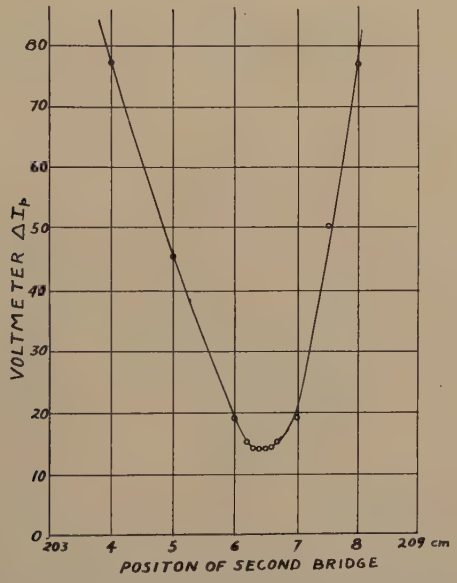

Fig. 11—The "dip" in the resonance curve using two No. 20 copper wire bridges for the determination of k for these bridges.

This result agrees reasonably well with the experimental value. A better agreement would hardly be expected, since the computed value does not take into account the corner capacitances of the bridge to the parallel wires. Since the experimental value is obtained by taking the difference between two readings, and since these were read only to the nearest millimeter, a difference of one millimeter between theoretical and experimental values is in any case small.

3. The Input Susceptance and Reactance of the Symmetrical Voltmeter

(a) Measurement of the input reactance and susceptance at a fixed value of the series capacitances C.

Since the end of the parallel wires is at $x_0 = 13.7$ centimeters on the tape scale, the input reactance of the voltmeter will be measured across this point. That is, the leads, capacitances, etc., beyond this point will be considered a part of the voltmeter.

For the particular value of C chosen for this case, the length S was given by

$$S = \Lambda/2 + 129.0 - 13.7$$

$$S = 20.9 \text{ cm}.$$

From formula (10), Part I, Section D,

$$NB_0 = -\cot \beta S. \tag{2}$$

With the above value of S this gives

$$NB_0 = -1.19$$

$$B_0 = -2.06 \times 10^{-3} \text{ mhos}$$

$$X_0 = -485 \text{ ohms}.$$

(b) Variation of the input reactance and susceptance with the capitances C in series with the tetrodes of the voltmeter.

The input reactance and susceptance of the voltmeter were computed for a wide range of values of the series capacitances in precisely the same way as for the type case above. The variation in the condensers is accomplished by turning up the upper plates, the lower ones being rigidly fastened to the control grids of the 224 tubes. This adjustment increases the plate separation, but simultaneously shortens the length of the telescoping threaded leads. It is clear, therefore, that the observed change in susceptance and reactance is not due to a change in the capacitances alone, but also to a change in the inductance in series with the condensers. If it is desired to estimate the change in capacitance of the condensers from the observed change in reactance or susceptance of the voltmeter, this can be done approximately by adding the separation of the plates to the observed value of S, computing the susceptance or reactance as before, and attributing the observed change to a variation in capacitance alone as is shown in Fig. 12.

4. The Measurement of the Reactance of Wires and Coils

Method (a). Low and intermediate reactances.

Reactances under about a thousand ohms may be measured conveniently using formula (11) of Part I, Section D. That is,

$$\tan \beta(s - S) = -X_s/N. \tag{3}$$

Before this formula can be used, the length S must be known for that particular input reactance of the voltmeter which is to be retained in the measurements. This can always be determined quickly and easily from the known equivalent length of the No. 20 copper wire bridge, and the position of a maximum using this bridge. When S has been determined, it is merely necessary to move the unknown reactance as

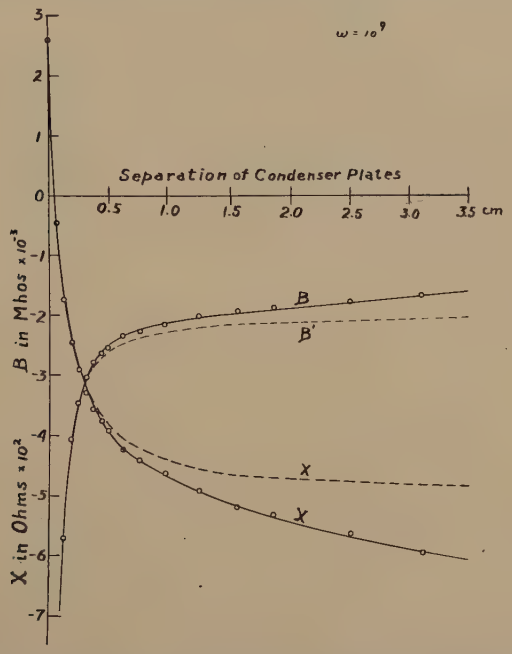

Fig. 12—Input reactance X and susceptance B of the symmetrical voltmeter as a function of the separation of the plates of the series capacitances C. X' and B' give the input reactance and susceptance, respectively, corrected to what they would be for changes only in the capacitances C, not including the change in inductance due to the shortening of the leads as the condenser plates are separated.

a bridge, (with properly adjusted tandem bridge), until a maximum deflection is observed in the voltmeter. If this maximum occurs at a value on the tape scale denoted by x_n, then $s = x_n - x_0$. The value of X_s is then at once obtained using the above formula and the known values of N and β. The reactances of a variety of wires and coils described in Table II and Fig. 13 were measured by this method. The results are tabulated in Table III.

Method (b). Intermediate and high reactances.

Method (a) presupposes that the effective resistance of the reactance which is to be measured is not so large that the voltage ampli-

TABLE II

DESCRIPTIONS FOR FIG. 13 AND TABLES III AND IV

Coil	Description
A	Rectangle of No. 20 bare copper wire, 5 × 10 cm.
B	Single turn of No. 18 insulated bell wire, 7.8 cm in diameter. Separation at bottom 1.6 cm.
C	Single loop of No. 18 insulated bell wire, 7.5 cm. in diameter; twisted once at the base.
D	Two turns No. 18 insulated bell wire, 7.5 cm in diameter. The turns are tightly taped together and twisted once at the base.
E	Ten turns No. 18 insulated bell wire; helix is ½ inch in diameter. The turns are spaced so that the coil proper is 3.1 cm long.
F	Five turns No. 18 insulated bell wire; helix is ½ inch in diameter. The turns are close together so that the coil proper is only 1.4 cm in length.
G	Five turns as for F but with the turns well spaced so that the coil proper is 3.1 cm long.
H	Nine turns No. 18 insulated bell wire tightly wound on a wooden cylinder 3.2 cm in diameter. The coil proper is 1.8 cm long; the leads are 2 cm long as shown in Fig. 1.
I	Rectangle of No. 20 bare copper wire, 10 cm × 10 cm.
J	Aluminum disk, 15 cm in radius. Short lengths of brass tubing are attached through two symmetrically placed holes in the disk. The parallel wires pass through these.

Thermocouple: Western Electric vacuum thermocouple; heater resistance 5 ohms; maximum safe current 75 ma. Used with Cambridge microammeter.
Meter 125: Weston radio-frequency thermal milliammeter, model 425; 125-ma range; resistance 4.5 ohms.
Meter 250: Same as above but 250-ma range; resistance 2.2 ohms.

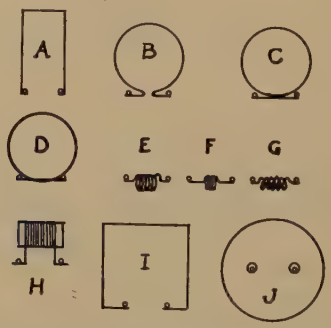

Fig. 13—Illustrations of coils and disk described in Table II; the small circles indicate the position of the parallel wires when the coils are connected in the support.

TABLE III

REACTANCES OF WIRES AND COILS

Wire or coil	Wire diameter	Measured Reactances in Ohms	
		Method (a)	Method (b)
Copper bar	1.27 cm	23.2	20.6
0.005-μf condenser		23.2	20.6
No. 12 copper wire	0.20	36.8	34.2
No. 20 copper	0.081	42.5	42.5
No. 32 copper	0.020	57.9	57.6
A		241	236
B		236	226
C		450	436
D		−283	−301
E		781	687
F		365	352
G		209	212
H		−730	−885
I		358	300
J		−34.8	

All values taken with $\lambda/2 = 94.4$ cm.
Distances are measured to the edge nearest the voltmeter.

tude V_0 is reduced to so small a value, that the maximum point is difficult to determine. In the case of coils made of copper wire, the effective resistance is primarily due to the distributed capacitance in parallel with the inductance. This simply means that coils which have large reactance because of this distributed capacitance, will also have correspondingly large resistance. If this is sufficiently large, Method (a) becomes unsatisfactory because of the small amplitudes and the breadth of the resonance peaks. On the other hand, coils which have a very high or nearly infinite reactance, cannot be measured by Method (a), even if the losses are low, without taking into account the impedance of the tandem circuit in parallel with the reactance of the coil to be measured. In either of these two cases, the following method is often useful.

Let the input susceptance B_0 of the voltmeter be measured across x_0 by the method described in Section 3(a) above. Then, let the unknown susceptance B_s be connected in parallel with the voltmeter across x_0. The susceptance of the combination is then determined by the same method as that used for the voltmeter alone. Let this be B_0'. Then,

$$NB_s = NB_0' - NB_0 = \cot \beta S - \cot \beta S'. \qquad (4)$$

The unknown susceptance is thus determined.

The reactances measured using Method (a) were remeasured by this method. The results are listed in Table III. It will be observed that they do not agree exactly with the previous ones, especially in the case of the higher reactances. This is due in part to the fact that the maximum amplitudes using Method (a) were very small for the large reactances because of their correspondingly high resistances. The resonance curves were, then, blunt, and the peak difficult to determine without plotting the curve. The differences in the results of the two methods are also due to a second, more significant fact. Although the same coils were used, their effective reactances in the two cases were not the same because of a slight difference in the circuit configuration. In Method (b), the coils were connected across the wires at x_0 by means of two small clips permanently fastened to the wires. In Method (a), the coils were simply placed in the wooden mount with no metallic connectors or clips. The effect of the clips used in Method (b) was to add a small capacitance from the clips to the adjacent turns of the coils; i.e., in parallel with a part of the inductance of the coil. The relative effect of this high reactance path was naturally greatest when the reactance of the coil as a whole was large. Evidently, if a given coil is to be used with binding posts, its reactance must be measured

with these in their correct positions relative to the coil. A small effect due to the parallel wires themselves, cannot be eliminated. But this usually is not important, since even if the reactance of the coil proper could be measured exactly, this measured value would not be quite correct for the same coil connected in any other circuit whatsoever.

Either of the two methods for measuring reactance is convenient and accurate. But it must not be forgotten that the reactance measured is the reactance of the entire circuit configuration. In Table IV a second set of reactance measurements is recorded. Some of the coils previously measured are included.

TABLE IV

REACTANCES OF WIRES AND COILS USING METHOD *a*.

Wire or coil	Wire diameter	Measured Reactance	Computed Reactance
No. 20 copper	0.081 cm	42.5 ohms	45.0 ohms
No. 32 copper	0.020	59.6	59.0
No. 20 Nichrome IV	0.081	44.4	45.0
No. 32 Manganin	0.020	59.6	59.0
No. 27 Advance	0.026	53.9	56.3
No. 35 Advance	0.014	62.5	62.4
No. 40 Manganin	0.008	66.0	68.1
Advance	0.005	73.5	72.7
No. 23 alloy	0.052	46.4	49.5
No. 21 steel	0.065	44.4	47.2
Coil A, vertical		234	
inclined toward voltmeter		189	
inclined away from voltmeter		250	251
Coil B, vertical		229	233
C		424	
D		−298	
E		746	
F		346	
G		210	
H		−810	
Thermocouple		162	
Meter 125		64.2	
Meter 250		64.2	
Meter 250, heater unit only		42.5	

All values taken with $\lambda/2 = 94.4$ cm. Distances read to nearest millimeter.

It is possible to check the measured values of reactance by comparison with theoretically computed ones in the simpler cases. These include straight wires of different diameter, single turn loops, and single turn rectangles. None of these calculated values takes into account "corner" capacitances, or capacitance to the parallel wires. The significance of this latter is brought out especially well in the measured values of the reactance of a rectangle inclined at different angles to the wires as recorded in Table IV. The measured reactance values of coils bring out very clearly the fact that reactance increases very much as the distributed capacitance is made larger by moving the turns nearer together.

5. Calibration of a Variable Condenser

The reactance of a small, five-plate General Radio variable condenser (rated at 15 micromicrofarads maximum) was measured first with the

shortest possible leads by Method (a); then with leads 3.5 centimeters long by both Methods (a) and (b). The reactance curves obtained are shown in Fig. 14. It is to be noted that the reactance becomes inductive even when the leads are as short as 3.5 centimeters, so that the condenser corresponds to a series resonance circuit.

In order to bring out the very significant effect on the susceptance of the condenser at ultra-high frequencies of the leads and mountings, the condenser was calibrated at a radio frequency (400 meters wavelength, or $\omega = 1.2 \times 10^5$). At this frequency the inductive reactance of the leads and mountings is negligibly small. Hence the value measured gives the actual static capacitance. By multiplying this by $\omega = 10^9$, one

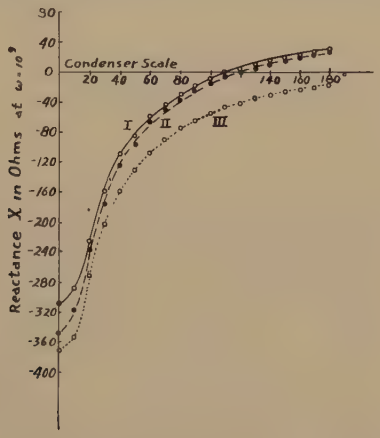

Fig. 14—Calibration curves of 5-plate variable condenser. I. Method *a*, 3.5-centimeter leads; II. Method *b*, 3.5-centimeter leads; III. Method *a*, short leads.

obtains the ideal susceptance of the condenser at that frequency without leads or extended mountings. In Fig. 15 this ideal susceptance is compared with the measured susceptance with the shortest possible leads (less than one centimeter), and the 3.5-centimeter leads. From these results it seems perfectly clear that any "capacitance" measured at ultra-high frequencies by dividing the susceptance by ω, has little or nothing in common with the static capacitance of the condenser. The parallel wire method usually employed is not a useful method for measuring capacitance; it is a very convenient and accurate method for measuring susceptances, small or large, at a definite ultra-high frequency.

6. Reactance and Susceptance of a Variable Length Coil

A small coil of variable reactance was constructed by winding 26 turns of cotton-covered wire of small diameter on a half-inch wood

dowel. By means of a wooden collar with a set screw, to which one end of the wire was fastened, the length of the coil could be varied by pushing the turns close together or pulling them apart. With the turns in close contact, the coil was 1.7 centimeters long. The reactance of this coil was measured using Method (b) for different lengths of the coil. The measured reactance and susceptance are plotted as functions

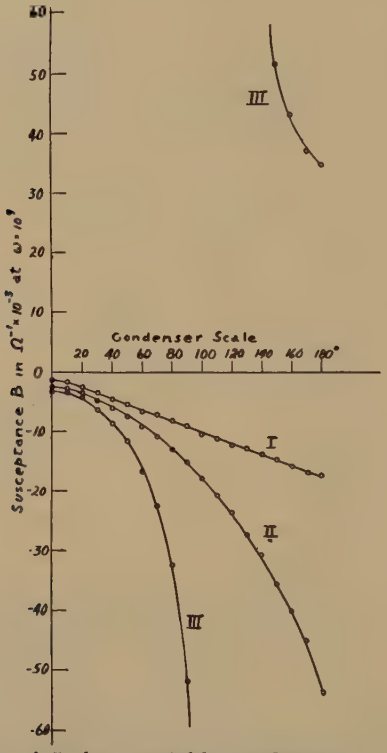

Fig. 15—Susceptance of 5-plate variable condenser. I. Ideal susceptance obtained by multiplying the capacitance measured at 400 meters by $\omega = 10^9$; II. Susceptance measured at $\omega = 10^9$, short leads; III. Susceptance measured at $\omega = 10^9$, 3.5-centimeter leads.

of the coil length in Fig. 16. The coil is seen to be an interesting parallel resonance circuit at this ultra-high frequency. Clearly a tuned coil of this sort may be adjusted to act as a high impedance choke coil at or near the natural frequency. Such a coil was used in the plate lead of the oscillator, as shown in Figs. 1 and 3. Here again it must be pointed out, that the reactance as measured is the effective reactance with the coil connected to the parallel wires across x_0 by means of the small clips already referred to. If connected in a different circuit con-

figuration, the effective reactance will necessarily differ somewhat from that shown in Fig. 16.

7. Interelectrode Susceptances of a 224 Tube

As a final reactance measurement, the interelectrode susceptances of a 224 tube were measured at $\omega = 10^9$. Since it was necessary to connect short lengths of wire to the tube terminals in order to arrange this in the mounting as a movable bridge, the measured reactances include the inductive reactance of these wires in series with the tube capacitances. A good approximation to the inductive reactance of these connecting wires is obtained by assuming them straight and using

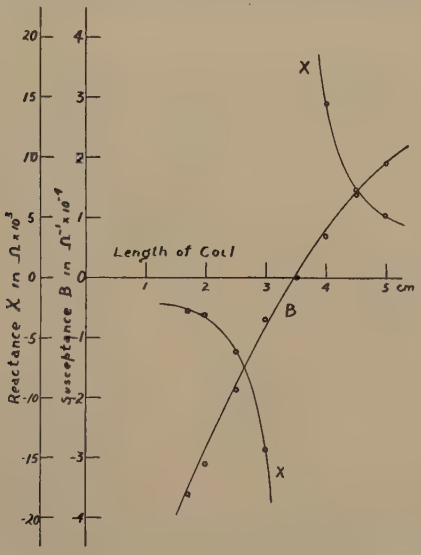

Fig. 16—Reactance and susceptance of single layer coil of variable length.

the measured value per centimeter of the size wire used. This reactance can then be subtracted from the measured interterminal reactances of tube and wires. This is done in Table V. From the resulting reactances it is simple to obtain the corresponding susceptances, since the resistance is small. If it is desired for comparison purposes, the susceptances so determined may be divided by ω and interterminal "capacitances" at this frequency obtained. This is also done in Table V.

C. Conclusions

Up to this point nothing has been said regarding the restrictions implied in the mathematical equations used in the computations. These are the restrictions of Special Case A of Part I, Section D. As a matter

of fact or good fortune, little need be said. The restrictions upon the wire system have already been shown to be easily satisfied in Table I of Part II. The conditions of the special case reduce essentially to the requirement that the reactance be large compared with the resistance. This is easily seen to be true; it will be definitely verified in Part IV when the resistances of the same coils are measured at the same frequency. The only exception is the case of the series resonance circuit, in which the reactance was made to vanish at one point. Actually, however, no measurements were taken at that point, and the continuity of the curves is sufficient to fix the value at small or vanishing reactances, where the equations are not quite such good approximations to experimental fact.

TABLE V

INTERTERMINAL REACTANCES OF 224 TUBE AT $\omega = 10^9$

Terminals	Measured Reactances	Length of Leads	Reactance of leads	Reactance between terminals	Susceptance between terminals	Susceptance divided by ω
	ohms	cm	ohms	ohms	mhos	
Plate-cathode	−95.0	3	27	−122	-8.2×10^{-3}	8.2×10^{-12}
Plate-screen	9.7	3.5	31.5	−21.5	−45.8	45.8
Screen-cathode	−46.4	3.5	31.5	−77.9	−12.8	12.8
Grid-screen	−21.2	8	72	−93.2	−10.7	10.7
Grid-plate	−114	8	72	−186	−5.4	5.4
Grid-cathode	−54.1	8	72	−126	−7.9	7.9

In conclusion it may be said that the parallel wire method outlined above and mathematically justified in Part I is a useful method for measuring reactances of all sizes at ultra-high frequencies. It is not a satisfactory method for measuring capacitance or inductance in the low-frequency sense; i.e., independent of frequency. Values of "capacitance" or of "inductance" obtained by dividing the measured ultra-high-frequency values of susceptance or reactance by ω are functions of frequency. In fact, they have a meaning only at that frequency at which the susceptance or reactance was measured. With reference to the accuracy of the measurements at a given ultra-high frequency, the following may be said. In the case of Method (a), the accuracy of the bridge setting depends upon the sharpness of the resonance peaks. This, in turn, is determined by the total resistance in the circuit. Since high reactances generally also have high resistances, the percentage error in measured reactances using a suitably designed wire system should be very low in so far as the actual experimental determination is concerned. In Method (b) the same statement is true if the reactance measured is sufficiently high or connected at a point such that the sensitivity of the voltmeter is not too much diminished. In both cases, however, the reactance measured is the effective react-

ance between the points on the wire system to which the unknown reactance is connected. Moreover, unless coils are very firmly wound and their connecting leads rigidly fixed, so that there is no possibility of even slight changes in their relative positions, the reactance may change as a result of handling the coils. This is seen by comparing the measured reactances in Tables III and IV of the same coils using the same method. Much of the difference in the results is due to actual changes in the reactances as a result of handling, connecting in position, etc. This was verified by taking successive readings for a given coil without removing it from its position across the wires, and then repeating the measurements each time removing the coil, and putting it back in place. In the first instance the bridge settings were consistently the same to the nearest millimeter, whereas in the second case they varied over several millimeters. Clearly, therefore, one may conclude that there is no great significance to be attached to precision measurements at ultra-high frequencies. Certainly the methods described are entirely adequate to measure reactances, and with reasonable precautions the results obtained will be accurate to within a few per cent even after the coil has been removed from its position in the wire system, and placed in another ultra-high-frequency circuit.

Part IV—The Measurement of Resistance

The purpose of this part is to describe methods for measuring low and high resistances and permeability at ultra-high frequencies.

A. Resistance at Ultra-High Frequencies

The effective resistance of a conductor or of a configuration of conductors at ultra-high frequencies differs from the low-frequency value as a result of several important factors. These will be discussed briefly in turn.

1. Skin Effect

The phenomenon of skin effect as a result of which current flows in an increasingly thin layer on the surface of conductors as the frequency is increased is analyzed in detail in many reference books.[14] The increase in resistance due to this effect is readily calculated for the case of straight, nonferromagnetic conductors of circular section. If the direct-current resistance of a given wire is denoted by R_0 and the resistance at an angular frequency ω by R, and a quantity q is defined by the relation

[14] *Loc. cit.*, p. 112.

$$q = 2\sqrt{\frac{\omega\mu}{R_0 \cdot 10^9}} \tag{1}$$

then the ratio, R/R_0 is obtained from tables and curves[17] as a function of q. For $\mu = 1$ and $\omega = 10^9$, (1) becomes simply

$$q = 2/\sqrt{R_0}. \tag{2}$$

Except in the case of the simplest circuit configurations, such as straight round conductors, the mathematical problem of skin effect becomes extremely complicated.

2. Capacitance in Parallel

In practically every ultra-high-frequency circuit the capacitive reactance between adjacent conductors, binding posts, and other circuit elements is sufficiently low, compared with the inductive reactance in parallel with it, to be significant. The effect of such a capacitance in parallel with the inductive parts of the circuit is to increase the effective resistance according to the approximate formula[13]

$$R = R_0/(1 - \omega^2 LC)^2. \tag{3}$$

3. Radiation

It has been pointed out by Brainard[3] that at ultra-high frequencies it is necessary to take into account energy radiated from circuit elements as well as the energy consumed in them in the form of heat. It was also indicated that this radiation resistance might be included conveniently in an effective resistance, although its nature is fundamentally different from ohmic resistance. The radiation resistance of a short, straight conductor in which the current distribution may be assumed uniform is given by the well-known Hertzian formula

$$R_r = 80\pi^2(s/\Lambda)^2 = 20\beta^2 s^2. \tag{4}$$

At high frequencies the radiation resistance of a conductor may be much larger than the ohmic resistance.

4. Current Distribution

At ultra-high frequencies current is a function of the linear dimensions of a circuit. Thus, for example, in a uniform coil of considerable length, there may be turns with a high current density, and others with a low current density if the circuit containing the coil is tuned to resonance. The energy dissipated in the form of heat and Hertzian waves from different parts of the coil will, then, not be the same. This

[17] Bureau of Standards Circular, No. 74, p. 309; Jahnke und Emde, "Funktionentafeln," p. 146.

effect can be illustrated experimentally in a most convincing manner. Let two small coils of resistance wire be connected opposite each other in the parallel wires of a Lecher wire system at a point, such that when the system is tuned to resonance by properly placing a bridge, a current maximum is set up across the coils. Let the voltage amplitude across (or the current through) one of the terminal impedances be read. Now let the same coils be connected in the parallel wire circuit at a point about a quarter of a wavelength removed from their former position, that is, at a current minimum. Suppose the circuit again tuned to resonance, (the adjustment will be found the same as before, if the coil turns are well spaced), and the voltmeter deflection recorded. By now comparing the two resonance amplitudes, it will be found that with the resistance coils at a current minimum, the voltage amplitude is practically the same as for a wire system of copper wire only, whereas the amplitude is very much reduced when the resistance coils are at a current maximum. The total series resistance, in the low-frequency sense, has remained unchanged by merely moving the resistance coils a short distance in the circuit; nevertheless the energy consumed in heat is entirely different in the two cases. Clearly, therefore, in measuring the resistance of a coil or other circuit element, it is essential to consider the current distribution, and not merely assume that the resistance is low because the energy consumed is small, where this may be due to the relative position of the element in the circuit. In the following resistance measurements it will be convenient to adopt the convention that the resistance of a coil or other circuit element is that resistance associated with the energy dissipated in, and radiated from it, when it is connected in a tuned circuit with a current loop at its center. That is, the position of the current loop is symmetrical with respect to the geometrical length of the coil or element. In particular, let resistance be defined as the resistance measured when the coil or element is placed across a pair of parallel wires as a bridge, and moved to a point at which a current loop is across the coil. This is indicated by a maximum deflection in a current or voltage indicator at the other end of the wire system.

5. High Resistance in Parallel

In using coils, condensers, and other circuit elements in ultra-high-frequency circuits, it is generally necessary and convenient to mount their terminals on a panel, bases, or supports of one kind or another. Such supports are naturally selected from insulators which have as high an effective resistance as possible. This means that a minimum amount of energy is consumed in leakage currents through the insula-

tor, or in molecular activity resulting from natural vibration periods of molecules or parts of complex molecules being approached by the ultra-high frequency concerned. In general, it is not at all a foregone conclusion that substances which are excellent insulators at low or radio frequencies, will be correspondingly good at ultra-high frequencies. It will be shown at a later point that considerable energy is consumed in such common insulators as wood, bakelite, paper, fiber, etc. This means that if a coil or other circuit element is connected between terminals mounted on such insulators, the measured resistance between the terminals is the effective resistance of the coil in parallel with the high resistance of the insulator. It can easily be shown that if a coil of reactance X in series with a low resistance R be shunted by a very high resistance R_m, the effective reactance X' and resistance R' are given by

$$X' \doteq X; \qquad R' \doteq R + X^2/R_m. \tag{5}$$

Hence, even though X be much smaller than R_m, it is clear that with R small, the term X^2/R_m may not be negligible as compared with R. Since the useful resistance of any circuit element is the effective resistance between its terminals, it follows that its resistance should be measured with its terminals mounted on the same material and in the same relative position as when the coil is in actual use in a given circuit. A small additional capacitance due to the parallel wires is unavoidable.

Summarizing this general discussion of resistance at ultra-high frequencies, it is important to bear in mind that the measured resistance between the terminals of a circuit element generally is determined by the direct-current resistance complicated by skin effect, capacitances in parallel, radiation, nonuniform current distribution, and high resistance in parallel.

B. The Measurement of Low and Intermediate Resistance

The measurement of the resistance component of impedances which satisfy the conditions of Special Case A, Part I, Section D, is based upon (7) of Part I, Section D. This equation may be written in the form

$$|V_0| = \frac{E_x}{\sqrt{b_0^2 + 1}} \left\{ \frac{1}{\alpha' s + \rho_0 + \rho_s} \right\} \tag{6}$$

where,

$$\rho_0 = \frac{g_0}{1 + b_0^2}; \qquad \rho_s = \frac{g_s}{1 + b_s^2}$$

$$\alpha' = \alpha + \frac{n\omega^4 s}{2N}. \tag{7}$$

If two different impedances Z_s' and Z_s'' are successively used as terminal impedances, then the ratio p of the maximum voltage amplitudes is given by

$$p = \left|\frac{V_0'}{V_0''}\right| = \frac{\alpha' s'' + \rho_0 + \rho_s''}{\alpha' s' + \rho_0 + \rho_s'}. \tag{8}$$

If the unknown conductance g_s' is to be determined from (8), all of the other quantities involved must be known. Even so, the equation is not very simple in form or convenient to use. It is, therefore, desirable to sacrifice a bit of rigor and precision for the sake of usefulness and convenience. In order to do this, let the following assumption be made. Let it be supposed that the length s at which the voltage amplitude $|V_0|$ becomes a maximum may be set equal to the fixed value S, (at which a zero reactance gives a maximum $|V_0|$), without thereby introducing a large error. If this is true, the entire quantity,

$$\gamma = \alpha' s + \rho_0 \tag{9}$$

is approximately constant. If this quantity, which depends entirely upon the wire system and the fixed impedance of the indicating device, is determined empirically, the following simple equation for the determination of ρ_s' results:

$$\rho_s' = \frac{1}{p}\left[\rho_s'' - \gamma(p-1)\right]. \tag{10}$$

To determine an unknown resistance from (10), it is necessary to know the value of γ, the experimentally measurable amplitude ratio p, and the quantity ρ_s'' of a standard impedance. If this standard is selected so that $b_s''^2 \gg 1$, then,

$$\rho_s'' \doteq R_s''/N. \tag{11}$$

This relation is true for straight conductors, as can be verified from Table IV of Part III. For the measurement of resistances (10) is a convenient and simple expression.

Before proceeding to make use of (10) to measure resistances, a few words are in order regarding the approximation made in obtaining (10) from (8). It might be supposed, indeed, that as a result of the assumption that the maximizing lengths s of unknown impedances are near S, that (10) is reasonably accurate for low reactances only. This is not

necessarily true. It may be noted that an impedance with a large reactive component generally has a correspondingly larger resistance component than an impedance with a small reactive part. This follows directly from the facts, that inductance and resistance of straight conductors both increase as the diameter of the wire is decreased, and that the effective resistance of a coil increases even more rapidly than the effective reactance, as the distributed capacitance is increased by moving the turns of the coil nearer together. This simply means that as s differs more and more from S with increasing reactance of the impedance concerned, ρ_s' will generally likewise increase, thus making the term $\alpha's$ less and less important. This compensating effect makes it possible to use (10) even for impedances with fairly large reactive components.

1. The determination of γ

To determine γ, the ratio of the maximum amplitudes obtained using two pieces of resistance wire as bridges is substituted in the following equation derived from (10):

$$\gamma = \frac{p\rho_s' - \rho_s''}{1 - p}. \tag{12}$$

The effective resistances of the two pieces of wire selected as standards were computed from formulas (2) and (4). The wires chosen were 5-centimeter lengths of No. 40 Manganin and No. 20 copper. Their effective resistances at $\omega = 10^9$ are

$$\begin{aligned} R_s'' \text{ (No. 40 Man)} &= R(\text{ohmic}) + R_r = 5.68 + 0.55 = 6.23 \text{ ohms} \\ R_s' \text{ (No. 20 Cu)} &= R(\text{ohmic}) + R_r = 0.066 + 0.55 = 0.62 \text{ ohms} \end{aligned} \tag{13}$$

From these,

$$\begin{aligned} \rho_s'' &= 1.076 \times 10^{-2} \\ \rho_s' &= 1.074 \times 10^{-3}. \end{aligned} \tag{14}$$

Upon substituting these in (12), one obtains

$$\gamma = 5.12 \times 10^{-3}. \tag{15}$$

2. The Measurement of Unknown Resistances

With the value of γ thus determined, the resistance component of any impedance can be measured, provided its reactive component is known, and a standard resistance is available. The measurement of reactance was discussed in Part III. For a standard resistance the computed value of 5 centimeters of No. 40 Manganin wire will be used. The formula for an unknown resistance derived from (10), (14), and (15) is

$$\rho_s' = (1/p)[1.076 \times 10^{-2} - 5.12 \times 10^{-3}(p - 1)] \quad (16)$$

where,

$$\rho_s' = \frac{g_s'}{1 + b_s'^2}; \quad (17)$$

or,

$$\rho_s' = R_s'/N \qquad \text{provided } b_s'^2 \gg 1. \quad (18)$$

In order to measure an unknown resistance, it is merely necessary to place it across the parallel wires as a bridge with a properly arranged tandem bridge. It is then adjusted to the point nearest S at which the voltmeter deflection is a maximum. The same process is repeated using the standard No. 40 Manganin wire. The ratio of the observed deflections (corrected to a linear voltmeter characteristic) gives p. It is, of course, advisable to average a number of readings. The usual precautions to avoid close coupling with the oscillator must also be taken.

TABLE VI
MEASURED RESISTANCES OF WIRES (5-CM LENGTHS)

Wire	Measured Reactances X	Measured Resistances R	$R - R_r$	Computed Resistances	Direct-Current Resistances
No. 40 Manganin	66.0 ohms	6.23 ohms	5.68 ohms	5.68 ohms	5.30 ohms
No. 20 copper	42.5	0.63	0.070	0.066	1.74×10^{-3}
No. 32 copper	59.6	0.85	0.30	0.26	2.62×10^{-2}
No. 20 Nichrome IV	44.4	1.17	0.62	0.53	0.101
No. 32 Manganin	59.6	2.35	1.80	1.60	0.73
No. 27 Advance	53.9	1.80	1.25	1.15	0.46
No. 35 Advance	62.5	3.25	2.70	2.32	1.50
Advance (0.005 cm)	73.5	13.2	12.65	12.25	12.05

All values taken at $\Lambda/2 = 94.4$ cm.
$R_r = 0.55$ ohms per 5 cm.

In Table VI are listed the measured resistances of 5-centimeter lengths of a variety of nonmagnetic wires, together with the computed values from skin effect and radiation formulas and the direct-current resistances. The agreement is reasonably good over the rather wide range of resistances measured. In Table VII are listed the measured resistances of the coils, the reactances of which were measured in Part III. A description of the coils was given in Table II and Fig. 13 of Part III. In measuring the coil resistances, the coils were all mounted on the wooden support previously used in measuring their reactances. The measured resistances, therefore, include the X^2/R_m values, where R_m is the effective resistance of the wooden support. (This term was negligible in measuring the resistances of straight wires, since the reactances of these are relatively low.) If it had been desired to mount any of the

TABLE VII

MEASURED RESISTANCES OF COILS AND METERS

Coil*	Measured Reactances	Measured Resistances	$R-R_r$**
A	235 ohms	1.29 ohms	
B	228	1.26	
C	435	6.74	
D	−296	12.2	
E	735	8.0	
F	355	2.76	
G	209	1.30	
H	−807	35.2	
Thermocouple	162	10.6	
Meter 125	64.2	5.9	5.3
Meter 250	64.2	3.6	3.0
Meter 250, unit only	42.5	2.9	2.3

All values taken at $\Lambda/2 = 94.4$ cm.

* For descriptions of coils see Table II and Fig. 13 of Part III.

** The energy radiated from the heater units is roughly the same as that radiated from a straight wire of the same length. The value $R-R_r$ is given to permit comparison of the ohmic resistances at ultra-high frequencies and at low frequencies as given in Table II.

coils permanently on, say, a bakelite panel, the resistances would have been measured with the coils mounted on a piece of the same bakelite. There is no check on the measured values of coil resistances other than the good agreement obtained in the case of the straight conductors covering about the same range of resistances. It may be concluded that the results are at least relatively correct, and of the right order of magnitude.

C. The Measurement of Permeability of Ferromagnetic Wires

The measurement of permeability follows directly the measurement of resistance. Thus, if the ultra-high-frequency resistance R of a given 5-centimeter length of a ferromagnetic wire is measured as described above, the ratio R/R_0 is at once available. From tables or curves[17] the value of q in (1) is obtained. Then (1) may be solved for μ, the desired permeability at the frequency ω. The current amplitude through the wire may be determined by a method described in Part II. In Table VIII are listed the measured resistances of 5-centimeter lengths of an iron-alloy wire, and of a steel wire. These were measured simultaneously with those of the wires listed in Table VI. The permeability was computed in each case by the method outlined above.

TABLE VIII

PERMEABILITY OF WIRES

Wire	Measured Reactances X	Measured Resistances R	$R-R_r$	D-C Resistances R_0	R/R_0	Commuted Permeability μ
No. 23 alloy	46.4 ohms	3.0 ohms	2.45 ohms	0.114 ohms	21.4	20.5
No. 21 steel	44.4	2.44	1.89	0.0213	88.5	63.0

All values taken at $\Lambda/2 = 94.4$ cm. X and R are per 5-cm lengths of wire.

D. The Measurement of Very High Resistance

The measurement of very high effective resistances depends upon (18) of Special Case B, Part I, Section D. This formula gives the maximum voltage amplitude obtained across Z_0 by moving a very high resistance, R_m, $(g=NG\doteq N/R)$, attached across the ends of a pair of parallel wires of continuously adjustable length. Here, as before, the requirement of adjustable length is inconvenient and undesirable. But, since R_m is a very high resistance, it is clear that even the maximum input impedance of a secondary or tandem section of parallel wires would certainly not be large compared with R_m. It might, indeed, easily be considerably smaller. Without carrying out the analysis in detail, it can be shown that if a tandem adjusted to maximum input impedance is used in parallel with a high resistance R_m, then the maximum voltage amplitude is given by the following expression:

$$|V_0| = \frac{E_x}{\sqrt{b_0^2+1}} \left\{ \frac{1}{\alpha' s + \rho_s + \rho_0 + g_m} \right\}. \tag{19}$$

Here the length s is the distance along the parallel wires between Z_0 and Z_s, where now Z_s is the second, or tandem, bridge of equivalent length k. The high resistance R_m is placed across the wires at a distance, $s-(\Lambda/4-k)$, from Z_0. It will be observed that this differs from all previous measurements using a tandem bridge. In these, the distance s was measured from Z_0 to the first bridge Z_s, while the tandem bridge was placed at a distance, $s+\Lambda/4-k$, from Z_0.

If the resistance R_m is infinite, i.e., no bridge is placed across the wires at $s-(\Lambda/4-k)$, then g_m in (19) vanishes. Hence the ratio of amplitudes without a high resistance R_m and with such a resistance is given by

$$\left| \frac{V_0'(R_m=\infty)}{V_0''} \right| = p = \frac{\alpha' s'' + \rho_0 + \rho_s + g_m}{\alpha' s' + \rho_0 + \rho_s}. \tag{20}$$

Now, since R_m is large so that its reactance is negligible as required by the restrictions of Special Case B, Part I, Section D, the length s must necessarily be $S-k$, and hence, since k is small, the approximation implied by (9) is satisfied. Then (20) becomes

$$p = 1 + \frac{g_m}{\gamma + \rho_s}. \tag{21}$$

This can be solved directly for R_m as follows:

$$R_m = \frac{N}{(1-p)(\gamma+\rho_s)}. \tag{22}$$

This is a convenient expression for evaluating R_m from the known value of γ and a known resistance factor ρ_s.

Using this expression, the resistances R_m of various grid leaks and dielectrics were measured. The results are listed in Tables IX and X. The effective resistance of the wooden support used in measuring the resistances of wires and coils is also given.

TABLE IX

EFFECTIVE RESISTANCES OF DIELECTRICS AT $\omega = 10^9$

Description of Dielectric (5-cm lengths)	Measured Resistances in Megohms
1/2" wood dowel (1.25 cm)	0.21
3/8" wood dowel (0.90 cm)	0.37
1/4" wood dowel (0.65 cm)	1.4
3/16" wood dowel (0.44 cm)	2.3
1/2" dowel with 1/4" hole	0.45
3/8" dowel with 1/8" hole	1.1
3/4" bakelite cylinder	1.45
Clear bakelite, 3/4" = 5/8" laid flat	0.25
Same, laid on edge	0.33
Hollow fiber tube, 1/2"	0.022
1/2" glass tube	∞
Wooden support for wires and coils with short strips of wire in place	0.08

TABLE X

EFFECTIVE RESISTANCES OF HIGH RESISTANCE LEAKS AT $\omega = 10^9$

Description of Leaks	Measured Resistances in Megohms
Blank filing card, 1½ × 4 cm with copper contacts	1.8
Same with very fine pencil line between contacts	1.8
Same with medium fine line	0.48
Same with heavy line	0.29
Same with medium fine line of India ink	0.85
Same with heavy ink line	0.72
Copper contacts hung from wires (The lines are 3 cm long)	∞

The experimental method consisted simply in placing the high resistance to be measured across the wires with a tandem adjusted to a maximum input impedance rigidly fastened to it. The bridges were then moved until the deflection of the voltmeter was a maximum. This was repeated with the high resistance removed. The ratio of the amplitudes (corrected to a linear scale) gave p. (A second tandem bridge beyond the first one was also used for obvious reasons.)

There seems to be no way to check the measured high resistances, since comparison with low-frequency values cannot give even a rough estimate. Thus, even in the case of pencil line grid leaks, the losses in the small piece of card upon which the lines were drawn, constituted an effective resistance comparable to the leakage resistance of the line itself. This is clear from Table X. In any case, the results obtained give an excellent measure of the relative effective resistances of dielectrics and leaks, and it seems reasonable to conclude that the order of magni-

tude is correct, even though there is no positive assurance that the numerical values obtained are not in considerable error.

E. Conclusions

This part of the present paper presents, to the best knowledge of the writer, the first theoretically derived and experimentally demonstrated method for measuring the effective resistances of circuit elements at ultra-high frequencies. The experimental technique and the formulas involved are relatively simple; the results obtained, though not accurate in the sense of low-frequency measurements, certainly provide excellent data for the intercomparison of resistances. The order of magnitude is without doubt correctly measured. In view of the great complexity of the physical problem of measuring resistances at ultra-high frequencies due to the number of parameters and variables which are concerned, the mathematical and experimental solutions seem very satisfactory.

Part V—The Analysis of Complex Frequencies

The purpose of this part is to describe a method for determining the component frequencies and their relative amplitudes in a complex oscillation.

The mathematical analysis and the methods of measurement described in the preceding parts depend upon the assumed sinusoidal driving electromotive force of the form

$$e = E \cos \omega t. \tag{1}$$

If the electromotive force is a function of several frequencies, it must be analyzed, since measurement of current, voltage, reactance, and resistance can be made only at one specified frequency. Thus, if

$$e = \sum_{i=0}^{n} E_i \cos \omega_i t \tag{2}$$

it follows from the principle of superposition[18] that the mathematical analysis carried out for a single frequency is true for each frequency independent of all others. The complete solution in any case involving several frequencies is then obtained by superposing the solutions for the individual frequencies.[19] Accordingly, resonance curves correspond-

[18] See, for example, Bush "Operational Circuit Analysis," p. 22, John Wiley and Sons, (1929).

[19] This presupposes systems characterized by linear differential equations with constant coefficients. It was shown in Part I, Section A that the long-line equations at ultra-high frequencies might be assumed approximately linear for the parallel wire system, and the solutions obtained depended upon this assumption.

ing to those described for a single frequency[6] must exist simultaneously for each frequency present in a complex oscillation, and the composite resonance curves in any given case must consist of a family of such curves for each frequency.

Resonance curves corresponding to those[6] of Special Cases 1, 2, and 3b will now be displayed for a driving electromotive force consisting of a fundamental and a second harmonic.

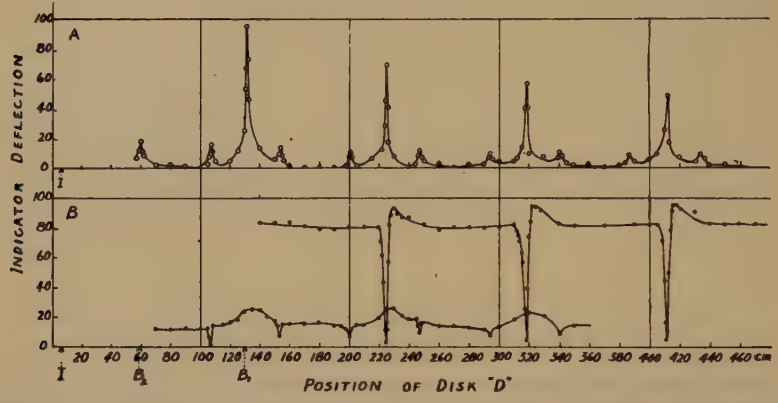

Fig. 17—A. Amplitude characteristics of type Special Case 3b for a fundamental with second harmonic. The curves were obtained by moving a low impedance bridge (disk) along the parallel wires.

B. Amplitude characteristics of type Special Case 2 for a fundamental with second harmonic. The curves were obtained by fixing one bridge (copper wire) at one peak, and then moving a second bridge (disk) along the parallel wires. The upper curve for the fundamental has the fixed bridge at B_1; the lower curve for the harmonic has the fixed bridge at B_2. For both A and B the oscillator was fixed at scale point 50 centimeters; the voltmeter was at the point marked *I*. The observed amplitudes as plotted are not corrected for the lower curvature in the voltmeter characteristic.

1. Special Case 3b

In Fig. 17 A are shown the experimentally determined resonance curves of this type. They were obtained by moving a low impedance bridge[20] along a pair of parallel wires, and recording the deflection (ΔI_p) of the screen-grid voltmeter connected across the wires at the

[6] *Loc. cit.*, Special Cases 1, 2, and 3

[20] When more than one frequency is involved it is not possible to use a tandem bridge to eliminate the effect of the secondary length of parallel wires, since the length of a tandem circuit cannot be adjusted to offer maximum, or even a high, impedance, to more than one frequency at a time. For this reason the aluminum disk (coil J in Table II of Part III) was used as a bridge. Although not a perfect screen because of its finite dimensions (a disk of very large radius acts as a perfect screen as is theoretically proved by Frenkel, "Lehrbuch der Elektrodynamik," vol. II, p. 398) the disk could be used very satisfactorily and conveniently with a little care to insure a detuned secondary. It was found that a secondary length reacted upon the primary only weakly and over a very short variation in secondary length near $\Lambda/2 - k_1 - k_2$. Here k_1 and k_2 are the equivalent lengths of the disk (negative) and the bridge (positive).

point marked *I* in Fig. 17. The oscillator generating the complex frequency was loosely coupled to the wires with its center at the 50-centimeter point on the tape scale.

2. Special Case 2

In Fig. 17 B are shown the resonance curves of this type for both fundamental and second harmonic. It is interesting to note that in the curve for the harmonic there is a small but unmistakable increase in amplitude at the points where the fundamental normally has its peaks. The filter action of the single circuit tuned to the harmonic is thus seen to be not quite perfect.

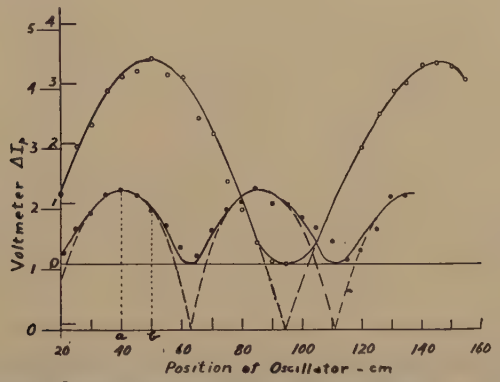

Fig. 18—Amplitude characteristics of type Special Case 1 for the fundamental and second harmonic. They were obtained by moving the oscillator with suitably fixed bridges. The true cosine curves for a linear calibration characteristic are shown dotted.

3. Special Case 1

The curves of this type for both fundamental and second harmonic are shown in Fig. 18. In accordance with the theory of Part II, the observed curves of Fig. 18 were corrected for the lower curvature in the voltmeter calibration characteristic. The true cosine curves for a linear characteristic are drawn dotted in Fig. 18.

The half wavelengths of the frequencies present are obtained by averaging the distances between those peaks in Fig. 17 A which belong to one frequency. To determine which belong together, if there is any doubt, the curves of Fig. 17 B may be used. Here there is a corresponding minimum for every peak in Fig. 17 A, and for a given adjustment of the fixed bridge, minima will occur only for a single frequency. In Table XI are listed the positions and observed voltmeter deflections for the different maxima of Fig. 17 A. The corrected amplitudes are also given.

TABLE XI

ANALYSIS OF FUNDAMENTAL WITH SECOND HARMONIC

Fundamental Peaks

Scale	Difference	Observed Amplitude	Corrected Amplitude
131.6 cm		1.05 ma	2.15 ma
225.1	93.5 cm	0.77	1.87
318.7	93.6	0.62	1.72
412.1	93.4	0.53	1.63

Av. 93.5 cm = A/2

Harmonic Peaks

Scale	Difference	Observed Amplitude	Corrected Amplitude	Corrected Amplitude Times a/b
60.2 cm		0.20 ma	1.10 ma	1.29 ma
107.1	46.9 cm	0.17	1.00	1.18
154.0	46.4	0.14	0.92	1.08
200.5	46.5	0.13	0.90	1.06
247.0	46.5	0.12	0.88	1.03
294.0	47.0	0.10	0.80	0.94
340.0	46.0	0.11	0.83	0.97
387.5	47.5	0.09	0.68	0.80
434.5	47.0	0.09	0.68	0.80

Av. 46.8 cm = A/2

Ratio a/b from Fig. 18 is 1.17

In order to determine the true relative amplitudes of the fundamental and second harmonic in the oscillator, two steps are necessary. The first of these is to determine the true relative amplitudes of the two frequencies on the wire system. This is done in Fig. 19, where the corrected amplitudes of the observed peaks are plotted to an arbitrary abscissa scale having the half wavelength of the second harmonic for its unit. Smooth curves (which have no experimental significance) are drawn through the two sets of points. The ratio of the ordinates of these curves for any value of abscissa gives the true amplitude ratio of the two frequencies on the parallel wire system. The second step, viz., to determine the amplitude ratio of the two frequencies on the oscillator, depends upon Fig. 18. Due to the fact that the current loops of fundamental and second harmonic are linearly shifted in phase on the oscillator, it is not possible to fix the oscillator at a point relative to the wires at which the amplitude of both frequencies induced on the wires will be a maximum. With the oscillator at the scale point 50 centimeters, the induced amplitude of the fundamental is a maximum, but that of the harmonic is less than maximum by a factor equal to the ratio of the ordinates at b and a in Fig. 18. Hence, by multiplying the amplitudes of all harmonic maxima by the ratio of the ordinates a/b, the required correction is made, and the true relative amplitudes of the

two component frequencies generated by the oscillator are obtained. This is carried out in Table XI. From the results of Table XI it is possible to write the equation for the driving electromotive force in the form

$$e = E[\cos \omega t + 0.52 \cos 2\omega t]; \quad \omega = 1.01 \times 10^9. \qquad (3)$$

The frequencies and the maximum relative amplitudes are given by (3), but phase angles are omitted.

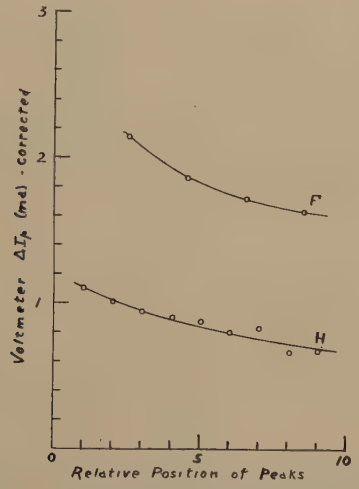

Fig. 19—Relative amplitudes of fundamental and harmonic maxima on the parallel wires. The abscissa scale is in units of the harmonic half wavelength.

The same method was successfully applied to carry out the analysis of a double oscillator generating simultaneously two fundamentals with their respective second harmonics. The amplitudes differed widely. It is, of course, not necessary to plot the complete resonance curves in making such an analysis. The composite frequency of the double oscillator was found to be,

$$e = E(\cos \omega_2 t + 0.42 \cos 2\omega_2 t + 0.49 \cos \omega_1 t + 0.08 \cos 2\omega_1 t)$$
$$\omega_1 = 0.68 \times 10^9; \qquad \omega_2 = 0.78 \times 10^9. \qquad (4)$$

With the components thus determined it is not difficult to separate the desired frequency from the others, and to carry out any of the measurements discussed in the preceding parts.[21]

The present paper has laid the fundamental mathematical and experimental foundations for electrical measurments at ultra-high fre-

[21] A similar analysis of the well-known central scientific demonstration 3.5 meter oscillator reveals a very strong second harmonic.

quencies using the parallel wire method. Only the salient points have been outlined, and no attempt has been made to take precision measurements. The emphasis has been placed on the development of useful methods and on their theoretical justification. Much refinement in the technique of measurement is certainly possible. But useful methods and a theoretical understanding of such methods, and of the approximations they involve must be made available first.

Acknowledgment

This investigation was carried out in the academic year 1933–1934 at the University of Wisconsin. It was supported in part by the Wisconsin Alumni Research Foundation, and in part by the Department of Electrical Engineering. The writer is indebted to the Foundation and to Professor Edward Bennett, Chairman of the Department.

Proceedings of the Institute of Radio Engineers
Volume 23, Number 8 *August, 1935*

A BROADCAST ANTENNA FOR "LOW ANGLE" RADIATION*

By

J. W. Labus

(Deutsche Technische Hochschule, Prague, Czechoslovakia)

Summary—*The present trend in broadcast engineering is to build transmitting antennas with reduced radiation at high angles of elevation. This increases the coverage of transmitters, within which no appreciable amount of "short range fading" takes place. A novel antenna of this kind is described below. It consists of a vertical radiator combined with a horizontal shield located near its top.*

In this paper both an experimental and a theoretical investigation of such an antenna are presented. The experiment was performed on a small scale model at a wavelength of five meters. A number of different antennas were tested having shields of various diameters located at various heights above ground. Their vertical plane field patterns were compared with the pattern of a vertical wire, a quarter of a wavelength long.

The experiment, as well as the theory, indicates that the current in the shield must be properly controlled in order to obtain the desired field pattern. Practically, this condition is met if the radius of the shield is such that the latter oscillates at its natural wavelength (current node in the center of the shield), and if the shield has a certain height above ground. Both from experiment and theory it is found that good results are obtained, even if the height is less than a quarter of a wavelength, which, from the point of cost, is a very important fact.

Introduction

FOR several years, it has been known that short range fading has limited the primary service area of broadcast stations. The generally accepted theory is that interference between the ground wave and the sky wave produces the observed fading phenomenon. While the ground wave is propagated along the earth's surface, the sky wave is emitted from the antenna at higher angles of elevation above ground and is reflected down to earth at some distance from the transmitter. The most severe fading occurs where the sky wave and the ground wave are approximately equal in intensity. This distance depends, to a great extent, on the attenuation of the ground wave and the vertical angle of radiation of the sky wave. On the average, the fading is generally most severe at a distance of the order of 100 kilometers from the transmitter.

In order to reduce this fading, or to extend the distance at which it occurs, it is necessary to increase the ratio between the ground wave

* Decimal classification: R120×R320. Original manuscript received by the Institute, July 25, 1934; revised manuscript received by the Institute, November 30, 1934.

and the sky wave. One method of attack is to design the transmitting antenna for so-called low angle radiation.[1]

Low angle radiation can be obtained by at least two methods: (1) by proper choice of the height of a vertical antenna; and (2) by arrays, whose radiation when added to the field of a short vertical antenna will produce the desired field pattern.

Several antennas of the first type are already in operation. Their heights vary between one quarter and three quarters of a wavelength. Therefore, for the longer wavelengths used for broadcasting, the cost becomes prohibitive.

In this paper we shall be concerned with an antenna, pertaining to the second type, which had been suggested by the author and investigated in 1930 at the South Schenectady station of the General Electric Company. This antenna consists of a vertical radiating wire and a horizontal shield or disk, suspended at a certain height (A) above ground (Fig. 1). In the discussion that follows it is frequently

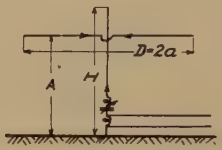

Fig. 1—Arrangement of a shield antenna.

referred to as an array. In order to obtain adequate design data, this antenna was investigated both experimentally and theoretically. Because of the low construction costs of a small scale model the experiment was performed at a wavelength of five meters. This incurred an undesirable complication due to the earth not being perfectly conducting. The mathematical part of this paper assumes perfect conductivity. This of course is approached only when the soil is fairly wet or the frequency is relatively low. How much the actual operating conditions will depart from this simple assumption, will, of course, depend on the wavelength and the nature of the ground as well. The currents in the shield are assumed to be known and to be controlled arbitrarily. However, in the greater part of the experiment the shield was excited through induction. The magnitude of the current is unknown.

[1] O. Böhm, *Hochfrequenz. und Elektroakustik*, Bd. 42, p. 137, (1933). P. P. and T. L. Eckersley and H. L. Kirke, *Jour. I.E.E.*, vol. 67, p. 507, (1929). A. Meissner, Proc. I.R.E., vol. 17, p. 1178; July, (1929). S. Ballantine, Proc. I.R.E. vol. 22, p. 564; May, (1934). C. A. Nickle, R. B. Dome, and W. W. Brown, "Control of Radiating Properties of Antennas," Proc. I.R.E., vol. 22, p. 1362; December, (1934).

Experiment

By means of a calibrated receiving doublet the vertical component of the field strength was measured at a horizontal distance of about one and three-fourths wavelengths away from the antenna. Throughout the experiment the height of the vertical radiating wire was a quarter of a wavelength. At its lower end it was connected to a system of sixteen ground wires, each 1.45λ long. The coupling of the transmission line and the tuning of the antenna are shown schematically in Fig. 1. The transmission line consisted of four diametrical wires (RCA system), so as to insure small radiation from the line. The shield was built up of sixteen radial wires. In some cases the several ends of the wires were open (type S_1). In other cases they were connected by means of a wire (type S_2).

Fig. 2—Experimental vertical field patterns of a plain vertical antenna ($H = \lambda/4$). These patterns were taken at a wavelength of five meters.

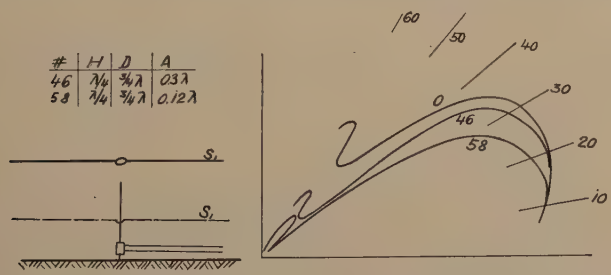

Fig. 3—Experimental vertical field patterns of a shield antenna having a shield diameter of 0.75λ. Shield at various heights, fed by induction.

Discussion of Results

The results of the measurements are shown graphically in Figs. 2 to 7. The field strengths are plotted against the angle of elevation (ψ). Difficulties encountered at short waves made it desirable to measure the field patterns of a number of various arrays and compare them with the pattern of an ordinary vertical antenna a quarter of a wavelength long. As seen in Fig. 2 the latter departs from the pattern of a

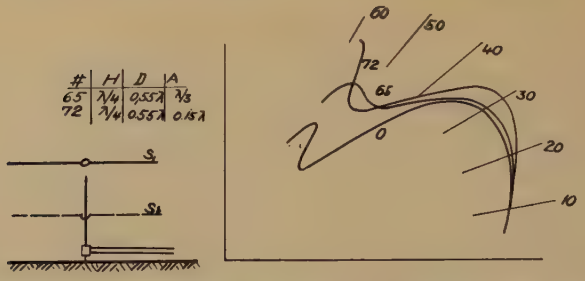

Fig. 4—Experimental vertical field patterns of a shield antenna having a shield diameter of 0.55λ. Shield at various heights, fed by induction.

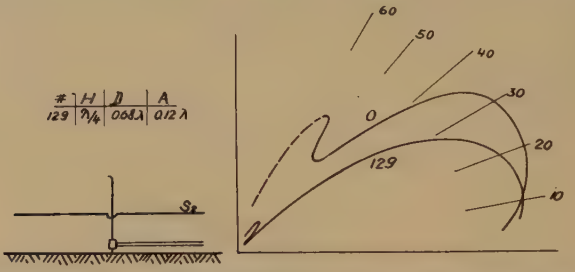

Fig. 5—Experimental vertical field pattern of a shield antenna having a shield diameter of 0.68λ. Shield 0.12λ above ground, fed by induction.

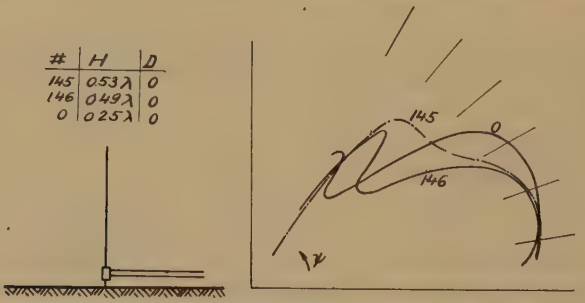

Fig. 6—Experimental vertical field patterns of a vertical antenna ($H > \lambda/4$).

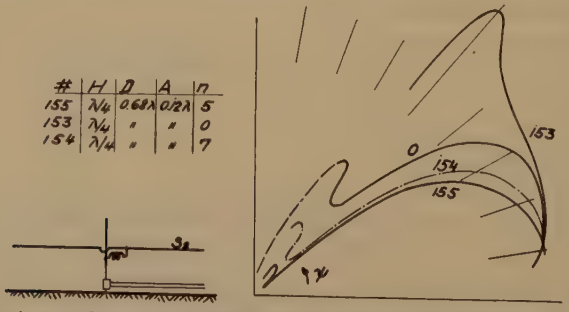

Fig. 7—Experimental vertical field patterns of a shield antenna. The shield is connected across a tuning coil of n turns.

short antenna operated at long waves (which approximately is a semicircle) in that it has a dip at a certain angle (of about 50 degrees) of elevation and the maximum field strength is not in the horizontal direction ($\psi = 0$). This is due to the finite conductivity of the ground as a result of which the refractive index becomes complex at these high frequencies.

Out of a great number of measurements taken with various arrays and at different times, only a few, which are particularly significant, are illustrated. The necessary explanations are given on the figures and in their captions. For purposes of better comparison the field pattern of the plain vertical wire is plotted on each diagram and designated by (0). The other numerals given on the figures refer to the numbers of the tests. Fig. 6 shows the variation of the pattern of a plain vertical antenna with heights greater than a quarter of a wavelength. In the tests shown in Figs. 3 to 5, the shield was not connected to the vertical wire. Instead it was excited by induction and without any tuning within the shield itself. In these cases the shield is most effective, only when it oscillates near its natural frequency. Under this circumstance there will be a node of current in the center of the shield. The experiment shows that this occurs at a diameter of about $2a/\lambda = 0.68$ to 0.75, depending on the type of the shield (S_1 or S_2).

Good results were also obtained by feeding the shield from the vertical antenna and using tuning coils as a medium of connection. (See Fig. 7.) It is interesting to note that in cases, where the shield was directly connected to the antenna (see for instance test No. 153) the vertical radiation increased materially instead of decreasing. This is because the shield is excited in a wrong phase as will be shown in the theoretical part of this paper. In practice the current flows from the vertical wire into the shield, whereas according to the theory the opposite direction of the shield current is necessary. Several tests were performed with excitation of the shield directly from the transmission line but finally coils were inserted between the antenna and the shield thereby making tuning possible.

From the tests described above it can be concluded that even at short wavelengths where ground conditions are unfavorable the shield antenna tends to produce the desired field pattern. Furthermore, it becomes evident that one of the most important factors is the phase of the shield current. If the shield is fed inductively, the diameter of the shield as well as the height above ground must be properly chosen. In cases in which these dimensions are fixed, the phases of the currents must be controlled.

Mathematical Analysis

In order to simplify the analysis, the following assumptions are made:

(1) The ground is assumed to be a perfect conductor and therefore, for purposes of the computation it can be replaced by the image of the array.

(2) The currents in the vertical wire and in the shield are known and can be controlled arbitrarily.

(3) The height of the vertical wire is a quarter of a wavelength.

(4) The distribution of the shield current along the radial direction is not known. However, for reasons of simplicity we assume it to be sinusoidal.

(5) The shield which in the experiment consisted of sixteen radial wires is replaced by a conducting disk.

With these assumptions, the current element at a distance x from the center of the shield is given by

$$i = \frac{I}{2\pi} \cdot \sin \gamma x \cdot d\phi$$

in which I is the total current at the maximum and $\gamma = 2\pi/\lambda_s$ (λ_s refers to the wavelength of the shield). (See Fig. 9.) When determining the field strength, produced by the shield S' in the vertical plane $X - X'$ at a distance r from the antenna, the current components parallel to $X - X'$ have to be considered only, because, on account of symmetry the effects of the other components compensate themselves. As the distance r will be chosen large as compared to the wavelength, the field can be expressed by that term which is inversely proportional to the distance. Therefore, assigning the positive sign to the field of the vertical wire, the field strength due to the symmetrical current elements in shield S' becomes

$$dF_s' = -2 \cdot \frac{2\pi c}{\lambda r_1} \left[\frac{I dx}{2\pi} \sin \gamma x \cdot d\phi \right] \sin \psi \cdot \sin (\omega t - \beta r_1) \qquad (1)$$

where $\beta = 2\pi/\lambda$ (λ wavelength in free space), c = velocity of light, and $\omega = 2\pi/T = 2\pi c/\lambda$. A similar expression holds for the field dF_s'' produced by the image S''. The currents in S' and S'' must, of course, have opposite signs. r_1 and r_2 are, for practical purposes, parallel. With reference to Fig. 9 we get

$$\begin{aligned} r_1 &= r - A \sin \psi - (x \cos \phi) \cos \psi \\ r_2 &= r + A \sin \psi - (x \cos \phi) \cos \psi . \end{aligned} \qquad (2)$$

The total field strength due to the shield and its image is obtained by integrating $dF_s' + dF_s''$ between the limits $\phi = 0$ and π and $x = 0$ and a. Thus, F_s becomes

$$F_s = \frac{2Ic}{r}\left(\frac{2a}{\lambda}\right) \cdot Q(a, \psi) \cdot \sin\psi \cdot \sin(2\pi\zeta \sin\psi) \tag{3}$$

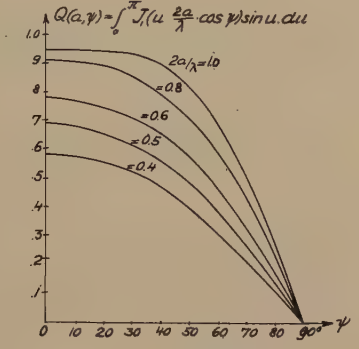

Fig. 8—Plot of the function $Q(a, \psi) = \int_0^\pi J_1(u \cdot 2a/\lambda \cdot \cos\psi) \sin u \cdot du$.

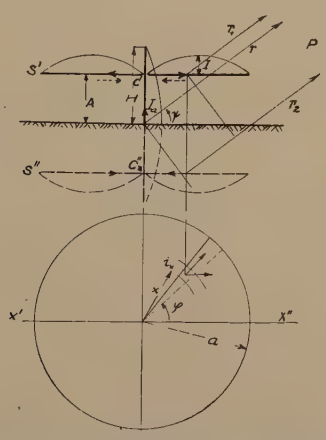

Fig. 9—Assumed current distribution in the array and its image. The direction of the shield current is opposite to that obtained in the analysis.

wherein,

$\zeta = A/\lambda$, a = radius of the shield

$$Q(a, \psi) = \int_0^\pi J_1\left(u \cdot \frac{2a}{\lambda} \cos\psi\right) \sin u \, du, \tag{4}$$

J_1 being Bessel's function of the first order. In Fig. 8 the integral $Q(a, \psi)$ is plotted against ψ for several values of the ratio $2a/\lambda$.

The field intensity due to a vertical wire, a quarter of a wavelength long, is known to be

$$F_v = \frac{2I_a c}{r} \frac{\cos\ (\pi/2\ \sin\ \psi)}{\cos \psi} \sin\ (\omega t - \beta r), \qquad (5)$$

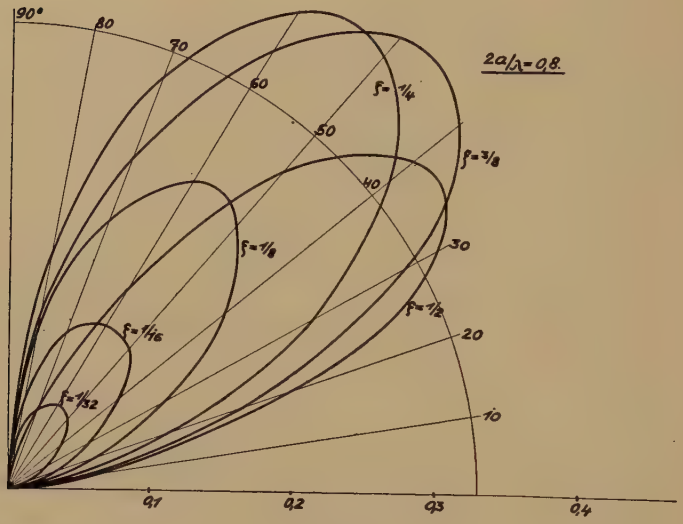

(a)

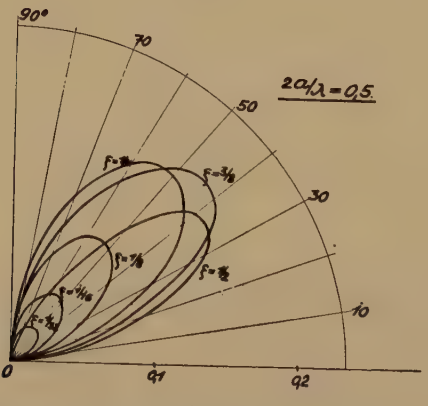

(b)

Fig. 10—Theoretical field patterns due to the shield and its image (perfect ground assumed).

I_a denoting the current at the grounded end of the wire. Finally the total field intensity at a distance r from the array is given by the sum

$$F = F_v + F_s = \frac{2I_a c}{r}\left\{\frac{\cos(\pi/2 \sin\psi)}{\cos\psi} + \frac{I}{I_a}\frac{2a}{\lambda}\cdot Q(a,\psi)\sin\psi\sin(2\pi\zeta\sin\psi)\right\}. \quad (6)$$

From this expression it becomes evident that in order to reduce the radiation for angles $\psi > 0$, the second term must be negative, and, therefore, the phase of the shield current must be opposite to that as-

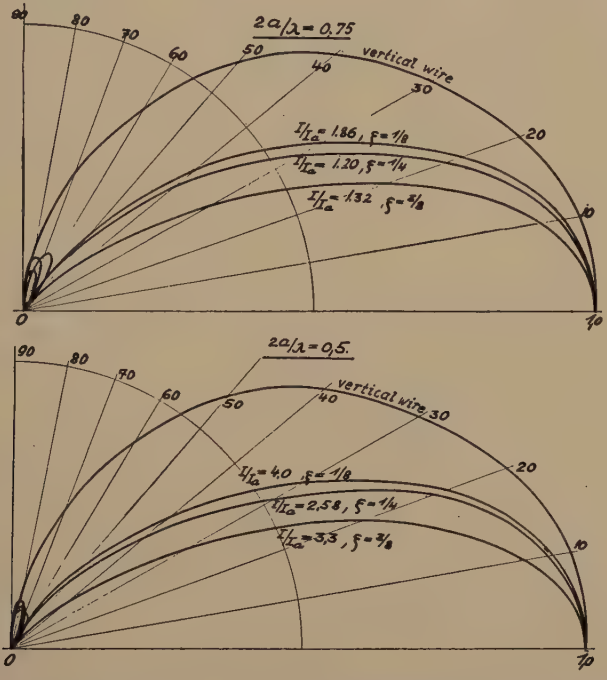

Fig. 11—Theoretical field patterns of shield antennas ($2a = D$), assuming perfect ground. $\zeta = A/\lambda$ for various sizes and heights of the shield.

sumed in Fig. 9. (Fig. 1 shows the proper direction of current flow.) From this it follows that, at a given instant, the currents in the vertical wire and in the shield will flow in the direction towards C' (Fig. 9) while in the image they will flow away from C''. We at once discern the difficulties encountered in feeding the shield. Obviously the simplest solution of this problem occurs when the total current at C' becomes zero. This always will be the case if the shield is excited by induction, either directly by means of a transformer or indirectly through radiation. The magnitude of the shield current and its phase with respect to the current in the vertical wire can be controlled by

tuning the shield and by proper choice of the height (A) above ground.

In the tests described above the optimum height proved to be $A = H/2 = \lambda/8$ and, as already pointed out, the tuning was achieved by variation of the diameter of the shield.

In Figs. 10 and 11 the field patterns of the shield and the complete array, as calculated by means of (6) are plotted against ψ. For purposes of comparison Fig. 11 also contains the pattern of the vertical wire ($H = \lambda/4$). From the condition that the total field intensity becomes zero for $\psi = 60$ degrees (and $\psi = 50$ degrees if $\xi = 3/8$), the ratio I/I_a between the shield and vertical wire current was determined.

Finally if we want to compare the results of experiment and theory, we may take test No. 58 in Fig. 3 and compare it with the case $2a/\lambda = 0.75$, $\zeta = A/\lambda = 1/8$ in Fig. 11. The same also holds for test No. 129 in Fig. 5. However, the shield diameter is 0.68λ instead of 0.75λ, because the shield S_2 was used in this test, instead of S_1 in test No. 58.

Proceedings of the Institute of Radio Engineers
Volume 23, Number 8 *August, 1935*

ANODE BEND DETECTION*

By

M. J. O. Strutt

(Natuurkundig Laboratorium der N. V. Philips' Gloeilampenfabrieken, Eindhoven, Holland)

Summary—*The anode direct current versus grid bias voltage characteristic of tubes is developed in a sum* $i=\sum A_n e^{a_n V}$, *where two or three terms suffice to represent the curves of some modern commercial tubes quite accurately. This development has two practical advantages. In the first place, as is shown in the first three sections, by comparison with measured values, detection slope and distortion effects may be accurately calculated from the static tube characteristics. In the second place, some general conclusions are obtained regarding the detection of various input waves. Finally, measured and calculated values of detection gain are compared and found to check fairly well.*

Introduction

RECENTLY, several commercial vacuum tubes were put on the market, either especially designed, or recommended for use as anode bend detectors. It is the purpose of the present paper to deal with the theory of anode bend detection and to describe the results of some experimental work conducted with a view to checking the theory. It would be desirable, ultimately, to obtain a detailed comparison between the merits of diode detectors and anode bend detectors. However, as anode bend detection presents in itself a considerable number of problems to be solved, the present paper is devoted exclusively to this type. Furthermore, the discussion here will be limited to tetrodes and pentodes.

In anode bend detection (Fig. 1), a vacuum tube is used with such a grid bias as to draw no grid current. The anode circuit contains a series resistance R, by-passed by a condenser C. The interior effective valve resistance R_i may be assumed large with respect to R. Furthermore, as usual, $R \gg 1/\omega C$, where ω is the angular frequency of the modulated input wave. If the input wave is given by

$$E(1 + M \cos pt) \cos \omega t,$$

where M is the depth of modulation and p the modulation angular frequency, a search is made for the voltage of frequency p to be taken from the resistance R. Besides this voltage, also voltages of frequencies $2p$, $3p$, etc., will be obtained at R, causing distortion of the modulation. These distortion effects will be discussed separately.

* Decimal classification: R134. Original manuscript received by the Institute, May 25, 1934.

Calculation of Detection Slope

In the anode circuit there will be a component of the current having a frequency p and an amplitude i_p. If E is the amplitude of the input wave, the *detection slope* of an anode bend detector is defined as:

$$S_d = i_p/E \tag{1}$$

If the detection slope of a tube and its anode circuit resistance R are known, the detection gain g_d may be found from

$$g_d = S_d R,$$

as long as[1] $R \ll R_i$.

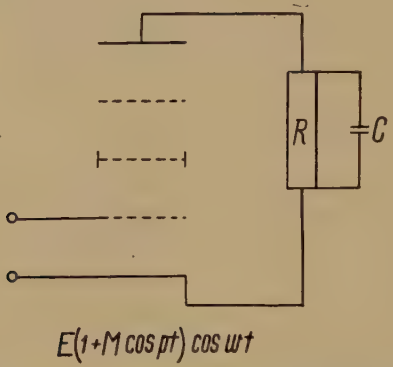

Fig. 1—Pentode used as an anode bend detector. R = resistance, about 10^5 ohms; C = capacity, about 100 micromicrofarads.

The static characteristic, i.e., anode direct current i versus grid voltage V is represented by an analytical expression

$$i = \sum A_n e^{a_n V} \tag{2}$$

In a previous paper,[2] this expression, using two or three terms only, was shown to give a very accurate representation of several commercial tube characteristics.

In (2), the voltage V is in our case

$$V = V_0 + E(1 + M \cos pt) \cos \omega t, \tag{3}$$

where V_0 is the grid bias. As shown previously, the anode current component i_1, which does *not* contain the angular frequency ω, is, by inserting (3) in (2), given by

[1] This restriction may be dropped if the static characteristic is measured while R is inserted in the anode circuit.

[2] M. J. O. Strutt, "Gleichrichtung," *Hochfrequenz. und Elektroakustik*, vol. 42, no. 6, pp. 206–208; December, (1933); Proc. I.R.E., vol. 22, pp. 931–1000; August, (1934).

$$i_1 = \sum A_n e^{a_n V_0} T_0\{j a_n E(1 + M \cos pt)\}. \tag{4}$$

Here $T_0\{\ \}$ is Bessel's function of order zero, of the first kind, and of argument $\{\ \}$ and $j = +\sqrt{-1}$. Expression (4) contains all the low-frequency components of the anode current, including direct current. We have now to pick out from (4) the current component i_p, of angular frequency p. This current component will be shown to be

$$i_p = i_{p1}M + i_{p3}M^3 + i_{p5}M^5 + \cdots \tag{5}$$

Hence, for small depths of modulation M, only the first term of (5) is essential. This is (see appendix)

$$i_{p1} = E \sum A_n a_n e^{a_n V_0} \frac{1}{j} T_1(j a_n E). \tag{6}$$

Here T_1 is Bessel's function of the first kind, of order one. The expressions for i_{p3}, i_{p5}, etc., are more complicated than (6) and are given by

$$i_{p3} = -\sum A_n e^{a_n V_0}\left\{\frac{3}{8} a_n^2 E^2 T_2(j a_n E) + \frac{1}{8} a_n^3 E^3 \frac{1}{j} T_3(j a_n E)\right\} \tag{7}$$

$$i_{p5} = \sum A_n e^{a_n V_0}\left\{-\frac{1}{128}\frac{1}{j} T_3(j a_n E) a_n^3 E^3 + \cdots + \right\}. \tag{8}$$

We shall now first consider (5) for small values of the input signal voltage E, such that $a_n E \ll 1$. Then, i_{p3}, i_{p5}, etc., are very small with respect to i_p, and hence

$$\begin{cases} S_d = \dfrac{i_p}{E} \sim M \dfrac{i_{p_1}}{E} = M \sum A_n a_n e^{a_n V_0} \dfrac{1}{j} T_1(j a_n E) \\ \qquad \approx \dfrac{M}{2} \sum A_n a_n^2 e^{a_n V_0} E = \dfrac{M}{2} \dfrac{\partial^2 i}{\partial V^2} E. \end{cases} \tag{9}$$

Equation (9) expresses the well-known result, that for small input voltages the detection slope is proportional to the product of this voltage and the second derivative of the anode current with respect to the grid voltage.

For moderate depths of modulation M, e.g., $M \leqq 0.3$, the second, third, etc., terms of (5) are only corrections, i.e., only a few per cent of the first one. This holds for all practical values of the input voltage E, with commercial tubes, as will be shown in the following section. We have then, for these values of M

$$S_d \sim M \sum A_n a_n e^{a_n V_0} \frac{1}{j} T_1(j a_n E). \tag{10}$$

If now the input signal voltage E and at the same time the grid-bias voltage V_0 are increased, so that a constant difference exists between them, in order to prevent grid current, the detection slope S_d *passes through a maximum.* This is seen as follows. For small values of E, we have

$$S_d = \frac{E}{2}\sum A_n a_n^2 e^{a_n V_0} m. \tag{10a}$$

Hence, S_d increases proportionally to E. For large values of E, such that $a_n E \gg 1$, we have

$$S_d = \frac{1}{\sqrt{2\pi E}}\sum A_n e^{a_n(V_0+E)} \cdot \frac{a_n}{\sqrt{a_n}} m \cdot \tag{10b}$$

Hence, as V_0+E is kept constant, S_d decreases with increasing E in this region.

It should be mentioned, that this conclusion, i.e., that S_d has a maximum as a function of E under the specified conditions, holds

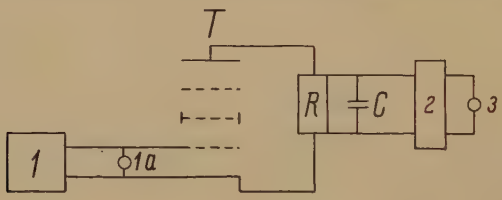

Fig. 2—Experimental set-up for measuring detector tubes. 1 is an oscillator of known depth of modulation. 1a is a voltmeter measuring the radio-frequency input to the tube T. R and C are as in Fig. 1. 2 is a filter circuit, passing only one audio frequency. 3 is a voltmeter for audio frequency.

also, if M is no longer small, such that (7) and (8) are taken into account. This may be seen by a numerical evaluation for given commercial tubes.

Measurements of Detection Slope

The detection slope may be measured, if a signal of known amplitude and known depth of modulation is put on the grid of an anode bend detector. This method involves the use of a signal oscillator of known modulation characteristic.

The experimental set-up is shown in Fig. 2. Oscillator 1 of known straight modulation characteristic is modulated by a pure sine wave of low frequency. The oscillator frequency is about 1000 kilocycles. The oscillator output is measured by a thermojunction voltmeter 1a and is connected to the grid and cathode of the tube under considera-

tion. A resistance R of about 0.1 megohm is in the anode circuit, bypassed by a condenser C of 100 micromicrofarads. The modulation frequency p is about 300 cycles and the low-frequency anode voltage is passed through a filter 2 and measured with the alternating-current voltmeter 3. The detection slope follows immediately from the readings of 3 and 1a, as R is known.[3]

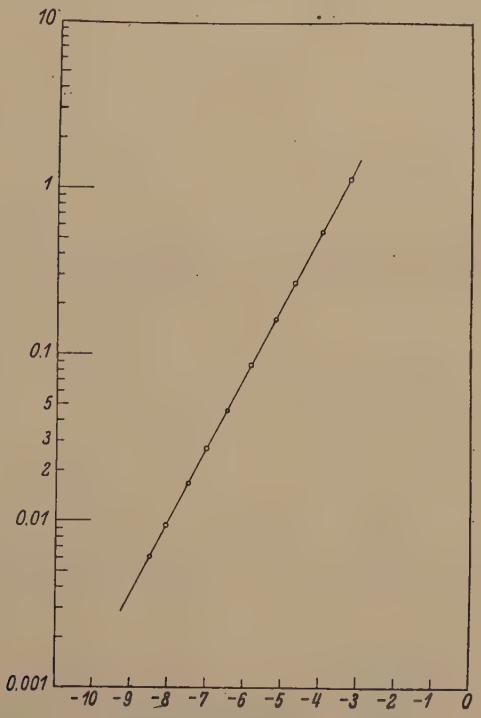

Fig. 3—Anode current i milliamperes (vertical) versus grid voltage V (horizontal) for Philips vacuum tube E 452 T. Points measured, curve calculated from $i = 28.7 \cdot e^{0.995V}$; $R = 0$; $V_{an} = 200V$; $V_{screen} = 100$ V.

In order to compare measured values with calculated ones, the anode current versus the grid voltage curve of several tubes was determined according to (2). Examples are found in Figs. 3 and 4. Calculated and measured values of detection slope are compared in Figs. 5 and 6.

If S_d is the detection slope and R the anode circuit resistance, the detection gain g_d is given by

$$g_d = RS_d.$$

[3] Of course, the resistance R used in the dynamic measurements must be equal to R used in taking the static characteristic.

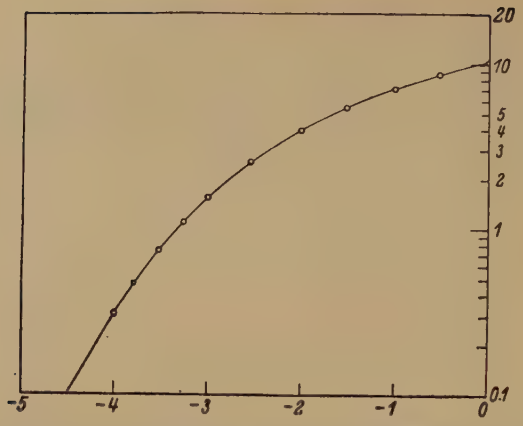

Fig. 4—Anode current i milliamperes (vertical) versus grid voltage V (horizontal) for Philips vacuum tube E 446. Points measured, curve calculated from $i = 11.5 \cdot e^{0.28V} - 1.2e^{0.377V} + 0.18e^{-4.10(V+3.5)}$; $R = 0$; $V_{an} = 200V$; $V_{screen} = 100V$.

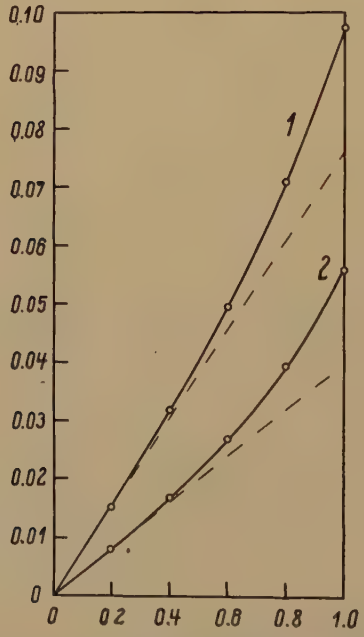

Fig. 5—Vertical axis, anode current component i_p (milliamperes). Horizontal axis, depth of modulation M. Points measured, curves calculated. Curve 1 for tube E 452 T. Curve 2 for tube E 446; $R = 0.1$ megohm; $V_{an} = 200V$; $V_{screen} = 100V$.

Insertion of a resistance R of about 100,000 ohms in the anode circuit decreases the anode direct voltage, which results in a decrease of the anode direct current. Therefore, S_d has to be measured under the anode voltage conditions which exist in normal use of the tube as an anode detector, i.e., inserting the resistance R inthe anode circuit.

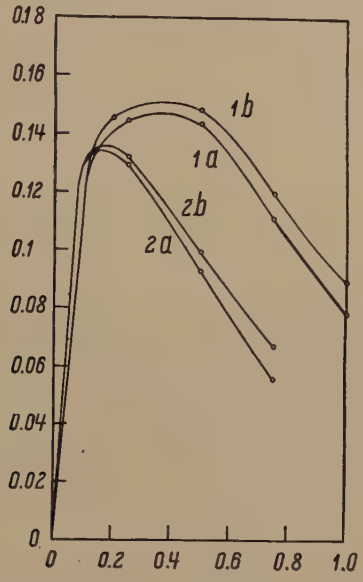

Fig. 6—Vertical axis, detection slope S divided by M' (ma/volts); horizontal axis; input signal amplitude E, while $V_0+2E=-3.5$ volts. Points measured, curves calculated. Curves 1 for tube E 452 T. Curves 2 for tube E 446. Curves 1a and 2a for M = 0.3. 1b and 2b for M = 0.8. Voltages and resistance as in Fig. 5.

Some measured and calculated values of S_d and of g_d are given below (for a depth of modulation of 30 per cent and a one-volt peak input signal for E452T and 0.75 volts for E446.

Tube	Grid Bias V_0	Anode Voltage	S_d calc. *ma/v*	S_d meas.	g_d on $R=$ 100,000 Ohms
Philips E452T	−5.5	200	0.078	0.075	7.8
Philips E446	−5.0	200	0.0166	0.0158	1.66

Owing to the effect on the anode voltage, mentioned above, an increase of R does not always result in an increase of g_d.

In Fig. 5 measured values of conversion conductance are also shown (dotted).

This conversion conductance is defined as follows: Put two alternating voltages on the grid and the bias V_0.

$$V = V_0 + E \sin \omega t + E_i \sin \omega_i t.$$

Then the anode current will contain a component $i_0 \cos \omega_0 t$, where $\omega_0 = \omega - \omega_i$. And the conversion conductance is i_0/E_i.

It appears, that *for small modulation depths M, the conversion conductance of a tube is equal to its detection slope divided by the modulation depth.* This conclusion may immediately be checked from the theoretical standpoint, as the conversion conductance S_c is rigorously given by

$$S_c = \sum A_n e^{a_n V_0} a_n \frac{1}{j} T_1(j a_n E), \tag{11}$$

as was previously shown.[4] This value (11) corresponds entirely to (10) for the detection slope. The curves of Fig. 6 show clearly the maximum of S_d, predicted in the foregoing section.

The difference between detection slope and conversion conductance at high values of the modulation depth M, as shown in Fig. 5, is due to the distortion effects of detection, expressed in the terms i_{p3}, i_{p5}, etc., of (5), (6), and (7). Particularly the term i_{p3} may give rise to serious distortion at high values of M, as will be shown in the following section.

As long as $M \leqq 0.3$, it is clearly seen from Figs. 5 and 6, that with these tubes the detection slope may be measured in quite the same way as conversion conductance, using an experimental set-up described previously.[4]

Distortion Effects with Input Signal of Ideal Wave Form

An ideal input signal wave is assumed to be of the form

$$E(1 + M \cos pt) \cos \omega t,$$

where $M < 1$. With such input waves, several possibilities of distortion occur.

The first distortion effect, to be discussed here occurs even if the modulation contains only a single frequency. By this effect, harmonics of the modulation frequency p are introduced. The anode current contains components $i_{2p} \cos 2\,pt$, $i_{3p} \cos 3pt$, $i_{4p} \cos 4pt$, etc. They are given by the expressions (see appendix)

[4] M. J. O. Strutt, "Radioempfangsröhren mit grossem inneren Widerstand, A. Hochfrequenz verstärkerröhren mit einem Steuergitter," *Hochfrequenz. und Elektroakustik*, vol. 43, no. 1, pp. 15–18; January, (1934); "B Modulator-(Detektor-) Röhren mit einem Steuergitter," pp. 18–22.

$$i_{2p} = i_{2p1}M^2 + i_{2p4}M^4 + i_{2p6}M^6 + \cdots; \quad (12)$$

$$i_{3p} = i_{3p1}M^3 + i_{3p5}M^5 + i_{3p7}M^7 + \cdots; \quad (13)$$

where, for small values of E,

$$i_{2p1} = \frac{1}{4}\sum A_n e^{a_n V_0} a_n E \frac{1}{j} T_1(j a_n E); \quad (12a)$$

$$i_{3p1} = -\frac{1}{8}\sum A_n e^{a_n V_0} a_n^2 E^2 T_2(j a_n E), \text{ etc.} \quad (13a)$$

Measured and calculated values of i_{p2} and of i_{p3} are compared in Fig. 7. The former were obtained by tuning the filter 2 of Fig. 2 to the frequencies $2p$ and $3p$, respectively.

A second distortion effect manifests itself, if more than a single frequency of modulation is present, as is usually the case with music or speech. Here, only two modulation frequencies will be assumed, of values p and q, respectively. Then, owing to the nonproportionality of detection slope to depth of modulation, combinations of the frequencies p and q occur in the detected low-frequency components. Thus the low-frequency anode current contains components

$$i_{p-q} \cos (p - q)t;\ i_{p+q} \cos (p + q)t;$$

$$i_{2p-2q} \cos (2p - 2q)t;\ i_{2p-q} \cos (2p - q)t,$$

and so forth. Generally, the first two components, just formulated, are the most important ones. They are (see appendix) for moderate depths of modulation

$$i_{p-q} = i_{p+q} = M_p M_q \sum A_n e^{a_n V_0} \left\{ \frac{1}{2} \frac{1}{j} T_1(j a_n E) a_n E - \frac{1}{2} T_2(j a_n E) a_n^2 E^2 \right\}, \quad (14)$$

where M_p and M_q are the depths of modulation of the input wave with the modulation frequencies p and q, respectively. As may be checked by equations (12a), (13a), and (14), we have

$$i_{p-q} = M_p M_q (2 i_{2p1} + 4 i_{3p1}), \quad (14a)$$

whence it is concluded that this combination tone distortion effect may be readily evaluated, if the harmonics have been measured. If more than two low frequencies are present in the modulation, a great variety of combination tones occur, of which the effect (14a) is generally the most important one.

Comparing the seriousness of the two distortion effects, discussed

above, on the quality of radio reception, it must be remarked in the first place, that their magnitude is of quite the same order, viz., (12), (13), and (14). The harmonics of (12) and (13) are already present in the primary music, as all musical instruments produce a certain

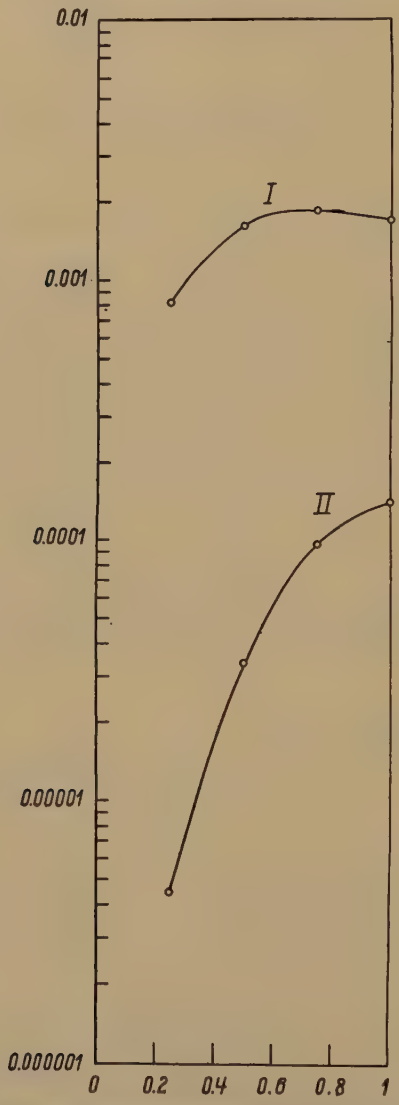

Fig. 7—Vertical axis, curve I = anode current component i_{2p} for $M = 0.3$. Curve II = anode current component i_{3p} for $M = 0.3$. Both curves related to vacuum tube E 452 T. Points measured, curves calculated. Horizontal axis, input signal amplitude E, while $V_0 + 2E = -3.5$ volts.

amount of harmonics. Hence, a slight portion of additional harmonics, introduced by the detector, will not give poor quality of reproduction. These things are different, however, with the combination tones, as, for example, in (14). These components are not present in the original modulating music and their occurrence after detection, even in slight quantities, may give rise to audible dissonances of the reproduced music. These dissonances are often responsible for what is called poor quality in reproduction.

By the methods set forth here, the detection and distortion effects on nonideal input waves (e.g., single side band) were also calculated and measured.

Appendix

The anode current i as a function of grid voltage V is given by

$$i = \sum A_n e^{a_n V},$$

where,

$$V = V_0 + E(1 + M \cos pt) \cos \omega t = V_0 + E_i \cos \omega t.$$

Now,

$$e^{a_n E_i \cos \omega t} = T_0(ja_nE_i) + 2\sum_{m=1}^{\infty} T_{2m}(ja_nE_i) \cos 2m\omega t + \frac{2}{j}\sum_{m=0}^{\infty} T_{2m+1}(ja_nE_i) \sin (2m+1)\omega t.$$

Hence, the component of anode current, which does not contain the angular frequency ω or one of its harmonics, is given by

$$i_1 = \sum A_n e^{a_n V_0} T_0\{ja_nE(1 + M \cos pt)\}.$$

But,

$$T_0\{ja_nE(1 + M \cos pt)\} = \sum_{k=0}^{\infty}(-1)^k \frac{(ja_nEM \cos pt)^k}{\lfloor k} \times (1 + \tfrac{1}{2}M \cos pt)^k T_k(ja_nE). \quad (15)$$

Inserting this into the expression for i_1 yields:

$$i_p \cos pt = (i_{p1}M + i_{p3}M^3 + i_{p5}M^5 + \cdots)\cos pt,$$

where,

$$i_{p1} = \sum A_n a_n e^{a_n V_0} \frac{1}{j} T_1(ja_nE) \cdot E;$$

$$i_{p3} = -\sum A_n e^{a_n V_0}\left\{\frac{3}{8}a_n{}^2E^2T_2(ja_nE) + \frac{1}{8}a_n^3E^3\frac{1}{j}T_3(ja_nE)\right\}$$

$$i_{p5} = \sum A_n e^{a_n V_0}\left\{-\frac{1}{128}\frac{1}{j}T_3(ja_nE)a^3{}_nE^3 + \cdots + \right\}.$$

These are equations (6), (7), and (8) of the text.

Consider the value of i_p, for small and for large values of input signal voltage E. In the former case,

$$\frac{1}{j}T_1(ja_nE) = \frac{1}{2}a_nE,$$

whence i_{p1} gives rise to (10a). In the latter case,

$$\frac{1}{j}T_1(ja_nE) = \frac{e^{a_nE}}{\sqrt{2\pi a_nE}},$$

whence (10b) results.

Coming to the harmonics of the modulation frequency p, generated by the detector, by (15) we derive

$$i_{2p}\cos 2pt = (i_{2p1}M^2 + i_{2p4}M^4 + i_{2p6}M^6 + \cdots)\cos 2pt$$

$$i_{3p}\cos 3pt = (i_{3p1}M^3 + i_{3p5}M^5 + i_{3p7}M^7 + \cdots)\cos 3pt, \text{ etc.},$$

where,

$$i_{2p1} = \frac{1}{4}\sum A_n e^{a_n V_0}\left\{a_nE\frac{1}{j}T_1(ja_nE + \cdots\right\}$$

$$i_{3p1} = \sum A_n e^{a_n V_0}\left\{-\frac{1}{8}a_n{}^2E^2T_2(ja_nE) + \cdots\right\}, \text{ etc.}$$

These distortion components are obviously

$$i_{2p1} = \tfrac{1}{4}i_{p1};$$

$$i_{3p1} = \tfrac{1}{3}i_{p3}, \text{ etc.}$$

where the latter equations hold only approximately, as long as a_nE is small with respect to unity.

In order to calculate the anode current components i_{p-q} and i_{p+q} of (14), the expression $M\cos pt$ in (15) of the appendix must be replaced by

$$M_p\cos pt + M_q\cos qt.$$

One obtains for moderate depths of modulation

$$i_{p-q} = i_{p+q} = M_p M_q \sum A_n e^{anV_0} \left\{ \frac{1}{2} \frac{1}{j} T_1(ja_nE) a_nE - \frac{1}{2} T_2(ja_nE) a_n^2 E^2 \right\}.$$

Hence, if a_nE is small with respect to unity, we have

$$i_{p-q} = M_p M_q (2i_{2p1} + 4i_{3p1}).$$

For literature on detection, reference is made to the bibliography, appended to a previous paper by the author.[5]

[5] M. J. O. Strutt, "On conversion detectors," Proc. I.R.E., vol. 22, p. 981; August, (1934).

Proceedings of the Institute of Radio Engineers
Volume 23, Number 8 *August, 1935*

RADIO-FREQUENCY POWER MEASUREMENTS WITH THE QUADRANT ELECTROMETER*

By

C. I. Bradford
(Ohio State University, Columbus, Ohio)

Summary—*This paper presents the mathematical theory and practical difficulties involved in the adaptation of the quadrant electrometer to radio-frequency power measurements. Two modified electrostatic wattmeter circuits are described and the limitations in their use are given. Data on typical measurements between 20 and 150 watts at 655 kilocycles are presented with the corresponding degree of accuracy for each case.*

I. Introduction

ONE OF the most valuable electrical instruments is the wattmeter, not only because of its use in the measurement of power, but also because of its value in circuit studies of impedance and power factor. At common power frequencies, the electrodynamometer type of instrument is indeed very satisfactory but at higher audio frequencies and radio frequencies the inherent inductance and stray capacitance of the elements make the instrument practically worthless.

The most common method utilized at present for the determination of radio-frequency power is that involving the measurement of current and resistance and the consequent I^2R calculation. Other methods which have been used include the calorimeter, the thermal wattmeter, and the vacuum tube wattmeter, all of which are cumbersome and indirect.

Since the time of Maxwell the quadrant electrometer has been recognized as an extremely valuable instrument not only as an electrometer but as a voltmeter, ammeter, and wattmeter on both alternating and direct currents. It has been the purpose of the study described in this paper to determine the possibilities and limitations in the adaptation of the quadrant electrometer to the measurement of power at radio frequencies.

II. The Electrometer

The quadrant electrometer, as the name implies, consists of four quadrants with a needle or vane suspended free to rotate within the quadrants. Diametrically opposite quadrants are connected together and a voltage, V_Q, is applied between the two sets of quadrants, and

* Decimal classification: R240×621.374.33. Original manuscript received by the Institute, August 6, 1934.

a second voltage, V_N, is applied between the needle and one set of quadrants. From a consideration of the energy of the system it can be shown[1] that the expression for the deflection is

$$\theta = \frac{r^2}{2k\pi t}(V_N - V_Q/2)V_Q \tag{1}$$

in which r is the radius of the needle, t is the distance between needle and quadrants, k is the suspension couple for unit twist, V_Q is the instantaneous voltage between quadrants and V_N is the instantaneous voltage between the needle and one set of quadrants.

The value of k in dyne centimeters per radian for a phosphor-bronze suspension is given by the empirical formula

$$k = \frac{7.3T^3W}{L} \tag{2}$$

in which T and W, are, respectively, the thickness and width of the suspension in mils and L is the length in centimeters. Also the total needle-to-quadrant capacity is

$$C_N = \frac{r^2}{4\pi t}. \tag{3}$$

Substituting these in (1) and inserting the necessary constants to convert electrostatic units to practical units, there results

$$\frac{\theta}{(V_N - V_Q/2)V_Q} = \frac{0.872C_NL\times 106}{T^3W} \tag{4}$$

and thus the sensitivity of the electrometer may be computed.

The electrometer normally possesses a mechanical zero and an electrical zero. The mechanical zero is the position taken by the vanes when no voltages are applied while the electrical zero is the position taken with $V_Q = 0$ and V_N equal to some operating value. It will be evident later that it is necessary that these two zeros coincide and that it is also necessary that the electrometer's deflections be linear in $(V_N - V_Q/2)$ and in V_Q in order that the instrument may operate satisfactorily as a wattmeter. Obtaining and maintaining these conditions involve the principal difficulties in the use of the electrometer.

In order to fulfill the above requirements, all unsymmetrical attraction of the vanes to the quadrants must be eliminated and a uniform change with deflection of the vane-to-quadrant capacity must be

[1] S. G. Starling, "Electricity and Magnetism," p. 158.

secured. This demands that the vanes be symmetrically located with respect to the quadrants and that they remain parallel with the quadrants at all deflections. The necessity of accurate mechanical design and assembly is obvious.

In the case for which the instrument is not properly adjusted there is an additional factor affecting the torque and the angle of deflection of the vanes which Beattie[2] calls the electrostatic control. He shows that in this case (1) becomes

$$\theta = \frac{K(V_N - V_Q/2)V_Q}{1 \pm K'(V_N - V_Q/2)^2} \tag{5}$$

in which $K = \frac{r^2}{2k\pi t}$ and K' is a new constant.

As a result of the electrostatic control term in the denominator the characteristic of the electrometer will not be a straight line but will be concave upward if the term is negative and concave downward if the term is positive.

The adjustments for linearity are best made by first leveling the instrument with a spirit level and adjusting the suspension so that each vane hangs in the middle of a cell and has equal capacity to all four quadrants. If the instrument were perfect, no further adjustment should be necessary. However, it will generally be necessary to adjust the leveling screws to obtain coincidence between the electrical and mechanical zeros. If a linear characteristic between θ and $(V_N - V_Q/2)$ is not then obtained the best method of procedure is to choose two operating points and adjust, by means of the leveling screws, for linearity between these two points. It will be found helpful if the approximate position of the linear characteristic has been previously determined from sensitivity calculations. After linearity has thus been obtained by these adjustments the zero adjustments will in general be satisfactory. Although numerous other possible procedures exist by which the above conditions can be obtained, it was found through a long period of experimentation that the above method is the most satisfactory.

III. The Electrometer as a Wattmeter

The most common circuit employing the electrometer as a wattmeter is shown in Fig. 1. The potential divider R_1R_2 supplies a fractional part of the source voltage, E, to the needle. Let n equal the ratio of these voltages.

[2] R. Beattie, "Sensibility and electrostatic control of the electrometer," *Electrician*, vol. 65, p. 729, (1910).

$$n = \frac{E}{V_N} = \frac{R_1 + R_2}{R_2}.$$

The load current, I_L, flowing through the resistance, R, supplies the quadrant voltage.

Simmons and Brown[3] have pointed out the usefulness of vector diagrams in the study of the behavior of the electrostatic wattmeter and from their suggestions the following analysis has been made.

In Fig. 2 let the load current, I_L, be the reference vector with the load voltage, E_L, leading it by an angle Φ. The drop across R, which equals V_Q, will be in phase with I_L, as shown exaggerated, and the source voltage, E, will be the vector sum of E_L and $I_L R$. V_N which equals E/n, is shown by the line AB.

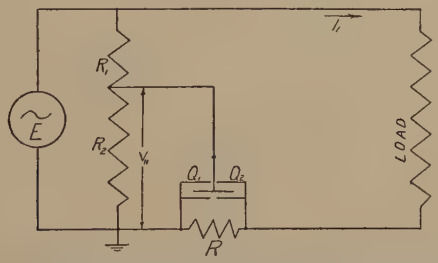

Fig. 1—The most common power measuring circuit utilizing the electrometer as an electrostatic wattmeter.

In setting up the analytic expression for the electrometer deflection, vector values will be designated by a bottom bar.

For convenience, let $\underline{V}_M = \underline{V}_N - \underline{V}_Q/2$. Then from (1) the average value of the deflection is proportional to the scalar product of $\underline{V}_M$ and $\underline{V}_Q$ or $\theta = K\underline{V}_N \cdot \underline{V}_Q$.

Since,

$$\underline{V}_N = \underline{E}/n$$

and,

$$\underline{V}_Q = \underline{I_L R}$$

$$\theta = K\left(\frac{\underline{E}}{n} - \frac{\underline{I_L R}}{2}\right) \cdot \underline{(I_L R)}$$

but,

[3] Simmons and Brown, "The electrometer for the measurement of dielectric loss," *Trans. A. I. E. E.*, vol. 43, p. 311, (1924).

$$\underline{E} = \underline{E_L} + \underline{I_L R}$$

$$\therefore \quad \theta = K\left(\frac{E_L/\underline{\phi}}{n} - \frac{\underline{I_L R}(n-2)}{2n}\right)\cdot\underline{(I_L R)}$$

$$\theta = \frac{K}{n}\left[E_L\cos\phi + jE_L\sin\phi - \frac{\underline{I_L R}(n-2)}{2}\right]\cdot\underline{(I_L R)}$$

or,

$$\theta = \frac{KR}{n}\left[E_L I_L\cos\phi - \frac{I_L^2 R(n-2)}{2}\right]. \tag{6}$$

If the potential divider is center tapped making $R_1 = R_2$, $n = 2$, and (6) reduces to

$$\theta = \frac{KR}{2}P_L \tag{7}$$

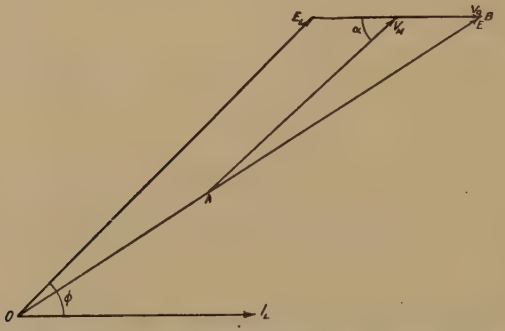

Fig. 2—Vector diagram of the instrument and circuit shown in Fig. 1.

where P_L is the power delivered to the load. Therefore the instrument can be made to indicate directly and linearly the power in the load. It will be noticed from Fig. 2 that for this case $V_M = E_L/2$ and $\alpha = \phi$.

The above analysis is for the simplest possible case, but at radio frequencies numerous other factors must be considered which were neglected in the derivation of (6). First, the needle-to-quadrant current flowing through R_1 will alter the magnitude and phase of V_N from the value used above; second, the resistor R will have some inherent inductance which will alter the magnitude and phase of V_Q, and third, the flow of current from the needle to high quadrant through R must be considered.

The error due to the first factor may be eliminated by placing a compensating capacity, C_c, across R_I of such size that the angle between current and voltage will be the same across both sections of the

potential divider. In other words, make the ratio of C_c/R_2 equal to the ratio of C_N/R_1. From an inspection of this circuit it is evident that under the above conditions a Wheatstone bridge balance is obtained and since no current flows from the junction of R_1R_2 to the junction of C_cC_N the potential divider may be removed and C_c placed in series with the needle. The currect value for C_c was determined by the bridge-balance method and from the 60-cycle calibration by making the electrometer deflection the same when the needle is connected to the junction of R_1R_2 as when in series with C_C. It is evident that C_c equals C_N for the case when $E/V_N = n = 2$ and this is the arrangement which was usually used in order to eliminate the correction term in (6).

The means of eliminating or minimizing the other two errors are better understood if the complete circuit is analyzed as was done for the simple case of Fig. 1. The complete equivalent circuit with C_c in series with the needle, a reactance in series with R, and needle-to-quadrant capacities, is shown in Fig. 3, in which C_L is the capacity

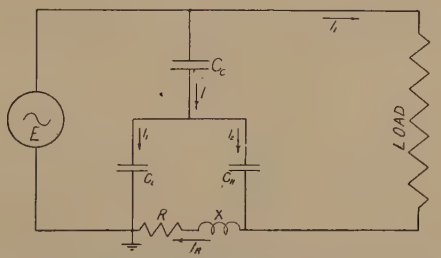

Fig. 3—Equivalent circuit of the electrostatic wattmeter at radio frequencies.

from needle to the low potential quadrant and C_H is the capacity from the needle to the high potential quadrant.

Since C_c, C_L, and C_H constitute a T of capacities, it can be transformed into an equivalent π. Furthermore, since the equivalent capacity across R and X is equal to one half the resultant series capacity of C_L and C_H, its reactance up to 1000 kilocycles is high in comparison to the impedance of R and X and therefore may be neglected. Thus, the problem is greatly simplified.

Now,

$$\underline{V}_Q = \underline{I}_R(R + jX)$$

but,

$$\underline{I}_R = \underline{I}_L + \underline{I}_2$$

and,

$$I_2 = \frac{jE_L \cos \phi - E_L \sin \phi}{2X_{CH}}.$$

Therefore,

$$\underline{V}_Q = (R + jX)\left(I_L - \frac{E_L \sin \phi}{2X_{CH}} + j\frac{E_L \cos \phi}{2X_{CH}}\right)$$

$$= RI_L - \frac{E_L R \sin \phi}{2X_{CH}} - \frac{E_L X \cos \phi}{2X_{CH}}$$

$$+ j\left(I_L X - \frac{E_L X \sin \phi}{2X_{CH}} + \frac{E_L R \cos \phi}{2X_{CH}}\right).$$

Now, $V_N = E/2$ through adjustment of C_c
and,

$$\underline{V}_M = \underline{E}/2 - \underline{V}_Q/2$$

but,

$$\underline{E} = \underline{E}_L + \underline{V}_Q.$$

Therefore,

$$V_M = \frac{E_L}{2} = \frac{1}{2}(E_L \cos \phi + jE_L \sin \phi)$$

and since,

$$\theta = K\underline{V}_M \cdot \underline{V}_Q$$

$$\theta = \frac{K}{2}\left(E_L I_L R \cos \phi - \frac{E_L^2 X \cos^2 \phi}{2X_{CH}} + E_L I_L X \sin \phi - \frac{E_L^2 X \sin^2 \phi}{2X_{CH}}\right)$$

$$\theta = \frac{KR}{2}\left(E_L I_L \cos \phi + E_L I_L \frac{X}{R} \sin \phi - \frac{E_L^2 X}{2RX_{CH}}\right)$$

$$\theta = \frac{KR}{2}\left(E_L I_L \cos \phi + \frac{E_L I_L X \sin \phi}{R} - \frac{E_L I_2 X}{2R}\right) \tag{8}$$

since, $$I_2 = E_L/X_{CH}.$$

This equation involves two correction terms which are introduced by the presence of I_2 and X. Since (8) reduces to $\theta = KR/2E_L I_L \cos \phi$ for $X = 0$, the importance of making R a noninductive resistance is evident.

Another circuit which is worthy of consideration is shown in Fig. 4. The current resistor, R, of the previous circuit is replaced by a condenser C_2. The load current flowing through this condenser will produce a 90-degree shift in quadrant voltage and consequently the needle voltage must be shifted through the same angle. If the $R_1C_1L_1$ circuit is made resonant with $X_{L1}=X_{C1}=R_1/2$ this requirement will be fulfilled and simultaneously V_N will equal $E/2$.

The derivation of the expression for the deflection as a function of load power is similar to the derivation of (6) and (8).

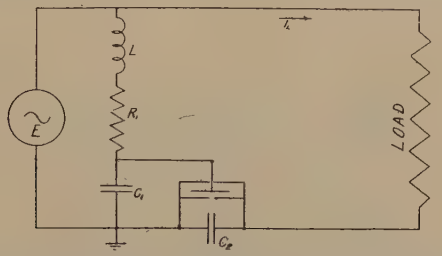

Fig. 4—A modified electrostatic wattmeter circuit utilizing a quadrant-to-quadrant condenser and a resonant potential divider.

In this case it is

$$\theta = \frac{KX_{C2}}{2}(E_L I_L \cos\phi - I_L^2 X_{C2}) \tag{9}$$

or this may be rewritten as

$$\theta = \frac{KX_{C2}}{2}(R_L - X_{C2})I_L^2 \tag{10}$$

since, $$E_L I_L \cos\phi = I_L^2 R_L.$$

Thus, to the wattmeter, the load resistance appears to be diminished by an amount equal to X_{C2}. The term $I_L^2 X_{C2}$ may be conveniently obtained and consequently the load power is obtainable from the electrometer readings.

From physical considerations of the circuit of Fig. 4 it can be seen that this circuit is essentially insensitive to the power involved in the harmonics of the frequency of resonance of the potential divider. For any frequency higher than the fundamental the impedance of $R_1L_1C_1$ is higher than R_1, its value at resonance, and simultaneously the reactance of C_1 is lower, therefore, V_N will be less than its correct value for two reasons. Also X_{C2} will be lower and the voltage V_Q will be low for the higher frequencies. Furthermore, the introduction of phase differ-

erences between V_N and V_Q will reduce $V_M \cdot V_Q$ and the deflection. This frequency discriminating characteristic of the circuit may or may not be an advantage depending upon the specific type of measurements desired.

The decided advantage of this circuit lies in the fact that the quadrant-to-quadrant capacity may be considered part of C_2 and the needle-to-quadrant capacity may be considered part of C_1.

Since E_L in (6), (8), and (9) is directly proportional to V_N, it is now evident that the electrometer deflections must be a straight line function of $(V_N - V_{Q/2})$ and that the deflections must be zero for operating values of V_N with $V_Q = 0$.

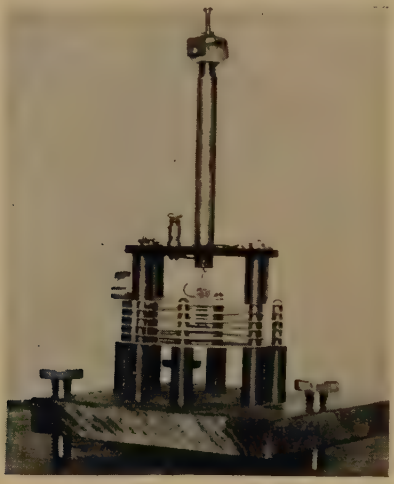

Fig. 5—The multicellular electrometer which was used as a radio-frequency wattmeter.

Experimental Work and Results

A close-up picture of the electrometer used in this investigation is shown in Fig. 5 with the shield removed. The total internal needle-to-quadrant capacity of this instrument is 138 microfarads and the sensitivity computed from (4) is

$$\frac{\theta}{(V_N - V_{Q/2})V_Q} = 0.000877 \text{ radians/volt}^2.$$

Since the instrument's deflections were read in centimeters with a telescope on a scale 60 centimeters away, in order to obtain actual readings from the above constant it must be multiplied by 2×60 or

$\theta_{read} = 0.105(V_N - V_{Q/2})V_Q = 0.0525P_LR$ in the case for $n = 2$.

This calculated value of sensitivity is shown as the broken line in Fig. 6 and checks the 60-cycle calibration curve to within about two per cent.

The complete circuit on which most of the power measurements at 655 kilocycles were made is shown in Fig. 7. The coil L is a radio-

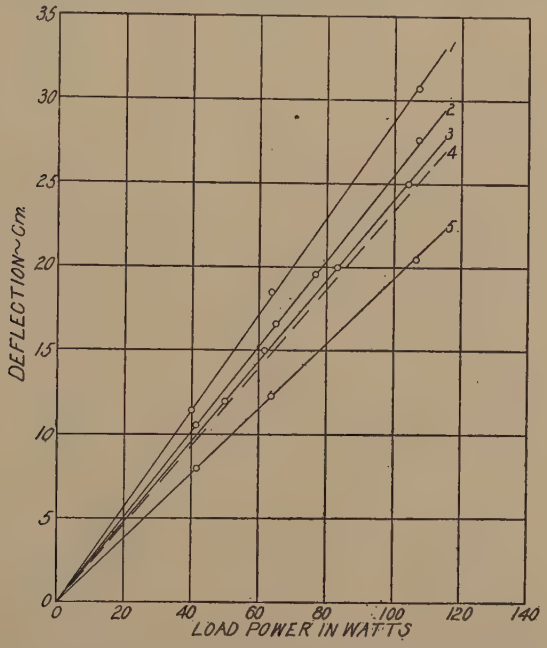

Fig. 6—Typical calibration characteristics of the electrostatic wattmeter obtained when the current resistor, R, is slightly inductive.
1. $Z_L = 518$. $\angle 48.5°$ at 655 kc.
2. $Z_L = 344$ and 457 $\angle 8°$ at 655 kc.
3. 60-cycle calibration.
4. Calculated calibration.
5. $Z_L = 456$ $\angle -41°$ at 655 kc.

frequency choke to prevent the division of direct plate voltage across the stopping condenser, the condenser C_c, and the electrometer, when Z_L is made capacitative by means of a series condenser.

The load impedance Z_L consisted of ohm-spun resistors with, or without, series inductance and capacity depending on the type of load desired. The quadrant resistor, R, consisted of a loop of wire about ten inches long with a resistance of 4.46 ohms.

The wattmeter was calibrated at unity power factor by applying a variable 60-cycle voltage across the circuit at points A and B in

Fig. 7 with L removed. The task then became one of checking the $I_L^2R_L$ values at radio frequencies against the power indicated by the wattmeter from the 60-cycle calibration.

An interesting set of data taken at 655 kilocycles is shown plotted in Fig. 6. These data were taken with a current resistor, R, with which reasonable care was taken in construction to eliminate any inductance. The wattmeter readings are approximately six per cent high for a load with an angle of lag of 8 degrees, approximately twenty per cent high for an angle of lag of 48.5 degrees, but approximately twenty-four per cent low for an angle of lead of 41 degrees. It is evident from these curves that a source of error exists which prohibits the use of this circuit with any degree of accuracy.

From a consideration of the last two terms of (8), which are correction terms, it was found that the characteristics of Fig. 6 are accounted for if $X=0.9$ ohms. Since this reactance represents an inductance of only 0.218 microhenry at 655 kilocycles this seems like the logical

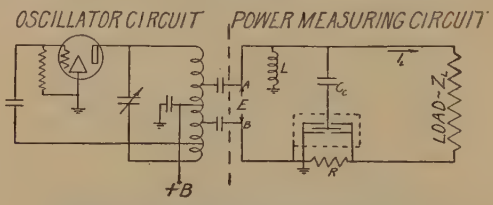

Fig. 7—Oscillator and power measuring circuit used in the experimental work at 655 kilocycles

source of error. It is evident from these data and calculations that the quadrant resistor, R, must have an extremely low inductance in order to obtain accurate measurements with this wattmeter circuit.

On the basis of this information a quadrant resistor was made by braiding six insulated pieces of wire having thirty ohms resistance per foot. The braiding was performed in a manner which would produce the maximum nullification of inductance; stray capacity effects can be neglected because of their negligible values in comparison to the low value of resistance. This new resistor had a resistance of 4.52 ohms and therefore the wattmeter constant K for this case was 4.46/4.52 times 4.13, the constant for the above case, or, $P_L=4.07\theta$. The values of power obtained under conditions similar to the above case are so nearly correct that a plot of the data yields a single curve coincident with the 60-cycle calibration curve.

These data are given in Table I with the difference, D, between $K\theta$ $I_L^2R_L$ as per cent of the $I_L^2R_L$ values for each case. It will be noted that this difference is always less than two per cent and that the average

TABLE I

I_L	Z_L	$I_L^2R_L$	θ	$K\theta$	D	$100\frac{D}{I_L^2R_L}$
0.38	343 +*j*45	49.5	12.3	50.1	0.6	1.21
0.50	343 +*j*45	85.8	21.4	87.1	1.3	1.49
0.58	343 +*j*45	115.5	28.6	116.4	0.9	0.77
0.33	455 +*j*60	49.5	12.3	50.1	0.6	1.21
0.42	455 +*j*60	80.2	20.0	81.4	1.2	1.48
0.5	455 +*j*60	114.0	28.5	115.7	1.7	1.49
0.38	343 +*j*342	49.5	12.4	50.5	1.0	1.98
0.5	343 +*j*342	85.8	21.5	87.5	1.7	1.94
0.58	343 +*j*342	115.5	28.3	115.2	−0.3	0.26
0.38	343 −*j*342	49.5	12.2	49.7	0.2	0.40
0.5	343 −*j*342	85.8	21.1	85.9	0.1	0.12
0.58	343 −*j*342	115.5	28.0	114.0	−1.5	1.31

Average $D = 1.14\%$

difference is 1.14 per cent, a value comparable with the accuracy of current and resistance measurements at this frequency. Furthermore,

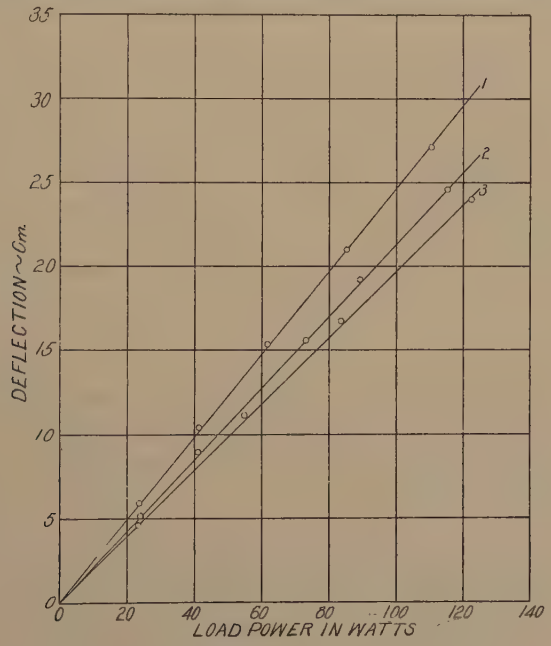

Fig. 8—Typical calibration curves of the electrostatic wattmeter utilizing the resonant potential divider.

For the curve marked

1. $Z_L = 455$. $\angle -41°$ at 655 kc.
2. $Z_L = 457$. $\angle 8°$ also transferred 60-cycle calibration
3. $Z_L = 454$. $\angle 41°$ at 655 kc.

the dissipation in the wattmeter circuit is due entirely to the I_L^2R loss in the quadrant resistor. In the measurements shown in Table I this loss reaches a maximum of 1.52 watts with a load current of 0.58 ampere.

Another set of data which was taken with the circuit shown in Fig. 4 is shown in Fig. 8. The circuit elements were as follows:

$$R_1 = 2360 \text{ ohms}$$
$$L_1 = 287 \text{ microhenrys} \qquad X_{L1} = 1180 \text{ ohms}$$
$$X_{C1} + X_{CN} = 1180 \text{ ohms}$$
$$C_2 = 0.055 \text{ microfarads} \qquad X_{C2} = 4.43 \text{ ohms.}$$

The unity power factor line agrees very well with the 60-cycle calibration but at leading and lagging power factors an error exists of approximately ten per cent. Although this error is much less than that involved in the characteristics shown in Fig. 6, it is large enough to prohibit the use of the instrument for measurements requiring a fair degree of accuracy. This fact combined with the disadvantage of the excessive loss in the resistance of the resonant potential divider did not justify a considerable amount of investigation on this circuit.

V. Conclusion

The question of the practicability of the quadrant electrometer as a radio-frequency wattmeter may be considered from two standpoints. First, what are the limitations in the use of the electrometer? Second, what are the limitations in the adaptation of the electrometer to this specific duty?

The electrometer in its present stage of development is purely a laboratory instrument because of the inherent difficulties in obtaining and maintaining the proper adjustments. On account of the extremely low values of torque developed it is necessary, practically, to use a suspension for supporting the vanes and supplying the restoring couple. Even if it were possible to build the vanes sufficiently light so that bearings could be used, the problem of linearity and zero adjustments would become more difficult. If a high sensitivity instrument utilizing bearings could be designed with provisions for making the required adjustments, there seems to be no reason why the electrometer could not be as portable and practicable as any of our magnetic type of instruments. Until this type of design becomes a reality the electrometer must continue as a laboratory instrument.

The utility of any electrical instrument is limited by its accuracy and its disturbing effects on the circuit in which measurements are to be made.

In the frequency range in which this investigation has been made, Table I and equation (8) indicate that the principal prerequisite for accurate measurements with the circuit shown in Fig. 7 is an absolutely

noninductive resistance, R, for use between quadrants. Naturally, the resistor used in obtaining the data in Table I was not absolutely noninductive and consequently precise measurements were not obtained. The fundamental and important fact is that the reduction of the the inductance of R reduced the error from twenty-four to two per cent. It must be remembered that although (8) states that the correction terms are zero if X is also zero, that simplifying assumptions have been made in the derivation. It was assumed that the reactance of the equivalent quadrant-to-quadrant capacity was negligible in comparison with the resistance of R and that the stray capacity of R was negligible. At higher frequencies these assumptions may not be justified. Thus, the accuracy of measurements is governed by the frequency, the inductive reactance of the resistor, R, and whether or not sufficient consideration has been given to the various parts of the circuit.

As to the instrument's disturbance of the circuit; it is evident that the electrometer used in the investigation could have been used to measure power at higher or lower current values by altering the value of the quadrant resistor, R. However, with R equal to approximately 4.5 ohms the drop across it and the consequent power loss were practically negligible. In Table I under column 1, are given the values of total current through the capacity C_e and the electrometer. Obviously, this is purely a capacity current and will increase with increase in frequency. Whether or not it is sufficiently large to have a disturbing effect on the circuit will be governed entirely by the conditions of the problem.

In brief, the conclusions are:

1. The electrometer, because of its critical adjustments, is suitable only for laboratory work at present.

2. For a given frequency the accuracy of power measurements is dependent upon the degree to which the quadrant resistor can be made noninductive.

3. The disturbing effects of the wattmeter circuit are governed by the value of the quadrant resistor and the amount of capacity current flowing from needle to quadrants.

Acknowledgment

The writer wishes to express his appreciation to Professor W. L. Everitt of Ohio State University, under whose direction this investigation was made, for his guidance, advice, and many helpful suggestions.

Proceedings of the Institute of Radio Engineers
Volume 23, Number 8 *August, 1935*

BOOK REVIEWS

Elements of Loud Speaker Practice, by N. W. McLachlan. Published by the Oxford University Press, 114 Fifth Avenue, New York, N. Y. 158 pages. Price $1.75.

This is an elementary text describing the construction and performance of loud speakers, with one chapter dealing very briefly with the effect of the room on loud speaker performance. Practically all of the loud speaker types which have been developed are described, including some, such as the condenser, inductor and piezoelectric, which have been of small commercial importance. The radiation from diaphragms is discussed, and the effect on the radiation of baffles and horns is taken up.

This book will be of most use to the radio engineer, or others—such as servicemen, patent attorneys and salesmen, who do not have the time or information to become loud speaker experts, but who would like to have some general information about the construction and performance of various loud speaker types. No mathematics is used in the presentation. The book is not suitable for the loud speaker designer, as it does not contain sufficiently detailed technical information.

* Irving Wolff

* RCA Manufacturing Company, Camden, N. J.

Seismographing for Oil, by E. G. McKinney. Published by E. G. McKinney, Box 845, Oklahoma City, Okla. 38 pages, price $2.00.

Devoted chiefly to the problems of seismographic prospecting for oil, this book presents a brief reference to the use of radio communication between members of the prospecting personnel.

† Alfred N. Goldsmith

† Consulting Engineer, New York City.

CONTRIBUTORS TO THIS ISSUE

Ataka, Hikosaburo: Born August 6, 1904, at Kanazawa, Japan. Graduated, electrical engineering department, Tokyo Imperial University, 1927. Instructor in electrical engineering, Meidi College of Technology, 1927 to date. Associate member, Institute of Radio Engineers, 1933.

Bradford, C. Irving: Born September 5, 1909, at Newport, New Jersey. Graduated, Bliss Electrical School, 1929. Radio development group, Bell Telephone Laboratories, 1929–1930. Received B.S. degree in electrical engineering, Rutgers University, 1933; Coffin Research Fellow, 1933–1934; received M.S. degree, Ohio University, 1934. Vacuum tube development engineer, Westinghouse Lamp Company, 1935. Nonmember, Institute of Radio Engineers.

King, Ronold: Born September 19, 1905, at Williamstown, Massachusetts. Received A.B. degree, University of Rochester, 1927; M.S. degree, 1929; Ph.D. degree, University of Wisconsin, 1932. American-German Exchange Student, Munich, 1928–1929; White Fellow in physics, Cornell University, 1929–1930; University Fellow in electrical engineering, University of Wisconsin, 1930–1932; research assistant, University of Wisconsin, 1932–1934; instructor in physics, Lafayette College, 1934 to date. Associate member, Institute of Radio Engineers, 1930.

Labus, J.W.: Born June 29, 1902, at Vienna, Austria. Received M.S. and Ph.D. degrees, Technical University of Prague, 1924. Assistant to Professor Siegel, University of Prague, 1924–1928. Engineering department General Electric Company, 1929–1930. Assistant professor (Dozent), Deutsche Technische Hochschule, Prague, Czechoslovakia, 1931 to date. Nonmember, Institute of Radio Engineers.

Strutt, M. J. O.: Born 1903, at Java, Dutch East Indies. Studied at University of Munich; Institute of Technology, Munich; Institute of Technology, Delft; graduated Munich, 1924, Delft, 1926. Assistant in physics department, Delft, 1926–1927. Doctor Technical Science, Delft, 1927. Research Staff, Philips' Incandescent Lamp Works, Ltd., 1927 to date. Nonmember, Institute of Radio Engineers.